Novel Methods for the Selective and Sensitive Detection of BMAA

by

Elliott Kerrin

Submitted in partial fulfilment of the requirements
for the degree of Master of Science

at

Dalhousie University
Halifax, Nova Scotia
August 2016

TABLE OF CONTENTS

LIST OF TABLES iv
LIST OF FIGURES v
ABSTRACT x
LIST OF ABBREVIATIONS USED xi
ACKNOWLEDGMENTS xiii
CHAPTER 1: INTRODUCTION 1
1.1 ALS/PDC in Guam 1
1.2 ALS/PDC in Other Foci 2
1.3 Initial Investigation 3
1.4 The BMAA Hypothesis 6
1.5 BMAA Controversy 10
1.6 Current Methods of BMAA Detection and Their Problems 11
1.7 Thesis Project Objective 14
1.8 Prospective Method: Differential Mobility Spectrometry 14
1.8.1 History and Potential Application to BMAA Analysis 14
1.8.2 Theory 15
1.8.3 Analyzer Geometries 20
1.8.4 Chemical Effects on DMS Separations 23
1.9 Prospective Method: Capillary Electrophoresis 28
1.9.1 History 28
1.9.2 Theory 29
1.9.3 Effects of BGE pH on Separation 31
1.9.4 BGE Composition and Concentration 31
1.9.5 Sample Stacking 32
1.9.6 Coupling CE with Mass Spectrometry 35
1.9.7 Variations of Sheath-Flow Interfaces 39
1.9.8 CE-MS BGE and Sheath Optimization 40
CHAPTER 2: SELECTIVE QUANTITATION OF THE NEUROTOXIN BMAA USING HYDROPHILIC INTERACTION LIQUID CHROMATOGRAPHY-DIFFERENTIAL MOBILITY SPECTROMETRY-TANDEM MASS SPECTROMETRY (HILIC-DMS-MS/MS)² 42
2.1 Introduction 42
2.2 Experimental 43
2.2.1 Chemicals, Reagents and Samples 43
2.2.2 LC-DMS-MS/MS Instrumentation 44

2.3 Results and Discussion 47
2.3.1 MS/MS and HILIC Behavior of BMAA Isomer Standards 47
2.3.2 Differential Mobility Spectrometry Optimization 49
2.3.3 HILIC-DMS-MS/MS Method Development 59
2.3.4 Identification of BMAA Isomers in Mussel Samples 62
2.3.5 Quantitative Analysis of BMAA with Isotope Dilution 65
2.4 Conclusion 69
2.5 Acknowledgments 70
CHAPTER 3: DETERMINATION OF THE NEUROTOXIN β-*N*-METHYLAMINO-L-ALANINE (BMAA) IN CYANOBACTERIA AND SEAFOOD BY CAPILLARY ELECTROPHORESIS-TANDEM MASS SPECTROMETRY 71
3.2 Introduction 71
3.3 Materials and Methods 72
3.3.1 Chemicals, Reagents and Samples 72
3.3.2 Sample Extraction and Cleanup 73
3.3.3 CE-UV Method Development 73
3.3.4 CE-MS Instrumentation 74
3.3.5 CE-MS Method Development 75
3.4 Results and Discussion 76
3.4.1 Method Development: Analyte Selection 76
3.4.2 Method Development: CE-UV 76
3.4.3 Method Development: BGE for CE-MS 81
3.4.4 Method Development: Improved CE-MS Interface 87
3.4.5 Method Evaluation and Application to Samples 89
3.5 Current Work 92
3.6 Conclusion 94
CHAPTER 4: CONCLUSIONS AND FUTURE WORK 95
BIBLIOGRAPHY 99

LIST OF TABLES

Table 2.1: Optimized detection parameters for BMAA isomers by HILIC-DMS-MS/MS.....48

Table 2.2: Quantitation of BMAA in matrix samples by HILIC-DMS-MS/MS.....70

Table 3.1: Quantitative results from final CE-MS method.....93

Table 3.2: Preliminary BMAA survey of aquatic matrices using HILIC-DMS-MS/MS.94

LIST OF FIGURES

Figure 1.1: Structure of β-*N*-methylamino-L-alanine (BMAA) 7

Figure 1.2: Chemical structures of BMAA, its isomers and the internal standard used...13

Figure 1.3: Three types of functional dependence of ion mobility on the electric field. Type A ions increase mobility with electric fields, type C ions see reduced mobility, and type B ion start out like type A ions but begin to behave like type C in even higher fields.....16

Figure 1.4: Schematic of the DMS ion filter setup and the hypothetical motion of a positive Type A ion (Blue) and a Type C ion (Red) when DV is applied without CV. If the correct CV is applied the path can be adjusted to fit the dashed line.....18

Figure 1.5: Dispersion plots showing all three types of ion behavior. The CV scan represents a cross-section of the dispersion plot at a DV of 1000. This image was adapted from Schneider *et al.* (2010) 19

Figure 1.6: Cross-section of a cylindrical FAIMS device. Ions are introduced with the gas, separated, and concentrated toward the detector.....21

Figure 1.7: Theoretical model of ion focusing in a FAIMS device. The paths of six identical ions starting at different radial positions have been traced. Ions below the focusing plane are pushed up by the larger migration due to DV while ions

above the focusing plane are pushed down by the larger migration due to CV.....22

Figure 1.8: Effects of carrier gas modifiers. The CV spectrums shows the same three of the 70 ions tested under different gas modifiers. The spectrum was collected using dry nitrogen as the carrier gas. The middle spectrum has 1.5% isopropanol added to the gas flow. The bottom spectrum is comprised of 44% helium and 56% nitrogen. Shifts in CV migration are explained by the models described. This figure was modified from Schneider *et al.* (2010) 25

Figure 1.9: CV of small organic ions (<700 *m/z*) as a function of percent acetonitrile composition in nitrogen carrier gas. This figure was adapted from Purves *et al*. (2014) 27

Figure 1.10: Model of standard capillary electrophoresis apparatus setup.....30

Figure 1.11: Model of conductivity based stacking.....34

Figure 1.12: Different concepts for CE-ESI interfaces. A typical sheath interface with the ESI voltage applied to the metal nozzle (a), a liquid junction interface with ESI voltage carried via sheath (b), a "junction-at-the-tip" interface (c), and a sheathless interface with ESI voltage delivered via wire (d) 38

Figure 2.1: Modification of DMS to allow for external metering of carrier gas modifier solvent.....46

Figure 2.2: Product ion spectra of BMAA isomers from collision induced dissociation of [M+H] *m/z* 119 for BMAA (A), BMAA-d_3 (B), BAMA (C), AEG (D), 2,4-DAB (E) and 3,4-DAB (F) with a collision energy spread of 15 – 20 V……49

Figure 2.3: HILIC-MS/MS (A) and HILIC-DMS-MS/MS (B) analysis of a 5 µM mixed BMAA isomer standard using selected reaction monitoring. Peak labels refer to isomers in Figure 1. Trace labels in B refer to DMS and SRM parameters in Table 2.1.....51

Figure 2.4: Effects of DMS parameters on BMAA isomer separation, including the effect of % acetonitrile modifier on compensation voltage (A) and sensitivity (B) at separation voltage = 2600 V and effect of separation voltage on compensation voltage (C) and sensitivity (D) using 0.35% acetonitrile modifier. The red line indicates optimum conditions used in HILIC-DMS-MS method.....53

Figure 2.5: CV spectra of a 5 µM isomer mixed standard before and after DMS modification. Part A shows the best parameters before modification collected with 1.5% (v/v) acetonitrile gas modifier and a dispersion voltage of 3600 V. Part B shows the same sample analyzed with the modified system with 0.35% v/v) acetonitrile gas modifier and a dispersion voltage of 2600 V.....57

Figure 2.6: Compensation voltage spectrum of a BMAA standard (A) and chemical noise separated by DMS (B), in full scan MS. Pane (C) shows DMS separation of BMAA (b) from its isomers BAMA (a), AEG (c), 2,4-DAB (d), 3,4-DAB (e) and isotopomer BMAA-d_3 (f), in SRM mode.....59

Figure 2.7: Identification of BMAA isomers in ASP-Mus mussel tissue reference material. Peak numbers correspond to analytes as in Figure 2.1 and trace labels correspond to DMS and SRM conditions in Table 2.1.....63

Figure 2.8: HILIC-MS/MS analysis of hydrolyzed ASP-MUS extract using selected reaction monitoring. Peak labels correspond to analytes in Figure 2.1.....65

Figure 2.9: DMS separation of BMAA from isomers and matrix interference in ASP-Mus mussel tissue reference material by HILIC-DMS-MS/MS. The 3D surface plots the total ion current of a product ion scan of *m/z* 119 carried out in a series of 30 LC runs at 1 V CV intervals.....66

Figure 2.10: Analysis of mussel sample M1 (A) and a calibration standard (B) using the targeted HILIC-DMS-MS/MS method. Retention time shifts occurred in matrix samples compared to standards, but relative retention time between BMAA/ BMAA-d_3 were constant and used, along with product ion ratios of *m/z* 102/44 as qualitative confirmation of BMAA identity.....67

Figure 2.11: Isotope dilution calibration plot showing the ratio of BMAA/ BMAA-d_3 plotted against the amount of BMAA injected.....69

Figure 3.1: Model of custom CE-ESI interface developed in-house.....75

Figure 3.2: Theoretical diagram for the relative concentrations of the different charge states of BMAA as a function of solution pH.....78

Figure 3.2: The effect of pH on migration times using 250 mM phosphate BGEs.....79

Figure 3.4: Final CE-UV method applied to an isomer mix standard at high concentration (1 mM) (a) and an extract of CRM-ASP-Mus (b). The known concentration of BMAA was too low to be seen in the extract of CRM-ASP-Mus. Peaks labels correspond to isomers in Figure 3.1.....81

Figure 3.5: Effects of pH on migration times for an acetic acid BGE.....83

Figure 3.6: Effect of formic acid BGE concentration on migration times.....85

Figure 3.7: Measured pH for formic acid BGEs at different concentrations and the effect on resolution and theoretical plate count.....87

Figure 3.8: CE-MS analysis of a standard mixture using final CE-MS conditions: BGE = 5 M FA with 10% MeCN; separation voltage = 20 kV; injection: 50 mbar for 120 sec; sheath liquid: 1.5 μL min^{-1} of MeOH/H_2O/FA (50:50:0.1) 89

Figure 3.9: CE-MS analysis of a CRM-ASP-Mus extract using the same conditions as in Figure 9. The peaks marked with an asterisk are unknown sample components.....91

Figure 3.10: Isotope dilution calibration plot showing the ratio of BMAA/BMAA-d_3 plotted against BMAA concentration.....92

ABSTRACT

β-*N*-methylamino-L-alanine (BMAA) is a neurotoxin first discovered in cycads and implicated as a possible cause of amyotrophic lateral sclerosis/parkinsonism dementia complex (ALS/PDC) in Guam's Chamorro population. Due to recent reports of the widespread presence of BMAA in cyanobacteria and seafood, there is concern over global public health. LC-MS is currently the method of choice for BMAA detection, but there are concerns over false positives from incomplete separation of isomeric and isobaric compounds or false negatives due to factors such as matrix suppression. Varying results from studies analyzing different samples with non-validated methods has led to considerable controversy within the field. In this study, hydrophilic interaction liquid chromatography-differential mobility spectrometry-tandem mass spectrometry (HILIC-DMS-MS/MS) and capillary electrophoresis-tandem mass spectrometry (CE-MS/MS) were developed as alternative complementary analytical methods for the determination of BMAA. These methods were initiated as part of an overall effort by the National Research Council of Canada to create certified reference materials (CRM) for BMAA in order to establish accuracy and traceability to the field.

LIST OF ABBREVIATIONS USED

2,4-DAB	2,4-diaminobutanoic acid
3,4-DAB	3,4-diaminobutanoic acid
AcOH	acetic acid
AEG	*N*-(2-aminoethyl)glycine
ALS/PDC	amyotrophic lateral sclerosis/parkinsonism dementia complex
AQC	6-aminoquinolyl-*N*-hydroxysuccinimidyl carbamate
BAMA	β-amino-*N*-methylalanine
BMAA	β-*N*-methylamino-L-alanine
CE	capillary electrophoresis
CFIA	Canada Food Inspection Agency
CNS	central nervous system
CRM	certified reference material
CV	compensation voltage
DIW	deionized water
DMS	differential mobility spectrometry
DP	declustering potential
DV	dispersion voltage
EPI	enhanced product ion
ESI	electrospray ionization
FA	formic acid
FLD	fluorescence detection
HILIC	hydrophilic interaction liquid chromatography
i.d.	internal diameter
IS	internal standard
LC	liquid chromatography
LOD	limit of detection

LOQ	limit of quantitation
MeCN	acetonitrile
MeOH	methanol
MRM	multiple reaction monitoring
MS/MS	tandem mass spectrometry
NRC	National Research Council
o.d.	outer diameter
SPE	solid phase extraction
SV	separation voltage
nd	not detected
RM	reference material
RSD	relative standard deviation
SD	standard deviation
S/N	signal to noise ratio
SRM	selected reaction monitoring

ACKNOWLEDGMENTS

I would like to thank my graduate studies supervisors, Dr. Michael Quilliam and Dr. Robert White for their encouragement and mentorship they provided over the past two years. I would also like to thank my supervisory committee, Dr. Alan Doucette and Dr. Louis Ramaley for their advice, support and helpful discussions.

I would also like to thank colleagues and staff at the National Resource Council in Halifax who provided practical advice and assistance, who were a wonderful team to work with, and who made for an incredible and enjoyable experience at the NRC. In particular I would like to acknowledge Dr. Daniel Beach for instruction and advice on DMS, Krista Thomas for her continuous support and encouragement throughout my graduate studies in addition to instrumental instruction, Sabrina Giddings for her BMAA extraction and analysis expertise, Dr. Pearse McCarron and Kelly Reeves for their help in preparation of freeze dried reference materials, Sheila Crain for acquiring NMR data for characterization of standards, Bill Hardstaff for providing ampouling expertise. I would also like to thank my family and friends for their support throughout my graduate studies.

Finally, I would like to thank the NRC and Dalhousie University for funding my graduate research.

CHAPTER 1: INTRODUCTION

1.1 ALS/PDC in Guam

Amyotrophic lateral sclerosis (ALS), sometimes called Lou Gehrig's disease, is an idiopathic neurodegenerative disorder that involves rapid progressive paralysis, ultimately resulting in patient death typically 2 to 3 years after initial symptom onset [1,2]. Globally, [1,3]. Of these cases, only 10% have an associated family history while the remaining 90% are considered sporadic, as they appear to occur randomly throughout the community [1,2].

In 1945, a high prevalence of motor neuron disease among the indigenous Chamorro population on the island of Guam was qualitatively described by Zimmerman [4]. Surveys by Koerner (1952) [5] and Arnold *et al.* (1953) [6] later revealed the island had over a 100-fold higher incident rate of ALS (196 cases per 100 000) than the rest of the world [7–9]. Their studies also suggested that males were almost twice as susceptible as females [6–9]. Interestingly, familiar components were associated with only 10% of the cases and a rationale for the elevated rate was not provided [6].

At the same time, another neurodegenerative disorder referred to as Parkinsonism-dementia complex (PDC) was of interest. It was present in one third of Guamanian ALS cases and responsible for 7% of Chamorro deaths over the age of 45 [10–12]. ALS and PDC were originally thought to be unrelated, as they have distinct manifestations and occur in separate parts of the brain (spinal cord/brainstem and the substantia nigra in the midbrain, respectively) [13,14]. In 1963, Hirano *et al.* [12] described an unusual pattern of neurofibrillary tangles occurring throughout the central nervous system (CNS) in PDC

patients that appeared to be identical in Guamanian ALS. Hirano *et al.* [12] concluded that the two conditions were in fact different expressions of the same disease [14].

The claim by Hirano *et al.* was later disputed by Oyanagi *et al.* (1994) [15] who surveyed 70 Guamanian patients with varying symptoms for tau-containing neurons, neurofibrillary tangles, Bunina bodies, and ubiquitinated inclusion bodies. They concluded that the two syndromes were independent, and that the Guamanian ALS fit the pathology of classical ALS [15]. Despite the possibility of PDC being a separate disease from ALS [9], it is of common belief that a single or several environmental factors in Guam are responsible for increasing the population's predisposition to both [3,14]. Furthermore, when looking for such factors, it has become of common practice to refer to both disorders interchangeably or as a single entity, ALS/PDC [3,13,16–18].

1.2 ALS/PDC in Other Foci

Around the same time of the Guamanian ALS/PDC studies (1940-1950), a high prevalence of ALS/PDC was observed in the Japanese population from the Kii Peninsula of Honshu Island (97 - 194 cases per 100 000) [19] and the Auyu and Jakai people from southern West New Guinea (147 cases per 100,000) [20]. As all three populations were effectively isolated from each other and came from distinct genetic lineages, hereditary causation was determined to be unlikely [8,21,22]. At the time, there was no reason to believe these three foci were isolated from neighboring regions, so the tightness of the clustering further decreased the likelihood of inherited susceptibility [8]. Though geographically isolated, the striking similarity in which the diseases presented, including the presence of neurofibrillary tangles, led some to believe a common environmental factor was present in all three locations [8,14,22].

If the environmental hypothesis is accurate, the agent appears to have a rather long incubation period. Epidemiological studies revealed an increase in risk factor only for the Filipinos and other immigrants who have assumed the Chamorro lifestyle for periods over 15 years [16,23]. In contrast, Chamorros who migrated to the United States and other countries may develop symptoms only after several decades [24,25].

A lifestyle component seems to be critical to the development of ALS/PDC, as no measurable increase in rate was observed in the 10,000 U.S. construction workers stationed in Guam over a 10 year period [26] or the 2 million Armed Forces personal that passed through Guam during the Second World War [16]. Furthermore, the steady decrease in incidence rate among the Chamorro people since the end of WWII has been attributed to adoption of a more "Western" lifestyle [9,16,19,27]. While there is no direct evidence for this conclusion, the reduction in occurrence over time has occurred too rapidly to be due to such factors as genetic mixing [9].

1.3 Initial Investigation

In 1956 the National Institute of Neurological and Communicative Disorders and Stroke initiated several projects to investigate the Guamanian phenomenon [9,22,23,28]. Though initially concerned with hereditary influences [9], ultimately four prevailing theories were investigated: genetic predisposition, a slow unidentified virus, an imbalance in water mineral content, and toxic agents present in cycad-based foodstuff [22,29].

Though some of the first theories at the time revolved around genetic and epigenetic predisposition, it is now generally agreed that these factors only account for a low percentage of documented cases due to the aforementioned distribution and propagation of

ALS/PDC in the three foci [1,3,8,30]. Nevertheless, there have been successes over the past 20 years identifying the superoxide dismutase 1 mutation [31], the survival of motor neuron 1 gene duplication, angiogenin gene, and ataxin-2 intermediate length polyglutamine expansions [17]. These discoveries have led to a large body of work examining how these polymorphisms relate within the foci. Despite these efforts, the penetrance of these mutations in appears to be very low [31], and have only been identified in half familial ALS patients and 11% of sporadic ALS patients globally [32]. Similarly, if underlying genetic components were responsible, epidemiological trends over the past 50 years would have required a highly disproportional number of those leaving Guam to be carriers for the problematic genes [9]. While it is possible that genetics can significantly increase an individual's susceptibility [3], the underlying environmental factor must be identified to continue research of this particular etiology.

The second theory of a temperate virus with a long latency period was proposed due to several studies linking CNS degenerative diseases with measles and polio contractions [28,33]. Despite many attempts, viral isolation from Guamanian ALS/PDC patients has been unsuccessful thus far [21,28,33,34] and no virus has been convincingly implicated with traditional ALS [1]. A viral infection would also fail to explain the epidemiological trends previously mentioned and a lack of recent publications suggest that the hypothesis has been abandoned [29].

The third theory of a mineral deficiency (or metal toxicity) was proposed by Yase in 1972 [16]. Although there have been several revisions, the main theory suggests a calcium and magnesium deficiency, caused by improper metabolism and/or inadequate environmental supply, results in increased intestinal absorption of neurotoxic aluminum and other

elements, which can be deposited in CNS tissues [8,16,20,35]. This theory seems promising as other heavy metals have been linked to neurodegenerative diseases and aluminum has been linked to Alzheimer's disease [36]. Analyses of drinking water and soil revealed low calcium and magnesium levels in all three foci with relatively high levels of aluminum, silicon, titanium, chromium, iron, and manganese [8,20,35,37]. Several studies have also found an accumulation of aluminum, calcium and silicon in Guamanian ALS/PDC patients' blood and intraneuronal tissues [16,35,37], though this has recently been disputed [13,38,39]. It should also be noted that no evidence of aluminum accumulation has been found in the spinal cord or brainstem [13,35]. Unfortunately, morphological evidence using animal models is weak and no long-term study using sub-lethal doses has been performed [40]. Those opposed to the metal toxicity hypothesis also point out etiologically important elements should be present before the pathological change, which does not appear to be the case [8,35]. Therefore heavy metal toxicity may be implicated with pathogenesis of neuronal death rather than the initial onset of the disease [8,35]. Lastly, this theory struggles to explain epidemiological studies, as aluminum toxicity would have to exert its effects decades after initial exposure. Neuronal loss during exposure would have to be asymptomatic for decades, with later symptom onset due to the natural process of aging [8,35]. While this model may appear to fit with the etiology of other neurodegenerative disorders, it is not compatible with ALS or PDC [8,35].

The Cycad Hypothesis was first proposed by Whiting and Fosberg in 1962 [41] and has subsequently become the most frequently cited environmental cause of the Guamanian ALS/PDC. Cycads belong to the family *Cycadaceae*, an ancient family of nonflowering plant that can be traced back into the early part of the Mesozoic Era [41,42]. These plants

are found in tropical and sub-tropical climates and six out of nine Cycadaceae's sub genera have demonstrated toxicity to humans and animals [41,42]. The Chamorro people have long been aware of the cycad's toxic nature, and wash with water for several days to make the seeds, leaves, and roots suitable for consumption [3,16,41,42]. Once prepared the cycad is used as feed for livestock, constructions of herbal remedies, and has become a staple food of the local Guamanian diet [3,16,41,42]. Though not initially known, evidence for the medical use of cycad seeds in both Japan and West Papua has been found[27,43]. Unfortunately the dietary habits in these areas have gone unstudied.

Symptoms of toxic exposure are common, particularly in cattle, which can manifest as the severe gastrointestinal disturbances and/or irreversible progressive paralysis starting in the hindquarters [41,42]. Locals believed male cattle are more susceptible, however this has not been verified [41,42]. Human casualties linked to cycad poisoning usually occur during periods of food shortage and can often be traced to inadequate preparation [41]. At the time, several lethal/carcinogenic glycosides had been isolated from cycads, but could not explain the paralysis observed [41,42]. Whiting and Fosberg hypothesized the unidentified paralytic agent may be responsible for the ALS/PDC epidemic [41].

1.4 The BMAA Hypothesis

Attempts to identify the neurodegenerative agent led to the isolation of the candidate neurotoxin α-amino-β-methylaminopropionic acid (later referred to as β-*N*-methylamino-L-alanine or BMAA) from *Cycas czrcznal* in 1967 [42]. BMAA is a non-coding amino acid had been isolated previously from several species in the genus *Lathyrus* [42]. Non-coding

amino acids are powerful toxins used by plants for protection from predation and nitrogen storage [3].

BMAA toxicity has been studied in mice, rats, chickens, and monkeys [44]. Initially interest was lost when exposure of mice to BMAA (0.5 mg g^{-1} day^{-1} for 11 weeks) failed

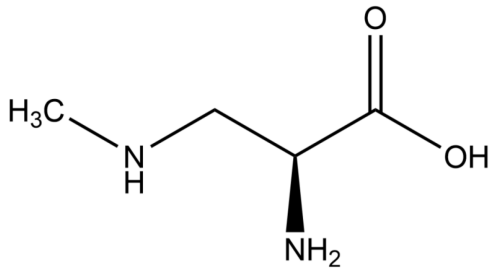

Figure 1.1: Structure of β-*N*-methylamino-L-alanine (BMAA).

to induce any appropriate neurologic symptoms [18]. The first study to observe a motor neuron-like disorder administered large doses of BMAA (100 to 250 mg g^{-1} day^{-1} for 12 weeks) to macaques [7]. Though subsequent studies using mice have failed to observe neurotoxicity, an LD_{50} of 3 mg g^{-1} administered intraperitoneally has been reported [45]. The same study also found that BMAA significantly accumulated in brains and livers of male mice more than female mice ($P < 0.01$), which they hypothesised may be due to differences in metabolic rate between males and females [45]. The fact that all studies administering BMAA orally to mice have failed to observe toxic effects [46] have led some to conclude that the mouse model may be a poor model for BMAA neurotoxicity [44].

Symptoms commonly described in BMAA toxicity studies with chicks, rats, and primates include convulsions, myoclonusm, shaking, ataxia, dragging or unsteady gait, hyperexcitability, and uncontrollable defecation [45]. Many studies that did not report any clinical symptoms have been presumed to have used insufficient doses of BMAA [45].

Despite some negative findings, a review by Karamyan and Speth (2008) [44] concluded that almost all *in vivo* studies on BMAA showed some neurotoxicity associated with motor function. It should be noted that only acute neurotoxicity has been demonstrated and to date there has been no confirmation of the delayed chronic form that is characteristic of Guamanian ALS/PDC.

BMAA appears to act as a glutamate agonist. Electrophysiological studies suggest that in the presence of physiological concentrations of bicarbonate, BMAA is an excitotoxin that activates the glutamate receptors NMDA, AMPA/kainite [47], and mGluR5 [48]. Exposure seems to result in a decreased number of glutamatergic receptors in the postsynaptic membrane and cell damage from oxidative stress [48,49]. Glutamatergic receptors have an important mechanism in memory function and for the sensory processing [45]. In addition to being a glutamate agonist, evidence has been found for the inhibition of the cystine–glutamate antiporter reducing cystine uptake [48], as well as incorporation into proteins potentially resulting in misfolding and loss of function [47].

Initially, the animal models cast doubt on the Cycad Hypothesis. Flour traditionally prepared from cycad had at most 150 μg g^{-1} BMAA, or about 10% of the original value prior to washing [18]. This would mean a 50 kg individual consuming 1 kg of flour daily would only ingest 20 mg kg^{-1} day^{-1}, an order of magnitude below that administered in the macaques study [7,18]. These findings led Spencer (1987) [16] to propose the "slow toxin(s)" model in which lower silent dosages of toxins have a minimum "incubation" period. A lower dosage may still damage pathways without fatal consequences, manifesting its clinical expression later in life [16]. Spencer [16] also suggested that larger doses may reduce the latency before disease onset. This theory was met with harsh

criticism from Duncan *et al.* [18], who argued that the theory lacked evidence and that the concept was "without precedence", as there is no known neurotoxin with delayed symptom onset after an initial exposure.

Interest in the Cycad Hypothesis was revived after a report suggested that the actual source of the BMAA was a cyanobacterium, *Nostoc sp.*, which lived on the cycad roots [50]. If true, cycad toxicity may fluctuate based on bacterial population [50]. Though not opposed to this theory, it should be noted that cycad's ability to produce BMAA without cyanobacteria was later demonstrated [51,52].

Even more intriguing were studies that suggested BMAA accumulation up the food chain. Flying foxes were considered a delicacy on Guam and were known to have a strong palate for cycad fruit [27]. Analyses of 50-year old museum specimens suggested that a single flying fox may have the same BMAA content as over 1000 kg of processed cycad flour [27,53]. This was orders of magnitudes higher than the doses required to induce neurodegeneration in primates (100 mg kg^{-1} day^{-1}) [7] and the authors suggested further investigation [27,53,54]. While other lipophilic toxins were known to accumulate in adipose tissue of flying foxes [27], the relatively polar BMAA would require a novel mechanism [54]. The bioaccumulation results suggested that there might be a secondary pool of BMAA that had thus far gone undetected.

Further investigation by Murch *et al.* (2004) [55] used an extraction with trichloroacetic acid to analyse BMAA in cyanobacteria, cycad flour, flying foxes, and 6 Chamorro patients clinically diagnosed with ALS/PDC. It was found that a secondary pool of BMAA could be released via hydrolysis of the insoluble protein-containing cycad fraction [55]. This secondary pool of "bound" BMAA contained up to 120 times that of the "free" BMAA and

was missed by previous studies [55]. “Bound” BMAA was observed in all samples, including cycad flour (80 mg g^{-1} BMAA), unaffected by the normal water-based detoxification process [55]. A slow release mechanism was proposed, where a free BMAA pool is maintained via normal cellular catabolism of proteins after initial exposure [55].

1.5 BMAA Controversy

The initial suggestion that BMAA was produced by cyanobacteria [50] coupled with the biomagnification theory caused concerns over possible widespread human exposure [21]. Cyanobacteria are an ancient phylum of bacteria that are found globally in terrestrial, freshwater, and marine environments. Cox *et al*. [56] tested 41 strains of cyanobacteria that covered all major taxonomic groups and reported BMAA in 37 strains. This started a worldwide search for the presence of BMAA in the environment.

Subsequently, BMAA production has been reported in many other cyanobacterial species and it has been suggested that the toxin may accumulate up the food chain in shellfish and other higher aquatic organisms (e.g. [27,50,55]). Even more alarming was the discovery of BMAA in the archived brain tissues of two Alzheimer’s patients from Canada (7 μg g^{-1}) [54].

There is considerable controversy, however, as reported concentrations have ranged over several orders of magnitude and some groups have not been able to detect BMAA in many previously reported species of cyanobacteria or other samples (e.g. [57–60]). These confusing results are exacerbated by the lack of reference materials and fully validated methods.

1.6 Current Methods of BMAA Detection and Their Problems

There are three major concerns with the analysis of BMAA: (a) isomers and isobaric compounds could be misidentified as BMAA; (b) false negatives could be caused by factors such as matrix effects; and (c) false positives could result from formation of interfering artefacts caused by derivatization chemistry. There is thus a need for a sensitive method to detect BMAA with the highest degree of selectivity in separation with the goal of resolving these three issues.

To date three methods have been employed for BMAA analyses. The first method employs reversed phase liquid chromatography (RPLC) with fluorescence detection after derivatization with 6-aminoquinolyl-*N*-hydrosysuccinimidyl carbamate (AQC) [61–63] or with dansyl chloride [64]. Such a method often suffers from low specificity as many compounds in a sample matrix can be derivatized and it can be difficult to completely separate all components in a sample extract and identify them by retention time alone. It has become apparent that this method drastically overestimates concentrations of BMAA in matrix samples and concerns over misidentification have been expressed [57,65,66]. The second method, RPLC with tandem mass spectrometry (MS/MS) after derivatization, was developed in response to these original concerns by providing more selectivity [61,62,64,67,68]. Unfortunately this approach still has the potential for artefact formation and interferences if there is inadequate chromatographic separation prior to MS. The third approach, hydrophilic interaction liquid chromatography (HILIC)-MS/MS, offers the ability for direct analyses without derivatization, while avoiding the potential of artefacts arising from derivatization [57].

Derivatization has the advantages of shifting BMAA and its isomers to a higher molecular weight range less impacted by chemical background and increasing retention on RPLC columns. However, the derivatization methods that used AQC [61–63] and dansylation chloride [64] rely on reactions with primary and secondary amines that are widespread in biological samples, so gains in selectivity are limited. A trend has emerged from the literature on BMAA analysis in cyanobacteria with positive findings reported using RPLC-MS/MS after derivatization and most negative findings reported by HILIC-MS/MS [58]. To date, it is still unclear whether these discrepancies in analytical results are due to false negatives by methods without derivatization, false positives by methods using derivatization, or differences in sampling or culturing conditions of algae [58].

In general, limits of detection reported for these different methods have varied as much between reports on the same technique as between techniques. HILIC methods have reported LODs between 90 and 600 ng g^{-1} dry algae [63,69] and 150 ng g^{-1} in freeze-dried shellfish tissue (about 45 ng g^{-1} wet) [69]. Limits of detection for AQC derivatization methods have ranged between 80 and 100 ng g^{-1} dry algae [61,63] and 10 ng g^{-1} in wet shellfish [62]. A similar LOD of 16 ng g^{-1} wet mussel tissue was also reported using dansyl chloride derivatization [64].

A major concern with any MS-based method is the possibility of chemical interference from analyte isomers that might be present in samples. Isomers are often difficult to distinguish by MS/MS and unless high resolution MS is used, isobaric compounds can also cause confusion. Analyses utilizing RPLC-MS/MS have reported interference due to 2,4-diaminobutanoic acid (2,4-DAB) and *N*-(2-aminoethyl)glycine (AEG) co-eluting with

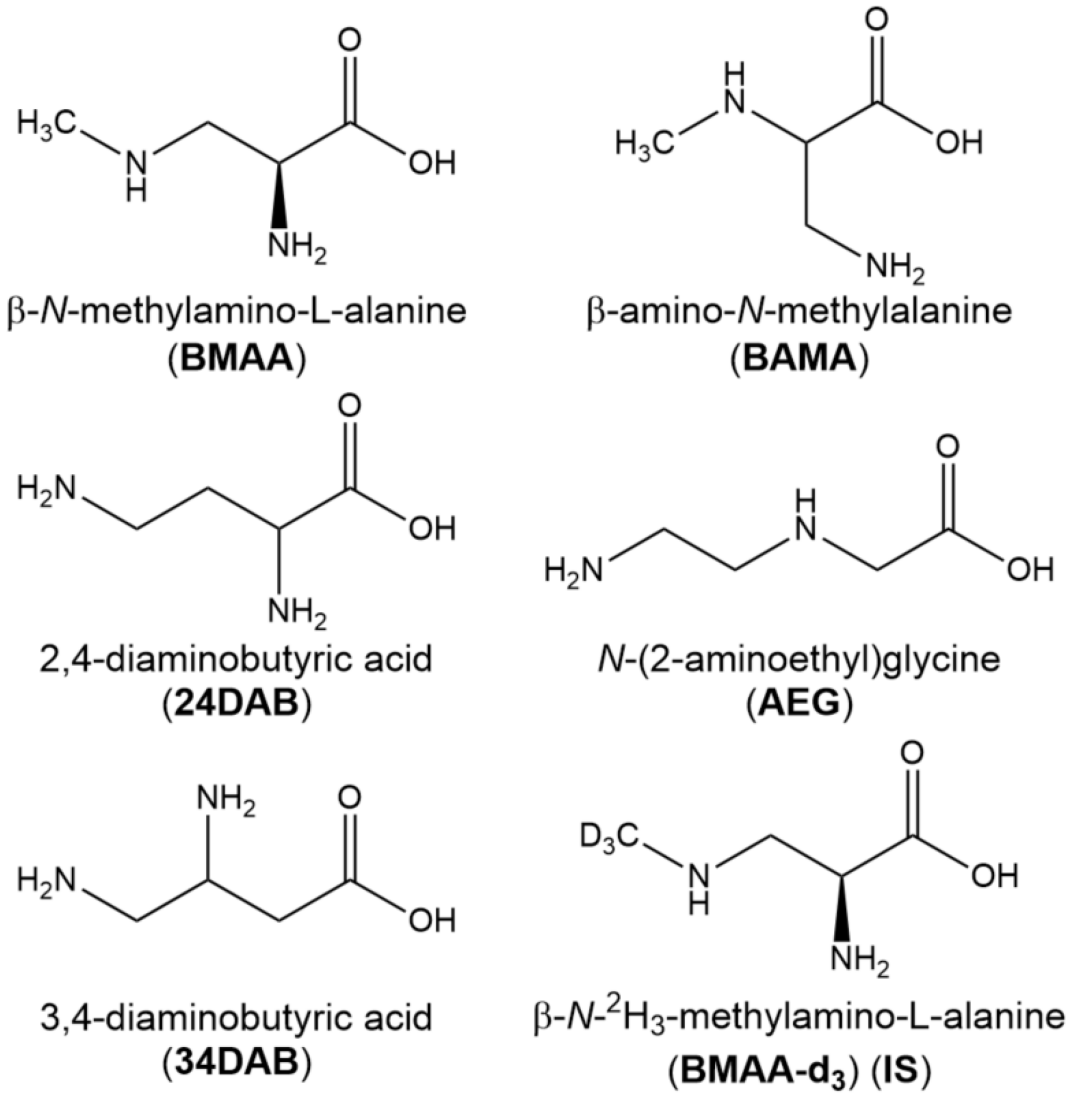

Figure 1.2: Chemical structures of BMAA, its isomers and the internal standard used.

BMAA. HILIC separations have observed similar interference from β-amino-*N*-methylalanine (BAMA) [60,62]. Of the seven isomers previously proposed as having a risk of interfering with BMAA analysis [61], only AEG, 2,4-DAB and BAMA (Figure 1.2) have been investigated due to lack of availability of chemical standards for the others [61,63,70]. All three of the isomers investigated to date have been reported in shellfish [61,69].

Recent reports of BMAA detection in shellfish have been more consistent than in cyanobacteria, and independent of analytical technique. Independent methods, all reporting validation data, have reported widespread BMAA detection in mussels at levels ranging from 0.02 to 0.9 μg g^{-1} wet [62], 0.3 to 1.6 μg g^{-1} wet [64], and 3 to 14 μg g^{-1} dry (about 1 to 4 μg g^{-1} wet) [69].

1.7 Thesis Project Objective

The objective of this thesis project was to help settle the "BMAA controversy" by developing two novel complementary methods for the detection of BMAA and its isomers, both of which should provide very sensitive and selective detection of BMAA free from interference. These methods could then be used in the production of a certified reference material (CRM) at the National Research Council so that others may evaluate the accuracy of their in-house methods. The two methods of separation that will be investigated in this study are HILIC coupled with differential mobility spectrometry and tandem mass spectrometry (HILIC-DMS-MS/MS) and capillary electrophoresis coupled with tandem mass spectrometry (CE-MS/MS).

1.8 Prospective Method: Differential Mobility Spectrometry

1.8.1 History and Potential Application to BMAA Analysis

DMS technology was first developed by the USSR as a means for on-site explosive detection. After over a decade of development in secrecy, the first English-language paper was published in 1993 [71]. It would be another three years before its potential was realized when a mining safety company proposed DMS for portable air quality analysis [72]. This device was developed further by a team led by Dr. Guevremont at the National Research

Council of Canada. They became the first group to interface DMS with ESI/MS in order to create a powerful new tool suited for biological and environmental analyses [73]. Dr. Guevremont later founded Ionalytics Corporation which produced the Selectra; a DMS unit designed to couple with MS. Since 2003, Selectra and similar devices have seen a steady increase in publications throughout many fields from pharmaceutical applications to LC/MS systems [73].

DMS was selected as it offers a separation mechanism that is orthogonal to both LC and MS and can operate in series with LC in a multidimensional LC-DMS-MS configuration. Methods with the highest degree of confidence in results of BMAA analysis can be achieved by applying at least two orthogonal methods [63,65]. While DMS has not yet been applied to BMAA detection, it offers potential for separating the various isomers and for reducing ESI background. This enhancement in selectivity from DMS has been shown to have a significant positive impact on the quantitative performance of LC-MS methods [74–78].

1.8.2 Theory

The theory of DMS is quite similar to that of ion mobility spectrometry, in which charged particles suspended in a gas are separated by a uniform electric field. The mobility of a charged particle can be described as being linearly dependent on the strength of the applied electric field (E). Ions with different sizes and shapes will accelerate differently under the same field strength and suspension media. Therefore, a mobility constant (K_0) that is

independent of electric field must be introduced to complete the mathematical model for drift velocity (V_d).

$$v_d = K_0 E$$

Any changes in temperature or gas composition will have a predictable effect on the mobility constant. Another constraint for this model is that the field strength must remain relatively low (E < 1000 V/cm) [71]. Under the influence of high electric fields (e.g., 5000 V/cm), the ion mobility constant becomes dependent on field strength and a non-directly proportional ion drift velocity is observed [71]. In high electric fields the ion mobility constant ($K_h(E)$) can be modeled with the following equation:

$$K_h(E) = K_0(1 + f(E/N))$$

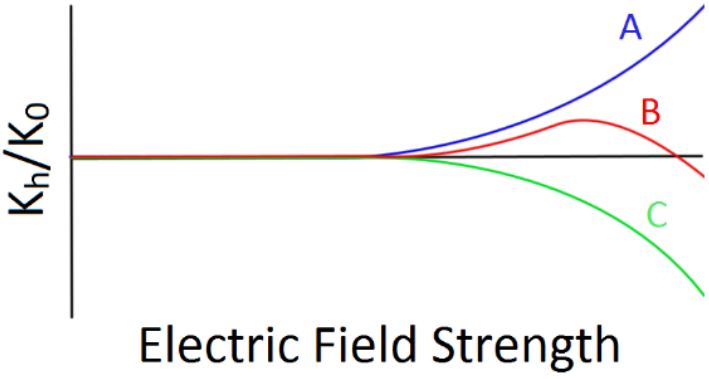

Figure 1.3: Three types of functional dependence of ion mobility on the electric field. Type A ions increase mobility with electric fields, type C ions see reduced mobility, and type B ion start out like type A ions but begin to behave like type C in even higher fields.

The electric field strength at which the mobility constant deviates from its K_0 value depends on the thermal energy of the system. If the energy gain from the electric field is small in comparison to the thermal energy input, then K is constant and dependent on the properties of the media. As the electric field is increased, the energy input on the ion becomes more significant and a deviation is observed. This is because the ion now has enough energy to affect properties of the media it is in, making it a function of its own propagation [79,80]. The field dependent part of the ion mobility function (*f(E/N)*) is referred to as the alpha function and is equivalent to the relative deviation from K_0. As indicated it is dependent on both the electric field and gas number density [80]. Alpha functions can be positive or negative but are never equal to exactly 0. Values corresponding to 30% deviation from K_0 have been reported [72].

When a plot of the ratio of K_h/K_0 versus electric field strength is created for a particular ion, it falls into one of three categories (Figure 1.3). *Type A* ions have a positive alpha function and thus have a higher mobility in strong electric fields than the linear model predicts [80]. *Type C* ions have a negative function and thus have a lower mobility constant in high electric fields [80]. *Type B* ions initially behave as Type *A ions*, but later see a decrease in mobility constant in a similar fashion as *Type C* ions [80]. The change in mobility is dependent on the size and rigidity of the ion as well as its interaction with the gas in which it's suspended [79,81]. It is this change in mobility constant that is the basis for the development of DMS technology. High field strength mobility is compound dependent. This means ions can be separated based on the difference in mobility observed at different field strengths.

A DMS device can be thought of as a system of two planar parallel plates on which a voltage can be applied to generate an electric field (Figure 1.4). A carrier gas with the ions of interest is allowed to flow between the two plates at a constant speed. The bottom plate is kept at a ground potential while the upper plate has an asymmetric waveform (*V(t)*) applied to it. This asymmetric waveform consists of a high field (E_{high}) portion for a duration of t_0 and a low field (E_{low}) portion of opposite polarity for a duration of t_1. The waveform is synthesized in such a way that the integral of the voltage time products is zero.

$$0 = E_{high}t_{high} + E_{low}t_{low}$$

In earlier works, E_{high} was referred to as the dispersion voltage (DV) or separation voltage (SV) [80]. However, DV and SV have more recently been used to describe the entire waveform. In the hypothetical set up displayed (Figure 1.4), E_{high} is four times that of E_{low},

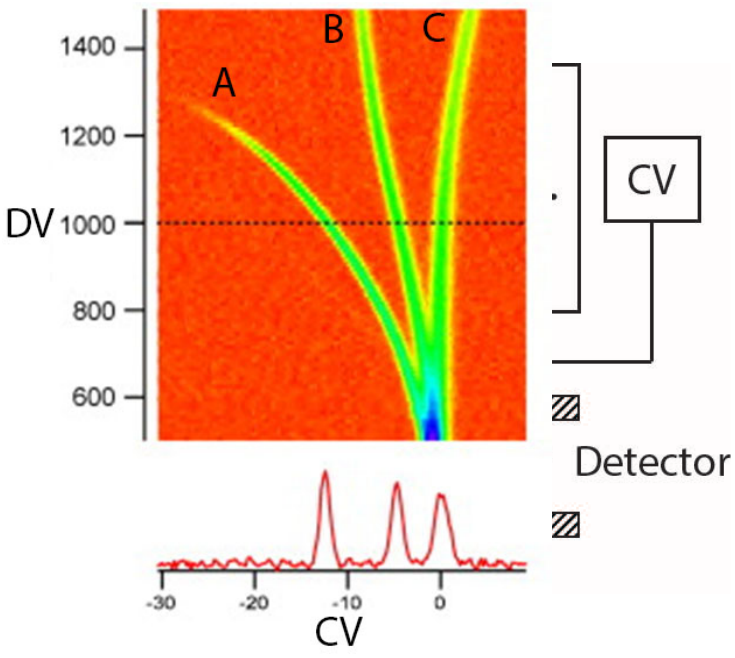

Figure 1.5: Dispersion plots showing all three types of ion behavior. The CV scan represents a cross-section of the dispersion plot at a DV of 1000. This image was adapted from Schneider *et al.* (2010) [79].

Distance is not to scale.

so t_{low} is four times longer than t_{high}. Under the high field strength an ion will be displaced by $K_h(E_{high})E_{high}t_{high}$ while the lower field produces a displacement of $K_0E_{low}t_{low}$. Ions that have an alpha function of zero will experience no net displacement as the displacement caused by the high field will be cancelled by the displacement under the low field. Ions with a positive alpha function (K_h larger than K_0) will gain a net displacement away from the upper plate if they are positively charged or towards the upper plate if they are negative [79,80]. The opposite is true for ions with a negative alpha function. After enough cycles, ions experiencing a displacement will collide with one of the plates and be lost.

To focus a particular ion into a detector, a constant correction or compensation voltage (CV) is applied between the two plates. This shifts the trajectory of the desired ion so that it passes between the two plates to a detector [79]. Under the same conditions, ions with a different alpha function will be lost. In this way DMS acts as an ion filter, allowing ions of interest through and eliminating background chemical noise. In principle, this should increase the signal-to-noise ratios and improve detection limits.

Unfortunately the CV required for a particular ion is quite unpredictable as it is dependent on the alpha function and the temperature and pressure of the carrier gas. There have been several papers published in which the CV values were calculated theoretically [81]. However, these values were only approximate. While prediction is still feasible, more work needs to be done. The physics of ions in high fields are simply not as well developed as with low fields [81]. A CV can be obtained experimentally by means of scanning a CV range to yield what is known as CV spectrum (Figure 1.5) [79]. CV spectra can also be collected and plotted topographically as a function of DV which is equivalent to mapping the alpha function (Figure 1.5) [79]. This is known as a dispersion plot.

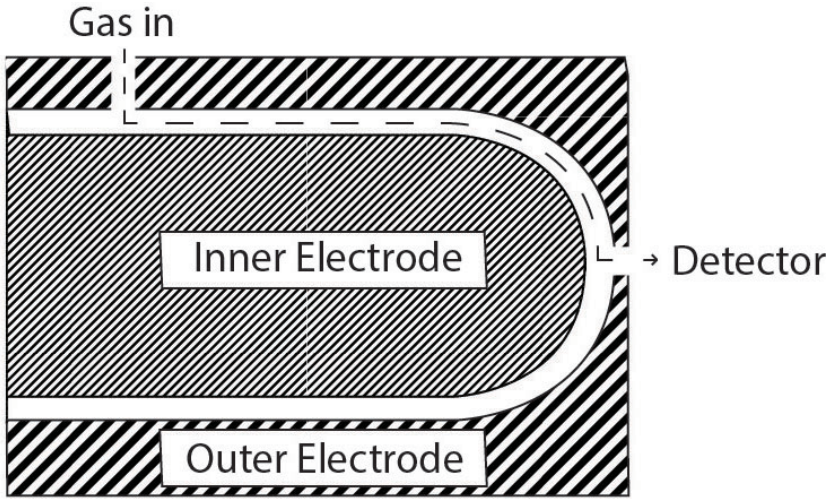

Figure 1.6: Cross-section of a cylindrical FAIMS device. Ions are introduced with the gas, separated, and concentrated toward the detector.

1.8.3 Analyzer Geometries

Currently, planar and cylindrical/dome differential mobility devices are the two most commonly used design. The planar design can be thought of as the example device used to describe the basic theory. The cylinder/dome design can be visualized as two separate metal cylinders with domed ends, one small enough to fit within the other while still leaving room for a gap (Figure 1.6). The carrier gas is allowed to flow through the gap as the DV waveform is applied to the inner electrode while the outer is kept at ground state [72]. Ions are separated in the same way as the planar device, concentrated, and then exit through the center of the dome. Though not abundantly intuitive or consistent, modern literature commonly refers to the planar geometry as DMS while the cylindrical setup is referred to as field-asymmetric waveform ion mobility spectrometry (FAIMS).

Different analyzer geometries are better suited for different applications. One of the key differences is the potential advantage of ion focusing in FAIMS devices. Unlike DMS,

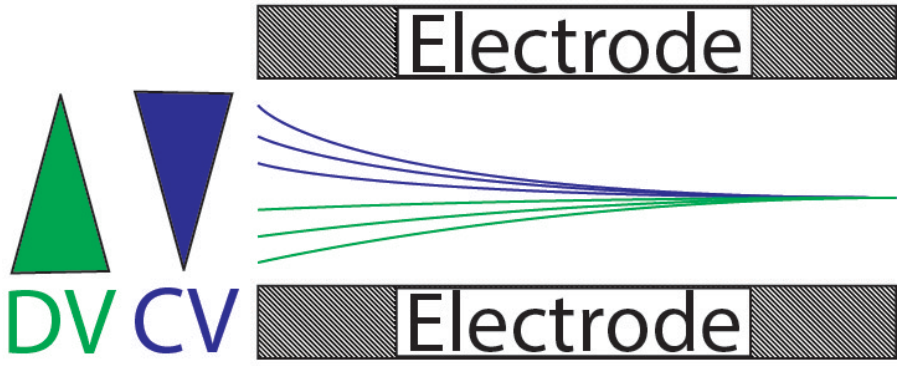

Figure 1.7: Theoretical model of ion focusing in a FAIMS device. The paths of six identical ions starting at different radial positions have been traced. Ions below the focusing plane are pushed up by the larger migration due to DV while ions above the focusing plane are pushed down by the larger migration due to CV.

reversing the polarity of the DV waveform on a FAIMS instrument has a profound effect on the observed CV spectrum. This is because the electric field generated by the curved electrode is actually stronger when it is closer to the smaller inner electrode then around the larger outer electrode. More highly curved electrodes produce more variable electric fields with greater focusing power [79]. Ions located at different radial positions experience different electric field strength in regards to both DV and CV [72,79]. The trajectory of the ion will be affected depending on its polarity and alpha function. This trajectory will eventually become level when the ion reaches a radial position where the migration due to the DV is equal to the counter migration due to the CV. Any displacement from this optimal radial position will result in the ion being pushed back into the plane by the now stronger CV or DV migration (Figure 1.7). Therefore, ions of a particular type will either be focused radially within the detector or defocused and lost via electrode collision, depending on the compatibility of their alpha function under the current conditions. If a particular ion of interest is being defocused, simply switching the DV polarity will result in ion focusing

[80]. Unfortunately this also means that two scans must be completed in order to get a complete CV spectrum. A DMS setup will only require one scan to collect an entire CV spectrum.

As ion transmission depends on alpha function and not the polarity of the ion itself, FAIMS instruments have a total of four modes. Two modes for positive ions with either a positive alpha function (P1) or a negative alpha function (P2) and two more modes for negative ions with positive (N1) and negative (N2) alpha functions [80].

Because focusing requires a variable CV that counteracts the DV, ions that migrate with a CV around zero cannot be focused and see a reduction in sensitivity [79]. This means that the focusing advantage the FAIMS offers is not universal to all ions under any condition. Despite this limitation, the possibility for ion focusing has made FAIMS the most common geometry for coupling with a mass spectrometer [79].

Recent work has suggested that the focusing properties of the FAIMS device are actually a hindrance. The varying strengths of electric fields required to produce the focusing effect also means that CV is less specific. This then reduces the resolving power [79]. Electrodes with less curvature will have higher resolving power but sacrifice focusing power. The best resolution is achieved with completely flat plates in a DMS setup. Focusing also requires ions to spend a longer time in the instrument and as a consequence will suffer greater ion loss due to diffusion [82].

When coupled with a mass spectrometer this residence time becomes an even larger problem. If multiple reaction ion monitoring mode is desired, the 100 ms or longer required switching time for the FAIMS instrument is significantly larger than the switching time on

a quadrupole mass spectrometer [79]. This can create cross talk between channels and reduce the sample rate of peaks if coupled with liquid chromatography separation.

DMS is arguably more convenient for research and troubleshooting. DMS allows for ion transmission when turned off with minimal losses. This is sometimes referred to as transparent mode [79]. This is useful in situations where ion transmission without discrimination is desired (e.g., method development and optimization). This is not possible with FAIMS as switching the device off will result in up to 93% loss of ions [79].

Other geometric properties to consider are the length and height of the electrodes. In either the DMS or FAIMS set up, longer electrodes increase resolving power at the cost of higher residence times and lower ion transmission. Gap optimization is more complicated. Larger gaps increase the total volume of a system and thus the residence time of the ions. If the device is laboratory-based and not limited by power constraints, DMS performance can be improved by increasing the electrode gap which allows for higher voltages and better transmission due to fewer wall collisions [72,79].

1.8.4 Chemical Effects on DMS Separations

Separation can usually be achieved under normal conditions with nitrogen as the carrier gas. If the ions of interest do not resolve, a chemical modifier can be added to the bath gas to enhance separation. Two different models have been developed to help explain this phenomenon better: the clustering model and the ridged sphere scattering model.

The clustering model dictates that under low electric field conditions, solvent molecules will rapidly form clusters around ions. Clustering would reduce the mobility of an ion and be observed experimentally as a lower K_0. The size of a molecule, steric hindrance around

the charge/functional groups, and the properties of the surrounding gas phase molecules all affect the clustering extent. The thermal energy input during the high-portion of the DV waveform would be enough to cause rapid declustering of the ion. This reduction in size would cause a sharp increase in ion mobility. The nature of the waveform would cause ions to dynamically switch back and forth between states millions of times a second. This field dependent shift in ion size amplifies the mobility differences, which are then reflected in a more positive alpha function for all ions and shift in CV spectrum. Negative deviations in the alpha function are not explained by this clustering/declustering model.

Sometimes the high field strength may not be enough to decluster the analyte ion. In this case several peaks on the CV spectrum corresponding to different cluster states may be observed. These clusters have extremely low bond energies and immediately break up in an MS vacuum, making peak identification easy. If the system is left unchanged and quantitation is desired, the peaks may be integrated separately and summed to obtain an accurate calibration curve.

Unfortunately, this model is highly complex which makes it difficult to predict how an ion will behave. The most recent computational model found in the literature was by Campbell *et al.* (2014) [81] who used the Gaussian 09 software package to study cluster formation around isomeric cations. Cluster energies were calculated by first computing possible cluster formations, selecting the clusters with lowest baseline energy, and subtracting the sum of the individual product total energies. Through studying the effects of steric hindrance and shielding, his group was able to explain how the degree of ion molecule clustering does not follow a trend predicted by the strength of dipole moments [81].

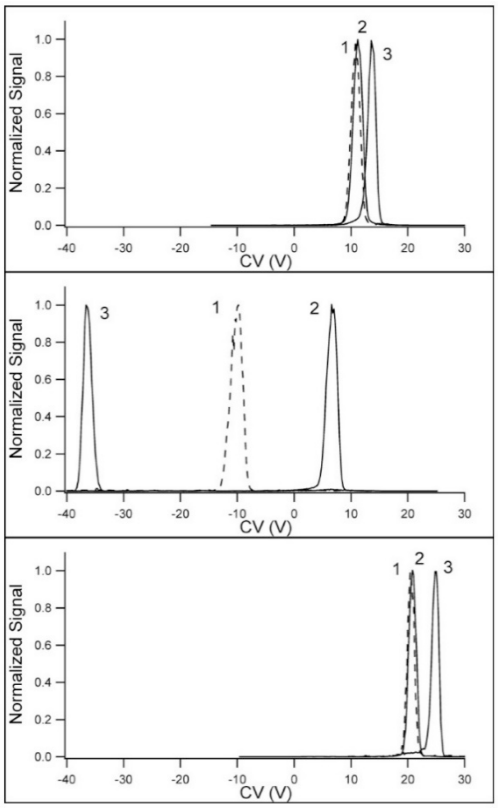

Figure 1.8: Effects of carrier gas modifiers. The CV specta show the same three of the 70 ions tested under different gas modifiers. The top spectrum was collected using dry nitrogen as the carrier gas. The middle spectrum has 1.5% isopropanol added to the gas flow. The bottom spectrum is comprised of 44% helium and 56% nitrogen. Shifts in CV migration are explained by the models described. This figure was modified from Schneider *et al.* (2010) [82].

In the absence of polar gases or chemical modifiers, the rigid sphere scattering model becomes dominant. All particles are treated like rigid spheres and the collisions with another particle are simulated as they move. The nature of these collisions and the law of diminishing returns prevent the velocity to increase linearly with field strength. This decrease in mobility in high field strengths is represented by a negative alpha function. Rigid sphere scattering is much easier to model and has been used to make very accurate computational predictions.

These orthogonal models can be used together to explain the complex alpha characteristics of individual ions. When long-range attractive interactions dominate the system, such as ion-dipole interactions, the ion mobility will increase with the field. If a less polar gas is used in a system, hard sphere interactions will start to decrease ion mobility with the field. This was demonstrated experimentally by Schneider *et al.* (2010) [82] who studied shifts in the CV spectrum of 70 different compounds as the control carrier gas was modified with 44% helium or 1.5% isopropanol (Figure 1.8). Unfortunately, only relative responses were reported and never discussed so the cost of increased separation remains unclear.

These two models also predict that there are no true type A ions. All ions will eventually see a reduction in mobility due to the rigid sphere scattering by overpowering any clustering affects at extremely high field strengths. This has led some review articles to refer to only two ion types instead of the three used in this work. One could argue that as ions may deteriorate in these extreme conditions before the effect is observed, the three ion classifications are still valid.

Although only isopropanol has been described, there are many other modifiers and gases that have been used. When selecting a modifier it is important to note that gas phase ion chemistry still applies. If the modifier has greater gas phase basicity then the analyte ion, a charge transfer can occur. This will result in reduction or loss of signal. The same is true with modifiers that have greater gas phase acidity and negative ions. As proton affinities for many chemical species are known, this effect can theoretically be used to further reduce chemical noise within a system [79]. Unfortunately, no literature in which this theory was practically applied could be found.

The amount of chemical modifier present need be considered as well. The presence of trace

level gases and changes in humidity have been shown to affect CV spectra and sensitivity between runs [80]. Guevremont *et al.* (2004) [83] were the first to recognize that trace amounts (1000 ppm) of gas additives could improve separation. For the curved FAIMS geometry, high concentrations of solvents are problematic as clustering/declustering appears to become a function of radial position [80]. Purves *et al*. (2014) [80] showed that optimal separation and sensitivity of small organic molecules in a FAIMS device could be achieved by using as little as 0.2% acetonitrile modifier (Figure 1.9). As little as 0.02% acetonitrile was enough to cause a dramatic negative shift in the CV spectrum which in turn dramatically improved the focusing power (100 fold). It can also be seen that isolation of different ions can be achieved by changing the percent modifier composition. Trace level modifiers work particularly well for small ion < 700 *m/z* separation. Conveniently, these types of molecules are most susceptible to contamination [80].

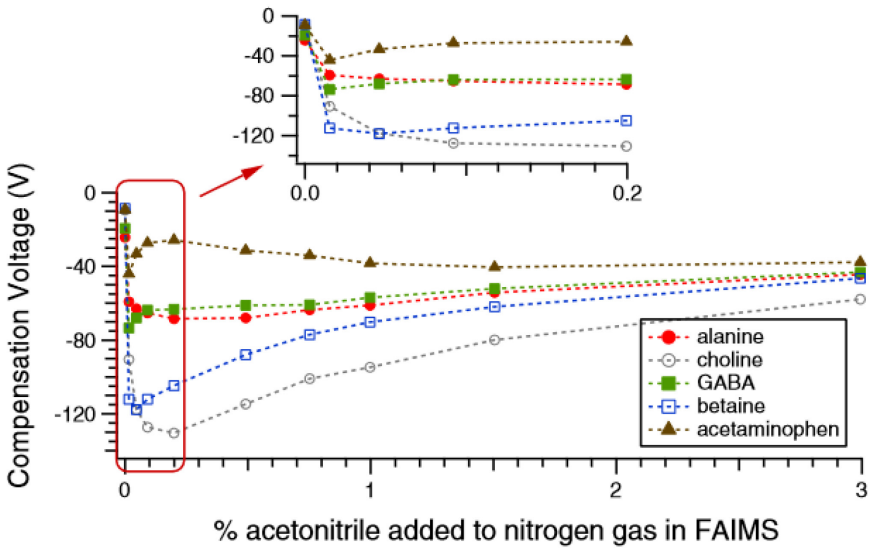

Figure 1.9: CV of small organic ions (<700 *m/z*) as a function of percent acetonitrile composition in nitrogen carrier gas. This figure was adapted from Purves *et al*. (2014) [80].

1.9 Prospective Method: Capillary Electrophoresis

1.9.1 History

Electrophoresis as an analytical technique was first described by Arne Tiselius in 1931 [84] based on principals described in the early 19th century. His work was expanded in the 1940s and 50s with the development of zone electrophoresis that employed supporting media such as filter paper or gels to enhance separations [84]. While zone electrophoresis is still sufficient for routine analyses in many laboratories, its resolution is still limited by band broadening due to joule heating [85]. This problem was ultimately solved by Hjertén (1967) by conducting separations in a narrow (300 µm I.D.) capillary that quickly dissipated thermal energy (this was later termed capillary electrophoresis or CE) [84,85]. The potential for free-zone capillary electrophoresis without a supporting gel was realised by Virtanen (1974) [86], who separated out alkali metal ions and described the importance of electro-osmotic flow [84]. Detection was initially limited to UV or fluorescence, however in 1987 Smith *et al.* [87] developed a method to couple CE with mass spectrometry.

CE has since developed into a powerful tool applied to food analyses, forensic, pharmaceuticals, proteomics, environmental studies, and biomarker discovery [88]. It offers a number of potential advantages for BMAA resolution, including very high resolving power, a novel separation mechanism complementary to that of LC, and an excellent ability to separate isomers and chiral molecules [89]. Though there have been many variations of CE separations developed for a wide range of analytes with particular

properties, the separation of charged analytes is commonly done with capillary zone electrophoresis (CZE) [90], which we will mainly consider here.

1.9.2 Theory

Similar to DMS, CE utilizes differences in ion mobilities in an electric field to achieve separations, however, the analytes are in the aqueous phase making the instrumentation setup less complex (Figure 1.10). A capillary is filled with an electrolyte solution (referred to as background electrolyte or BGE) and the ends are placed into two BGE reservoirs. Some BGEs are designed to have buffering characteristics and are referred to as running buffers for distinction. A sample plug can be introduced by temporarily inserting the capillary inlet into a sample vial and applying pressure for a short time (1-3 seconds). After returning the inlet to a buffer reservoir, a high voltage (10-30 kV) is applied across the capillary to generate an electric field. Analytes migrate towards or away from the cathode at a rate dependent on the electric field strength and the analyte's charge, size and shape, which affect its interaction with the BGE. Analytes that pass through the detector window near the outlet end of the capillary are recorded in an electropherogram and separated compounds appear as peaks with different migration times.

In addition to analyte mobility, migration time is effected by the electroosmotic flow (EOF) of the BGE inside the capillary. The most common type of capillary is a bare fused-silica capillary with walls that are covered with free silanol groups (Si-OH). When a BGE above pH 4 is used, the silanol groups are predominantly ionized to negatively charged silanoate groups ($Si\text{-}O^-$) [91]. Cations within the BGE are drawn to the silanoate groups, forming

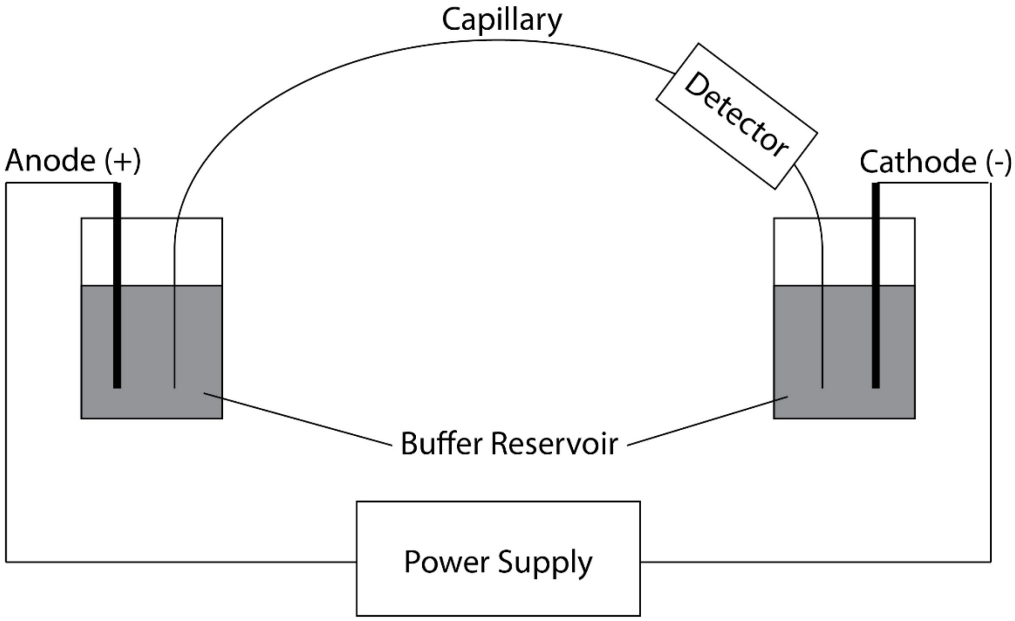

Figure 1.10: Model of standard capillary electrophoresis apparatus setup.

several layers of cations covering the interior wall [92]. While the innermost layer of cations is bound too tightly to be considered mobile, the outer cationic layer will migrate toward the cathode in the presence of an electric field, pulling the BGE solution and analytes with it. In this way, analytes migrating away from the cathode can still be detected provided their mobility is less than that of the EOF. EOF is dependent on the electric field strength and the charge density on the capillary wall. Experimentally, the electroosmotic mobility can be determined by measuring the migration time of a neutral analyte. It should be noted that EOF offers an alternative form of injection known as electrokinetic injection. This is similar to the hydrostatic injections previously described but use the combined EOF and analyte migration to draw in a sample plug. This form of injection tends to be more reproducible but is more biased toward analytes with higher mobilities [93].

1.9.3 Effects of BGE pH on Separation

Buffer pH is the most critical parameter to consider when optimizing a separation, as it directly determines analyte charge [94]. While separation of two interfering compounds can be accomplished by selecting the pKa/isoelectric point of one of the analytes as the buffer pH [94], this does not hold true for more complex matrices, as many other neutral species may be present for a given pH. Most method developments employ a univariate optimization, evaluating separations over a pH range. Other optimization techniques include computational modeling and response surface analyses by means of a central composite design to help reduce the number of "wet" experiments required [94]. Both these methods have drawbacks, as neither method can optimize for complex matrices [94]. Additionally analyte migration order should ideally remain constant during response surfaces optimization [95].

One last consideration is the effect pH has on the EOF. As previously mentioned, surface charge density effects the EOF, which is determined by the surface material and the pH. Surface charge can be modeled using the Henderson–Hasselbalch approximation, as it can be shown that some EOF will be present at 1 pH unit below the pKa of a silanol group (pKa 3.8-5) [91]. At lower pHs the EOF is considered suppressed and analytes' migrations are solely dependent on their electrophoretic mobility.

1.9.4 BGE Composition and Concentration

The primary criteria when selecting a BGE is compatibility with the system detector. This often means low UV absorbance or fluorescence interference but other detectors such as surface enhanced Raman spectroscopy and mass spectrometry can be more restricting [92].

Other than compatibility, BGEs are usually selected for having a buffering range within the target pH. Phosphate and borate buffers are the most commonly selected for CE separations due to meeting these criteria. Other considerations are sometimes made for BGE that can interact with the analyte of interest, potentially increasing the selectivity. For example, borate buffers have been used to form five- and six-membered ring complexes with 1,2-diols and 1,3-diols, respectively [96].

Organic modifiers can be used to reduce sample precipitation inside the capillary. Modifiers like methanol can also increase solution viscosity, while acetonitrile can be used to decrease it. These changes can effect migration times by effecting analyte mobility and EOF. Lastly, organic modifier interactions can alter the degree of ionization of analytes, thus changing migration order and time. Modifiers such as cyclodextrins and proteins can be used to selectively interact with analytes, providing separations based on chirality. Lastly, BGE concentration and organic solvents can be used to change solution conductivity, ionic strength and viscosity. High conductivity/ionic strength results in greater joule heating but can improve on-line pre-concentration or "stacking". Stacking requires an ionic strength mismatch between BGE and sample plug and thus having higher BGE concentrations reduces or eliminates the need for sample dilution [92].

1.9.5 Sample Stacking

One major area of focus is on the improvement of LOD for CE methods. The low capillary I.D. (50-75 μm) required limits the LOD two-fold by reducing sample injection volume and path length for optical detectors [97]. The use of bubble cells and laser induced fluorescence detection have greatly improved sensitivity but can still be orders of

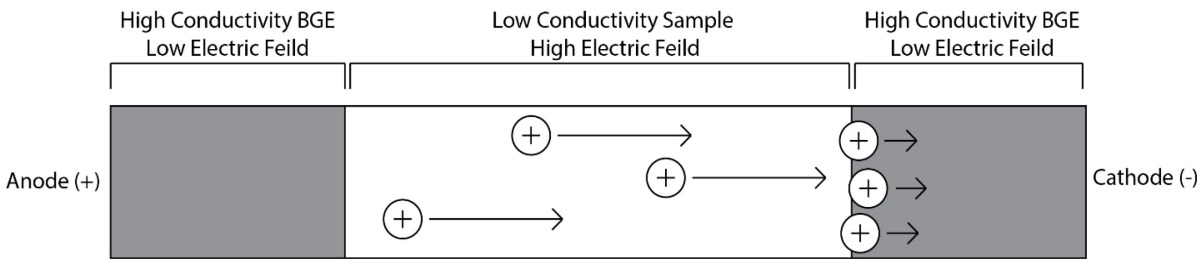

Figure 1.11: Model of conductivity based stacking

magnitude less than HPLC counterparts [97]. Stacking helps to alleviate this problem by increasing the amount of sample that can be loaded.

As previously stated, a sample must be in a solution with lower conductivity than the BGE for basic stacking to occur (Figure 1.11). This ensures that the electric field within the sample plug is greater than that of the BGE. The lower the sample conductivity, the higher the voltage drop is across the sample plug and hence the stronger the electric field that the analytes experience. Analytes within the sample plug will have a higher mobility then those in the BGE. Once analytes reach the concentration boundary, a reduction in mobility is observed, allowing ions still present in the sample plug to catch up or "focus" before proceeding with the separation [98]. As the differences in mobility and efficiency of stacking are directly related to the difference in conductivity, the increase in concentration due to stacking can be modeled with the following equation:

$$C_{stack} = C_{sample} \times \gamma$$

where γ is equal to the field strength in the sample plug divided by field strength in the BGE [99]. Experimental concentration factors may be worse than predicted by this formula due to mixing between the ionic boundaries via diffusion. Mixing can be considerably

higher if differences in EOF between the BGE and sample plug exist [99]. Mixing is the main limiting factor for ionic-based stacking, as larger injection volumes require more time to complete stacking and allow more time for mixing at the ionic boundary. As a consequence, injection volumes are normally limited to 5-10% of total capillary volume [100]. Ten-fold improvements in sensitivity are normally reported with this technique [97–99].

Even larger volumes can be injected by pushing the sample plug out of the capillary using reverse pressure or EOF after the initial stacking event, followed by another injection and stacking procedure. Sample plug ejections using reverse EOF is preferred, as a change in capillary resistance can be used to accurately measure the volume of matrix still present [97]. Ejection of the sample plug at the end of the stacking procedure is beneficial to reduce mismatches in EOF [97]. This method is not commonly practiced do to difficulties with replication and automation but spectacular 100- to 5000-fold improvements in LOD have been reported [97–99].

One variation to ionic strength based stacking employs an isotachophoretic mechanism. Here, the sample plug is situated behind a plug of low mobility, high conductivity leading electrolyte and in front of a plug of high mobility, low conductivity tailing electrolyte [97]. Upon the application of an electric field, the tailing electrolyte progresses through the sample plug, thus increasing analyte mobility [97]. Analytes near the front of the plug get caught in the tailing electrolyte and focused [97]. This mechanism requires a very strict range in BGE pH, concentration, and counter-ion in each plug in order to function properly. Isotachophoretic stacking does not see much improvement over the normal ionic strength mediated approach and is not frequently employed [97–99].

If the ionic strength of a sample cannot be reduced, a pre-concentration mechanism known as a pH-mediated stacking can be employed. Following the electrokinetic injection of a sample plug, a plug of strong acid or base is injected [98]. An electrokinetic injection must be used so that BGE counter-ions migrate into the sample plug prior to separation [98]. Upon the application of an electric field, the acid/base titrates the counter-ions present in the sample reducing conductivity [98]. Analyte mobility increases abruptly at the pH gradient front, resulting in a narrow focused band [98]. Up to 100-fold increases in concentration factors have been reported [98].

An alternate form of pH mediated stacking utilizes vast differences in pH between the sample plug and BGE. Analytes that leave the sample plug are reduced and consequently see a loss in mobility [101]. 500-1000 fold improvements in sensitivity have been reported when employing this method [98,101].

Though powerful on their own, combinations of stacking techniques can be used to multiply their effectiveness [102]. One particularly complex combination gave rise to a million-fold increase in sensitivity while still maintaining an efficiency of 350 000 plates [103].

1.9.6 Coupling CE with Mass Spectrometry

Unfortunately the commonly employed UV and fluorescence detectors traditionally used with CE separations are not suitable for the detection of BMAA. Even with stacking, the lack of a chromophore in the structure of BMAA means a very poor response would be expected without some form of derivatization. This was seen in a CE-UV method reported by Baptista *et al*. (2011) [104] who demonstrated the ability to separate BMAA from 2,4-

DAB, however, a LOD of 0.5 mg L^{-1} or 4.2 μM was reported [104]. This LOD is orders of magnitude higher than levels reported in natural sample extracts [58] and it is believed that MS detection may be a solution. In addition to greater sensitivity, mass spectral detection offers a number of advantages for CE analysis of BMAA including structural confirmation, an orthogonal level of selectivity, and the ability to use an isotopically labeled internal standard [105–107].

Isotopically labeled internal standards are particularly useful, as pressure driven injections in CE are notoriously variable, making quantitation by external calibration irreproducible and potentially inaccurate [93]. Factors affecting hydrostatic injection variability include differences between sample viscosities, temperature gradients altering BGE viscosity, local atmospheric pressure/humidity, and incomplete seal between sample vial and capillary. Internal standards correct for differences in injection volume between runs as well as providing an additional level of confidence in peak assignment.

While there have been many methods of coupling CE with MS, the most common approach is via an electrospray ionization source (CE–ESI-MS) [88,108], which will be the focus of this study. ESI is a relatively soft ionization method particularly well-suited for polar organic molecules like peptides and amino acids. Though ESI does solve the problem of getting analytes into the gas phase, it comes with several problems of its own, the largest being completing the circuit for the separatory voltage (10-30 kV) across the capillary while keeping the capillary exit at sufficient potential for proper electrospray (4-7 kV) [88]. This has been solved via two distinct mechanisms, each with advantages and disadvantages.

One approach uses a secondary ESI compatible sheath liquid introduced coaxially at the capillary exit [88,109] (Figure 1.12a). The sheath serves as the buffer reservoir to which the CE system can be grounded and the ESI voltage applied. The sheath is usually delivered at 5-10 μL min^{-1}, making up the majority of the electrospray volume and carrying analytes that migrate out of the capillary exit into the MS [88,109]. The sheath is also responsible for supplying counter ions that would normally be supplied by a buffer reservoir in the traditional setup. This setup is considered the more versatile option but comes at the cost of reduction in S/N due to sample dilution [107].

The alternative approach commonly referred to as the sheathless interface is considered the more sensitive (8-30 fold) approach [105,109]. Sheathless interfaces rely on the EOF within the capillary to make up the entire volume of the electrospray. Circuit completion occurs at the capillary exit, usually through conductive capillary coatings or a permeating wire (Figure 1.12d). Manufacturing these emitters is often complex and hard to reproduce [105–107]. Though still commonly used, many consider this method harder to

implement and the lack of sheath adds a number of restrictions [105–107]. As the BGE makes up the entire electrospray for the sheathless approach, concentrations/ionic strength is normally limited to ~10 mM as background noise and sensitivity are highly dependent on BGE composition [110]. Specific BGEs and/or capillary coatings are also required in order to maintain a high EOF for stable electrospray. While high EOF is feasible for some analytes, this may not be the case with BMAA. Most reports of separation of similar molecules such as peptides and amino acids typically required EOF suppression [111–114]. Furthermore, one study comparing the two approaches in peptide separations found no difference in sensitivity [110]. A sheath flow interface was selected for this study.

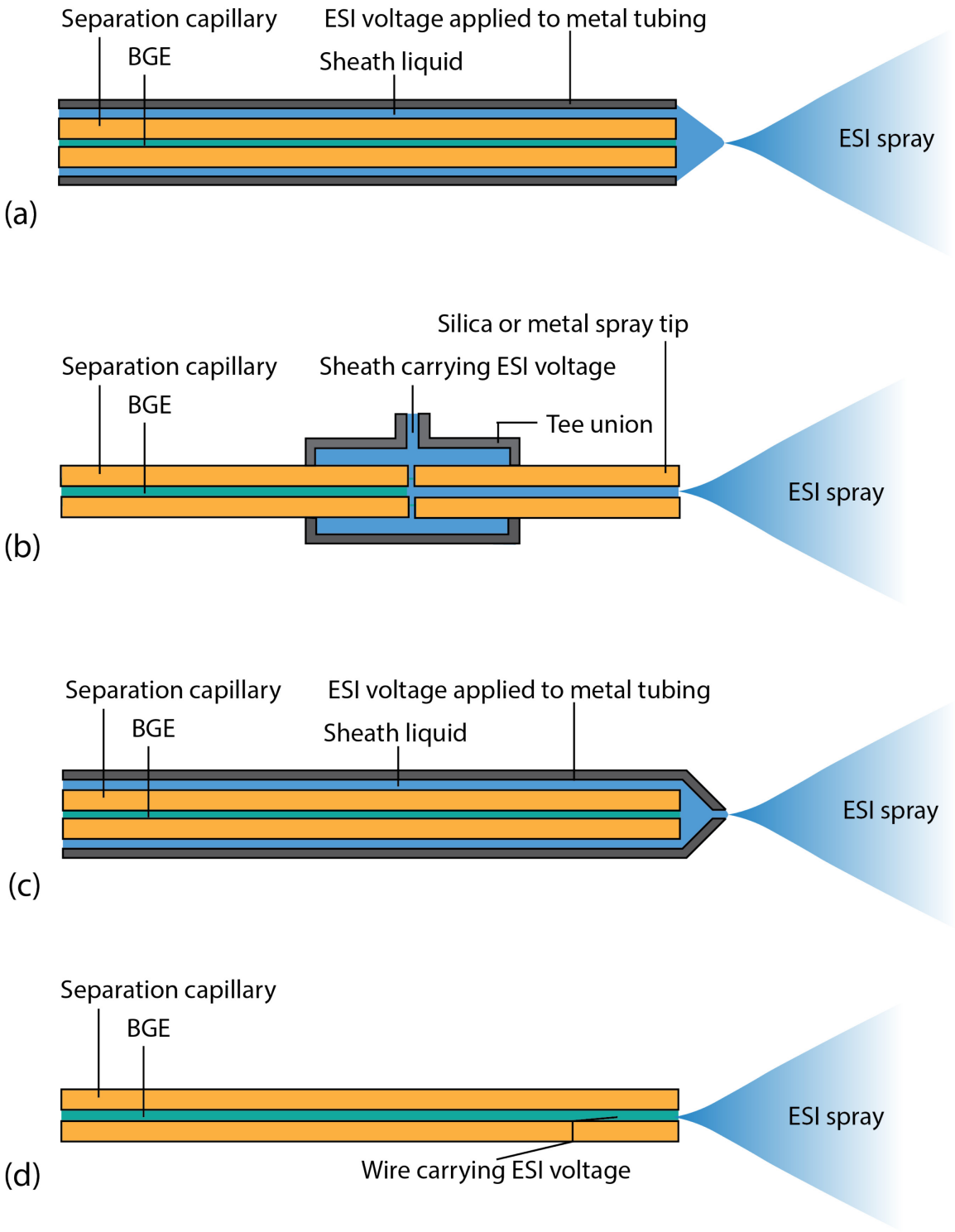

Figure 1.12: Different concepts for CE-ESI interfaces. A typical sheath interface with the ESI voltage applied to the metal nozzle (a), a liquid junction interface with ESI voltage carried via sheath (b), a "junction-at-the-tip" interface (c), and a sheathless interface with ESI voltage delivered via wire (d).

1.9.7 Variations of Sheath-Flow Interfaces

Typical coaxial interfaces require between 2 and 10 μL min^{-1} of sheath-flow [105–107]. As well as analyte dilution, flow-rates this high often require the supply of a nebulizing gas for achieving ESI stability. The high flow rate of a nebulizer gas can result in a negative pressure at the capillary tip, causing peak broadening, reduced migration times and additional sample dilution in the gas phase [105–107]. Most variations of sheath-flow interfaces center on attempting to reduce the flow-rate to less than 1 μL min^{-1} to overcome these effects.

One of the more common approaches is known as the liquid-junction interface (Figure 1.12b). Here the separation capillary is connected to a sprayer tip via tee union. Sheath liquid permeates through the gap between the capillary and sprayer tip, allowing for the completion of both CE and ESI circuits. Negative pressure from the ESI pulls sheath liquid to the emitter tip rather than pneumatic pressure required for the coaxial approach [105–107,109]. This approach comes at the cost of reduced separation efficiencies due to difficulties aligning the capillaries and an increase in dead volume. Dead-volume can be reduced by applying pressure to the liquid junction interface, but implementation requires a precise balancing of pressures [115]. These drawbacks in conjunction with improved coaxial setups mean this approach has been largely abandoned [105–107,109].

Reducing the ESI sprayer orifice diameter can reduce the amount of sheath required for stable ESI. Chen *et al.* (2005) [116,117] were able to use flow rates as low as to 500 nL min^{-1} by tapering the metal tube and capillary of a traditional coaxial setup. An alternative

to capillary etching is the "junction-at-the-tip" approach in which the separation capillary is inserted inside a tapered emitter [118] (Figure 1.12c). Here analytes are mixed with the sheath in a small dead-volume before exiting through the emitter orifice [118]. This method has been shown to operate with sheath flow-rate of 200 nL min^{-1} but suffers from band broadening and irreproducible capillary positioning [118].

Lastly, Dovichi *et al*. (2015) [119] reported a setup similar to the "junction-at-the-tip" interface that used electrokinetically driven sheath flow and an etched capillary (tapered from 350 μm to 15-35 μm) that further reduced dead-volume. Sensitivity was shown to be inversely related to orifice size, but smaller orifices were susceptible to plugging and had a reduced lifetime [119]. Electrokinetic sheath delivery was believed to be more consistent that traditional pumping, and an estimated flow rate of ~50 nL min^{-1} was reported [119]. One drawback of this method is the need for coated capillaries that have limited lifetimes [119].

1.9.8 CE-MS BGE and Sheath Optimization

Although sheath flow interfaces are more versatile, a BGE composed of a volatile electrolyte is still required for compatibility with ESI. For the most part, electrolytes are restricted to formate, acetate or ammonium ions [105–107]. Non-volatile BGE have been used when the EOF was suppressed but frequent system maintenance was required [120–123] and lower S/N by increasing spectral backgrounds was reported [120,123,124]. These effects can be reduced by scheduling MS data collection and using lower concentration BGEs with <60 mM for a phosphate buffer [123]. Unfortunately, much higher concentrations are often required for proper separation and stacking [123].

The ionic composition of the sheath liquid must also be compatible to that of the BGE. As previously described, the sheath acts as a buffer reservoir when there is no EOF, supplying the counter-ions in order to maintain electro-neutrality in the presence of a current [121]. If the counter ions differ from those in the BGE, a secondary separation environment is created at the cathode, which expands over the course of a run [121]. This environment can have vastly different conductivity, ionic strength, molecular interactions, and pH. These differences have been reported to result in suppressed or inverted separations [121]. In some cases, ionic boundaries can be minimized by using sheath counter-ions with a similar pKa to that of the BGE, but this approach should be avoided if possible [121].

In addition to matching the counter-ions in the BGE, sheath composition and flow rate should be optimized. Flow rate is usually kept as low as possible while maintaining system ESI stability and supplying sufficient counter-ions to the CE [107]. Composition, on the other hand, is analyte dependent and optimal conditions are found experimentally [107]. Soga and Heiger (2002) [113] investigated volatile salts in the sheath liquid for the analysis of 19 free amino acids and found that ammonium acetate provided the highest sensitivity for 15 of the amino acids. The same analyte dependent trend was observed when optimizing organic modifier type and concentration [113]. Ultimately methanol/water (50:50) with 5 mM ammonium formate gave the best overall performance [113].

CHAPTER 2: SELECTIVE QUANTITATION OF THE NEUROTOXIN BMAA USING HYDROPHILIC INTERACTION LIQUID CHROMATOGRAPHY-DIFFERENTIAL MOBILITY SPECTROMETRY-TANDEM MASS SPECTROMETRY (HILIC-DMS-MS/MS) [1,2]

2.1 Introduction

As described in Chapter 1, Differential mobility spectrometry (DMS) is a relatively new analytical tool that separates ions in the gas phase at atmospheric pressure based on differences in their mobilities at high and low electric field strength [80,125,126]. DMS was selected as it offers separation mechanism that is orthogonal to both LC and MS and can operate in series with LC in a multidimensional LC-DMS-MS configuration. In the LC-DMS-MS configuration, DMS has the potential to improve the selectivity for an analyte with respect to three important types of interference: isomers, co-eluting matrix compounds and chemical background originating in ESI. This enhancement in selectivity from DMS has been shown to have a significant positive impact on the quantitative performance of LC-MS methods [74–78].

In the current work, the enhancements in method selectivity achieved when DMS is used as a chemical filter between a HILIC separation and MS/MS detection is investigated in

[1] This chapter has been adapted from the publication Analytical and Bioanalytical Chemistry 407, 8397-8409 (2015). DOI: 10.1007/s00216-015-9012-8 titled "Selective Quantitation of the Neurotoxin BMAA Using Hydrophilic Interaction Liquid Chromatography-Differential Mobility Spectrometry-Tandem Mass Spectrometry (HILIC-DMS-MS/MS)". The authors of the publication were Daniel G. Beach, Elliott S. Kerrin, Michael A. Quilliam. The copyright © is held by Her Majesty the Queen in Right of Canada, as represented by the Minister of by the National Research Council of Canada, 2015.

[2] Elliott Kerrin carried out all experiments and data analysis as part of his MSc research. Elliott also contributed to the planning of the study as well as writing and editing of the manuscript. The in house reference material and internal standard were prepared by Sabrina Giddings at the NRC.

order to develop a method with added confidence in BMAA detection and quantitation. This study was driven equally by the general controversy in the field of BMAA analysis as well as by the specific separation problems identified between BMAA and its isomer BAMA using an existing optimized HILIC method in our laboratory. Some technical limitations of the commercial DMS system used are also discussed and simple workarounds are implemented that are widely applicable and that will increase its practical utility in other analytical applications.

2.2 Experimental

2.2.1 Chemicals, Reagents and Samples

HPLC grade acetonitrile, methanol, acetone and 2-propanol were obtained from Caledon (Georgetown, ON, Canada) and formic acid (> 98% ACS grade) from EMD (Gibbstown, NJ, USA). β-*N*-methylamino-L-alanine hydrochloride was obtained from Tocris Bioscience (R&D systems, Minneapolis, MN), β-amino-*N*-methylalanine from Enamine Ltd. (Kyiv, Ukraine), N-(2-aminoethyl)-glycine from TCI America chemicals (Portland, OR), 2,4-diaminobutyric acid dihydrochloride and hydrochloric acid from Sigma Aldrich (Oakville, ON Canada), and 3,4-diaminobutyric acid dihydrochloride from FCH Group (Chernigiv, Ukraine). The internal standard, BMAA-d_3, was synthesized in-house as described previously [62]. The structure and purity of all BMAA isomers was verified by ^{1}H-NMR, which was also used to establish the concentrations of stock solutions of each isomer and the internal standard [127]. Individual and mixed working 5 μM solutions were then prepared in 30/70/0.1 $H_2O/CH_3CN/HCOOH$ (v/v/v) and used for method development.

Samples included four mussel tissue reference materials certified for marine algal toxins (CRM-ASP-MUS, CRM-Zero-Mus, CRM-PSP-Mus and CRM-DSP-Mus) acquired from National Research Council Canada (Halifax, Canada) as well as two of the un-processed mussel tissues used in preparation of these materials (M1 and M2). Other samples included an in-house positive control reference material made from the homogenized tissue of a cycad plant (*Cycas debaoensis*), obtained from Jurassic Plants Nursery (Halfmoon Bay, BC) and a recently developed pilot-scale cyanobacterial reference material containing other cyanotoxins [128].

BMAA extraction was carried out using a modified version of a previously described method [63]. Total protein hydrolysis of 50 mg freeze-dried samples was carried out in 1 mL 6 M HCl at 110 ºC overnight. Samples were then dried under nitrogen at 55°C, spiked with BMAA-d_3, reconstituted in 2.5 mL of 2 mM HCl, and filtered to 0.22 µm (Ultrafree-MC).

2.2.2 LC-DMS-MS/MS Instrumentation

All experiments were carried out on an AB Sciex (Concord, ON) QTRAP 5500 mass spectrometer equipped with a Turbospray® ionization source and an AB Sciex SelexION differential mobility spectrometer. Mass spectrometer settings included a spray voltage of + 4000 V, dispersion voltage of 140 V, entrance potential of 10 V, exit potential of 13 V, curtain gas of 20 psi, collision gas of 5 psi, desolvation gases of 45 psi (GS1) and 50 psi (GS2), and spray temperature of 400 °C.

Liquid chromatography was carried out as described previously [63] using a 5 µm TSKgel Amide-80 column (25 cm x 2 mm ID) (Tosoh, Grove City, OH) held at 40 °C and a mobile phase of 50 mM formic acid in both water (A) and 95 % acetonitrile (B). A linear gradient from 10 to 35% A over 15 min was followed by a 6 min isocratic period, a one minute increase to 45 % A and an additional 8 minute isocratic period. The column was then flushed by decreasing A to 10% for 5 min and re-equilibrating at 90% A for 10 min.

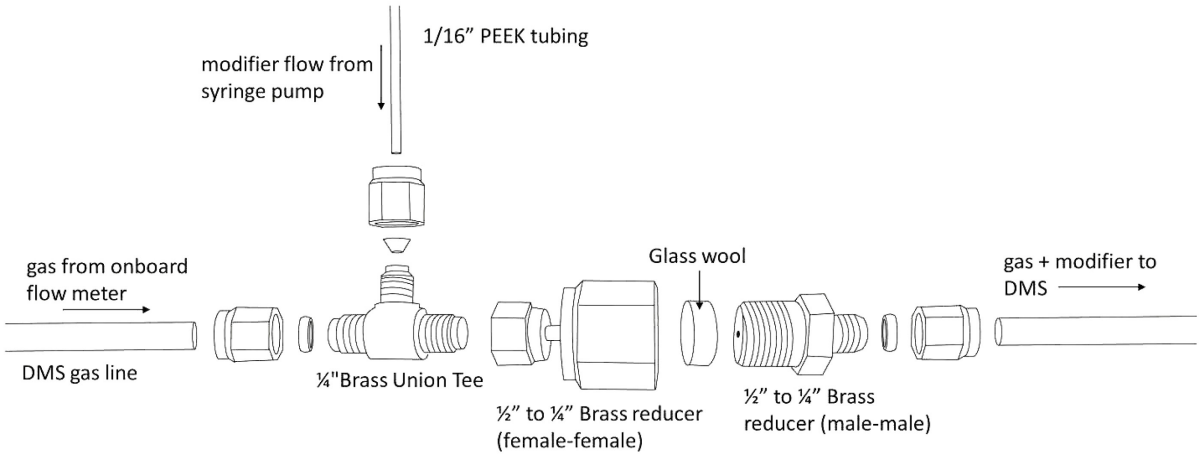

Figure 2.1: Modification of DMS to allow for external metering of carrier gas modifier solvent

The DMS gas modifier delivery system was modified by introducing an externally metered flow of solvent into the DMS carrier gas as shown in Figure 2.1. The DMS gas line was cut after the gas out line from the onboard flow regulator and a 1/8″ Swagelok tee was used to deliver the modifier to the gas stream via PEEK tubing inserted at the perpendicular position making contact with the back wall of the tee. Initially observed signal instability was corrected by introducing a small mixing chamber loosely filled with glass wool in-line after the tee. An Agilent 1200 isocratic LC pump, a Harvard PHD Ultra syringe pump and an ISCO SFC-500 microflow pump were all successfully used to deliver modifier flow.

DMS method development was performed by infusing ~5 μM solutions at 10 μL min^{-1} into a 340 μL min^{-1} flow of 50 mM formic acid in 70% acetonitrile (representing the elution conditions of BMAA off the HILIC column) by ESI-DMS-MS(/MS) using full scan, product ion and SRM scan modes to monitor BMAA isomer separation during compensation voltage scans. Optimized DMS settings included a separation voltage of 2600 V, carrier gas modifier of 0.35% acetonitrile, DMS temperature of 150 °C and a DMS offset of -3 V. Product ion spectra in Figure 2.2 were acquired in ESI-DMS-MS/MS mode by operating the DMS at the fixed CV maximum of each analyte and ramping the collision energy from 5 V to 50 V.

The HILIC, SRM and DMS parameters used for identification and quantitation of BMAA and its isomers by LC-DMS-MS/MS are shown in Table 2.1. For sample screening and isomer identification, scheduled SRM scan mode was used with acquisition windows centered at the retention times of each analyte ± 45 sec. A targeted method monitoring only transitions for BMAA and the internal standard BMAA-d_3 was used for BMAA quantitation.

Table 2.1: Optimized detection parameters for BMAA isomers by HILIC- DMS-MS/MS

Analyte	Retention time [b] (min)	Precursor *m/z*	Product *m/z*	Collision energy (V)	CV (V)
BMAA	18.2	119	102	13	-23.6
			44	25	
BMAA-d_3	18.2	122	105	13	-23.2
			47	25	
dummy [a]	-	-	-	-	+ 20
BAMA	18.1	119	102	15	-26.2
			56	20	
2,4-DAB	22.4	119	101	10	-18.1
			56	17	
AEG	21.0	119	102	15	-20.8
			56	15	
3,4-DAB	24.5	119	101	10	-21.5
			84	20	

[a] An additional entry in the SRM table used to eliminate DMS crosstalk between BMAA and BAMA.

[b] Retention time in mussel matrix matched standard

2.3 Results and Discussion

2.3.1 MS/MS and HILIC Behavior of BMAA Isomer Standards

In addition to the commonly considered isomers 2,4-DAB and AEG, two additional isomers of BMAA were obtained for testing (Figure 1.2). The first, BAMA, was previously analyzed by RPLC-MS/MS after AQC derivatization and identified in shellfish [61], but its behavior in HILIC-MS/MS has not been reported. The other, 3,4-DAB, has not previously been analyzed by either method. The MS/MS spectra for all 5 isomers, and the BMAA isotopologue BMAA-d_3, at an intermediate collision energy spread are shown in

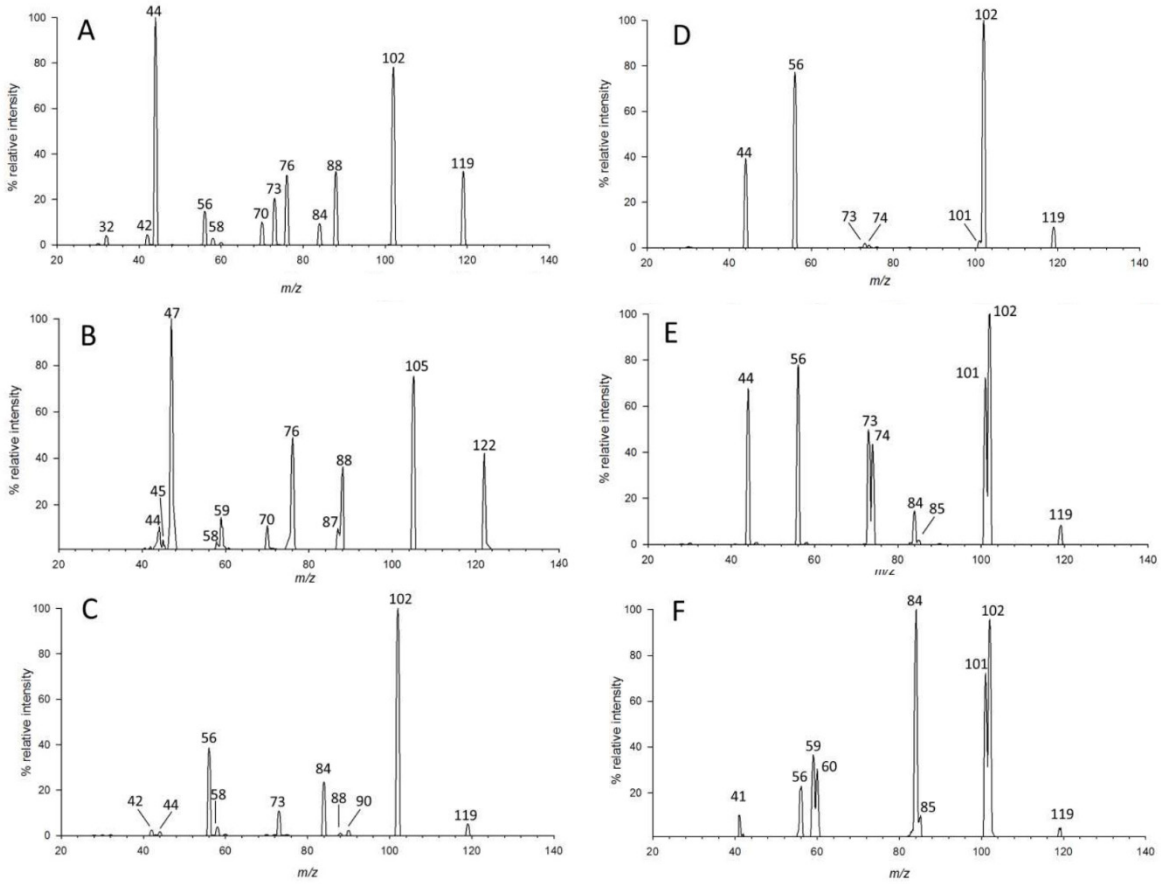

Figure 2.2: Product ion spectra of BMAA isomers from collision induced dissociation of [M+H] *m/z* 119 for BMAA (A), BMAA-d_3 (B), BAMA (C), AEG (D), 2,4-DAB (E) and 3,4-DAB (F) with a collision energy spread of 15 – 20 V

Figure 2.2. All isomers appear to have potential for interference in MS/MS analysis of BMAA. The relatively insensitive *m/z* 119>76 transition for BMAA is the only selective transition for BMAA detection, while 119>88 only shows a small contribution from BAMA. Because of the similarities of product ions of BMAA isomers, effective separation of all isomers by another technique is required prior to MS/MS detection in order to allow for selective quantitation of BMAA.

The HILIC-MS/MS method previously reported by McCarron *et al.* [63] was optimized for the separation of BMAA from only 2,4-DAB and AEG as those were the only standards

available at the time. Analysis of a mixture of BMAA and its 4 isomers (Figure 1.2) using this method showed significant chromatographic overlap between BMAA eluting at 18.5 min and BAMA at 18.3 min, as shown in Figure 2.3A. While the partial separation observed might be sufficient to differentiate BMAA from BAMA in neat standards, retention time shifts that have been observed in the analysis of BMAA in crude extracts of samples [69] could easily lead to misidentification or interference between these isomers. Furthermore, the presence of BAMA in mussels has been reported recently [61]. These same shifts in migration time were observed in later analyses of different matrices here, with a collapse in resolution between BMAA and BAMA. The rarely used transition *m/z* 119 > 44 offers the best sensitivity for BMAA, but with an approximately 10 times higher background signal in HILIC-MS/MS, leading to poor signal-to-noise compared with *m/z* 119 > 102, especially in matrix samples. Further work by the NRC group failed to improve the HILIC separation. Some effort in this project was spent exploring alternative stationary phases but there was no success to report.

2.3.2 Differential Mobility Spectrometry Optimization

The ultimate goal of this work was to implement DMS as an ion filter after HILIC to separate isomers from one another by DMS. A particular focus was placed on the separation of BMAA and BAMA, which co-elute in HILIC and share precursor and product ions in MS. The separation of BMAA isomers was investigated by infusing standards into ESI-DMS-MS(/MS) and collecting CV spectra. Recent DMS literature has been dominated by the use of chemical modifiers in the carrier gas to enhance the clustering/declustering behavior of analytes and improve DMS separation [77,129,130].

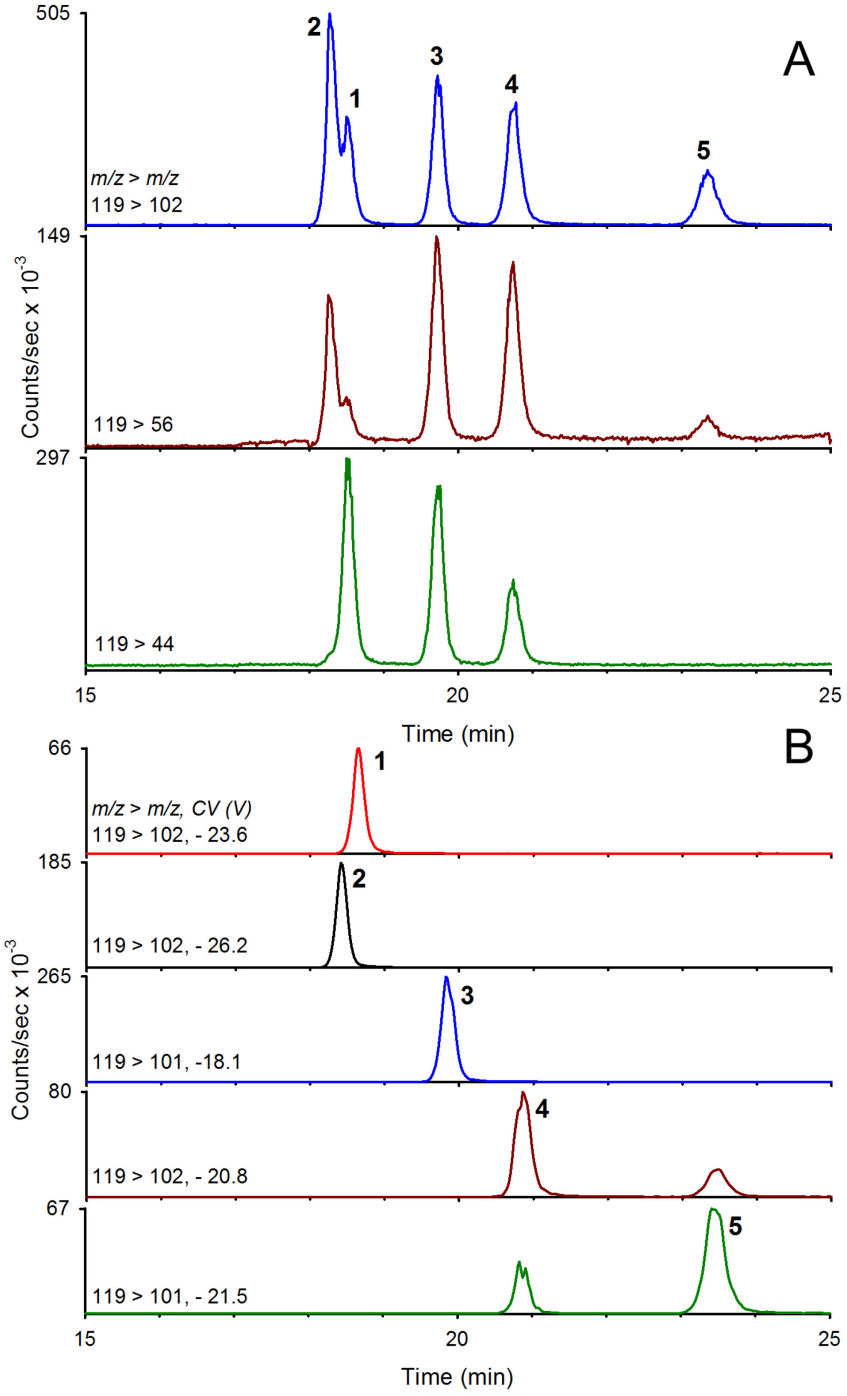

Figure 2.3: HILIC-MS/MS (A) and HILIC-DMS-MS/MS (B) analysis of a 5 µM mixed BMAA isomer standard using selected reaction monitoring. Peak labels refer to isomers in Figure 1.2. Trace labels in B refer to DMS and SRM parameters in Table 2.1.

Without the use of any gas modifier, BMAA failed to separate from any isomers, and migrated through at 0 CV over the range of tested separation voltages (1500-4000). Several commonly used gas modifiers including deionized water (DIW), isopropanol, methanol, acetonitrile and acetone were screened for their ability to enhance the separation of BMAA and its isomers.

This identified acetonitrile as the most promising modifier, separating the BMAA isomer mix into 3 peaks using the pre-set limit of 1.5% modifier. Each peak represented a different isomer with BMAA and BAMA completely interfering with each other (Figure 2.5A).

By comparison, both methanol and isopropanol gave poor sensitivity with no enhancement in separation. Acetone yielded a total of 7 peaks within the scan range, each with contributions from several isomers, indicative of multiple cluster formations for each analyte. Our initial investigation of DMS parameters and MS source conditions including dispersion voltage, throttle gas, DMS offset and modifier flow rate did not yield any conditions where BMAA and BAMA were separated.

The Analyst software used to control the DMS imposes 2 levels of gas modifier: high corresponding to 3% (v/v) carrier gas modifier concentration and low corresponding to 1.5% (v/v) carrier gas modifier concentration. The lower limit is likely imposed out of respect for patent law [80]. In all cases, using the high modifier flow rate showed a rapid deterioration of separation and sensitivity in comparison to the low setting. These observations coupled with the recent literature examining the impact of modifier concentration on separation [77,129] led to conclusion that lower concentrations of

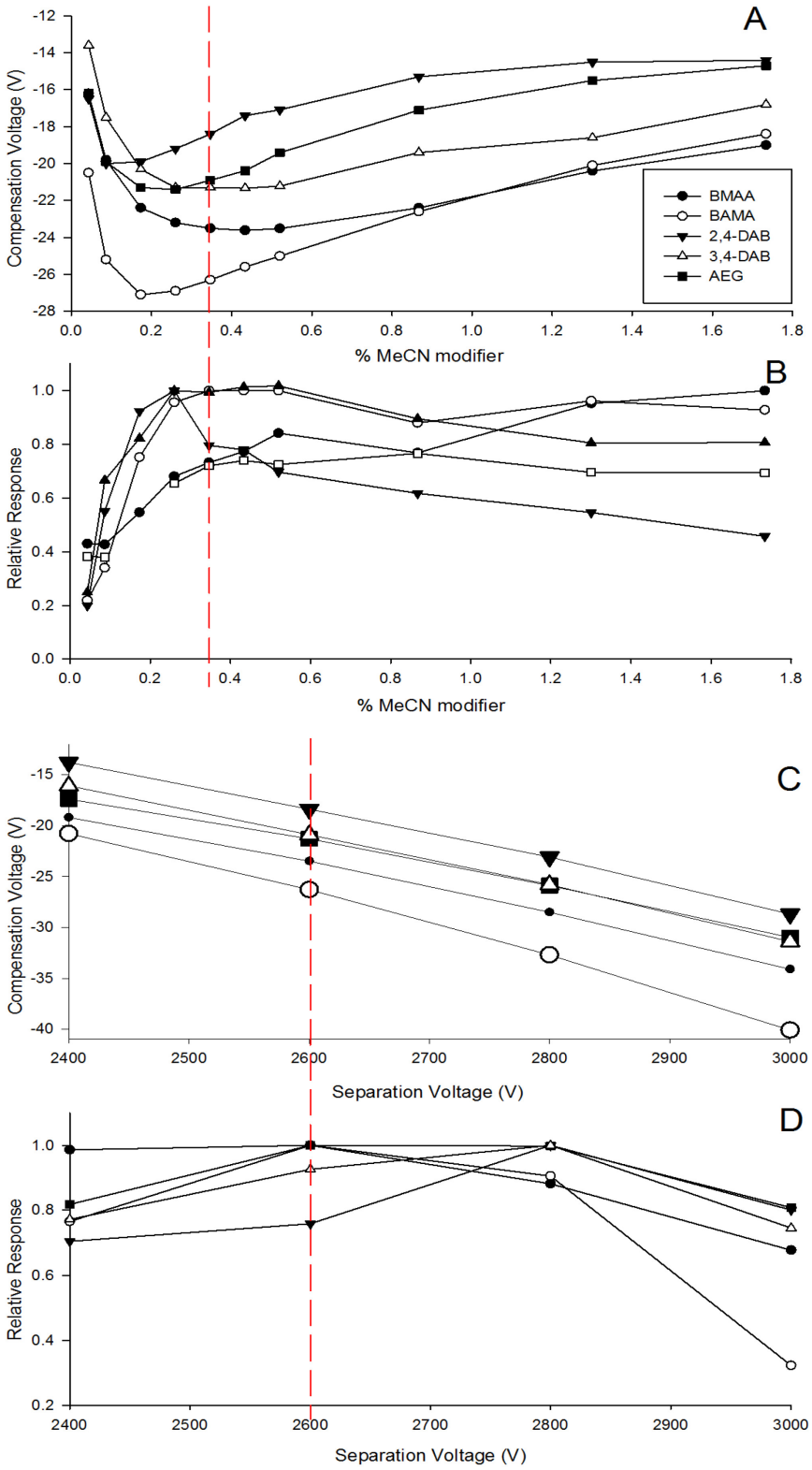

Figure 2.4: Effects of DMS parameters on BMAA isomer separation, including the effect of % acetonitrile modifier on compensation voltage (A) and sensitivity (B) at separation voltage = 2600 V and effect of separation voltage on compensation voltage (C) and sensitivity (D) using 0.35% acetonitrile modifier. The red line indicates optimum conditions used in HILIC-DMS-MS method.

acetonitrile should be investigated so see if separation of BMAA and BAMA occurred anywhere between 0 and 1.5% (v/v).

The instrumental and software modifier limitations were overcome by introducing an externally metered flow of liquid modifier into the carrier gas flow. This was accomplished by teeing in a liquid flow from a syringe pump or an HPLC pump directly into the flow of modifier gas before it enters the analyzer gap. This allowed for stable concentrations of gas modifier down to 0.01% to be investigated for the separation of BMAA isomers by DMS.

The effects of varying the externally metered acetonitrile concentration in the carrier gas on the separation of BMAA isomers by DMS are shown in Figure 2.4. The co-migration of BMAA and BAMA observed at 1.5% MeCN can be overcome by decreasing the modifier concentration to 0.35%, as shown in Figure 2.4A. This is consistent with clustering-declustering of analyte ions with neutral solvent molecules during low- and high-field portions of the waveform, respectively.

At lower levels of modifier, clustering occurs predominantly during the low-field portion of the waveform, increasing the collisional cross section relative to that at high-field. As the % modifier is increased, more clustering occurs, but during both the low- and high-field portion of the waveform, leading to a smaller relative difference in collisional cross section than that observed at lower % modifier and a corresponding loss of resolution between BMAA and BAMA. At very low modifier composition (< 0.2%) the sensitivity of the analysis decreased significantly for all analytes as shown in Figure 2.3B. The separation voltage (SV, also known as dispersion voltage (DV)) has a significant impact

on the CV of transmission of BMAA isomers, but less of an impact on their resolution, as shown in Figure 2.3C. Some improvement in separation at higher SVs was observed, but at the cost of a large decrease in sensitivity, as shown in Figure 2.4D. In general, as the % modifier was decreased, an accompanying decrease in SV was required to achieve good sensitivity. This was advantageous because operating at high SVs (> 3500 V) and high modifier concentrations ($\geq$ 1.5 %) led to frequent electrical discharge that prevented operation of the device. Thus, optimized conditions of SV = 2600 V and modifier concentration of 0.35% were chosen as having the best sensitivity while maintaining baseline separation of BMAA and BAMA.

A comparison of the two optimal conditions before and after modification is shown in Figure 2.5. In addition to complete isomer separation from BMAA, better signal stability, DMS peak shape and overall sensitivity were observed after the modification. The higher quality pump used after the modification is believed to reduce instabilities in modifier delivery previously present, leading to better signal stability. Additionally, better separation means less defocusing inside the DMS due to fewer analytes of similar charge.

Figure 2.6 shows the separation of BMAA from its isomers as well as ESI generated chemical background achieved by DMS. Unlike LC, DMS is able to separate analytes from chemical background produced by ESI prior to MS analysis. This is demonstrated by the abundant background observed in Figure 2.6B, showing DMS-MS detection while infusing a BMAA standard. These background species represent a mixture of adducts of acetonitrile, water, mobile phase modifiers and system contaminants, and many can be observed throughout an LC-MS analysis, leading to high background signal at low *m/z*.

The absence of background in the product ion spectra of BMAA isomer standards collected by ESI-DMS-MS/MS (Figure 2.2) can also be attributed to DMS. As shown in Figure 2.5B and 2.6C, analysis of an infused mixture of BMAA isomers by ESI-DMS-MS/MS in SRM mode gave good separation of BMAA and BAMA, but co-migration of AEG and 3,4-DAB. However, since these isomers are effectively separated by HILIC (Figure 2.3A), they need not be separated by DMS. Of the six standards investigated, only 2,4-DAB showed an additional CV peak, at -14.5 V in Figure 2.5A and 2.6C. This peak showed the same product ion spectrum as the major peak at CV = - 18.1 V and only *m/z* 119 was observed at CV = - 14.5 V in full scan MS. The species transmitted at CV = - 14.5 V had the identical HILIC retention time in LC-DMS-MS analysis (below) as the one transmitted at - 18 V. This evidence, along with ^{1}H-NMR spectroscopy confirmation of the purity of the 2,4-DAB standard, indicate the additional peak is a different gas phase conformation of 2,4-DAB rather than another isomer in solution. More work is required to determine the nature of this species and whether it would have any impact on quantitation of 2,4-DAB by HLIC-DMS-MS/MS. If accurate quantitation of 2,4DAB is required, reverting back to the initial 1.5% (v/v) gas modifier concentration pre-set can force all analyte into one conformation while still separating BMAA and other isomers.

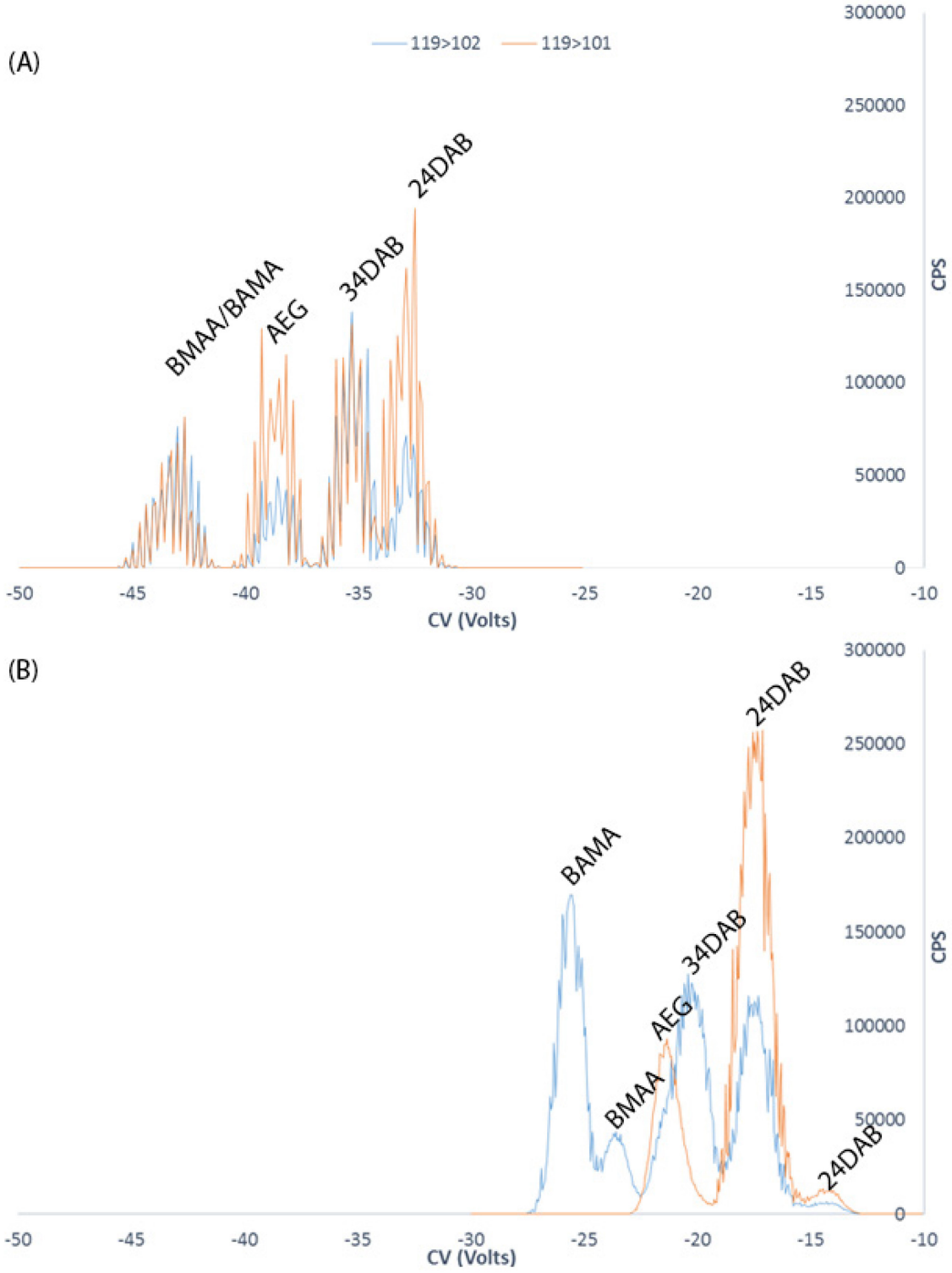

Figure 2.5: CV spectra of a 5 µM isomer mixed standard before and after DMS modification. Part A shows the best parameters before modification collected with 1.5% (v/v) acetonitrile gas modifier and a dispersion voltage of 3600 V. Part B shows the same sample analyzed with the modified system with 0.35% v/v) acetonitrile gas modifier and a dispersion voltage of 2600 V.

Another metric that is critical for robust quantitation by LC-DMS-MS/MS is stability of the CV of transmission. Previous versions of the DMS device suffered from CV values that were highly dependent on MS source conditions and sample flow rate and composition, as well as high sensitivity to moisture present in the sample and atmosphere [130,131]. The mobile phase used in chromatography can act as gas modifier in DMS separations, changing the CV required for detection. This can be particularly challenging during gradient chromatographic separations with analytes with changing retention times, such as the separation here. If the mobile phase is different due to an earlier elution, the CV might be altered enough so that transition through the DMS cannot occur, preventing detection. Fortunately, excellent CV stability was observed between replicate analyses of mixed BMAA isomer standards, including different MS source conditions, sample compositions and a broad range of sample flow rates. The average deviation of the CV maxima of BMAA isomers from the mean values in Table 2.1, over a three month period, was 0.2 V (n = 43). Considering the 3 - 4 V CV peak widths, this CV stability was more than adequate to allow reproducible operation of a HILIC-DMS-MS/MS method.

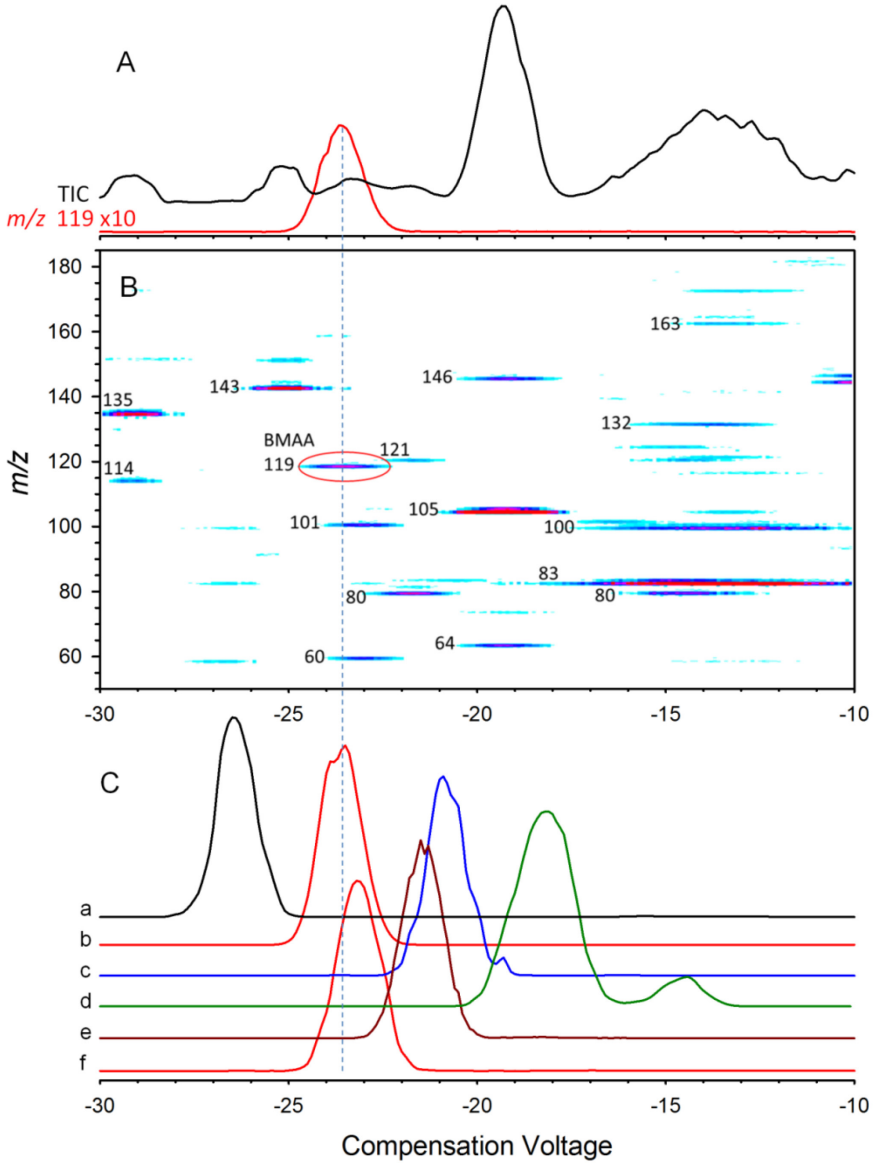

Figure 2.6: Compensation voltage spectrum of a BMAA standard (A) and chemical noise separated by DMS (B), in full scan MS. Pane (C) shows DMS separation of BMAA (b) from its isomers BAMA (a), AEG (c), 2,4-DAB (d), 3,4-DAB (e) and isotopomer BMAA-d_3 (f), in SRM mode.

2.3.3 HILIC-DMS-MS/MS Method Development

One of the limitations of using DMS as an ion filter in LC-MS experiments is that the switching time between different CV values of DMS is relatively slow (msec) compared with switching times in SRM (μsec). This greatly limits the number of different analytes that can be monitored simultaneously compared to LC-MS/MS. Additionally, SRM transitions that would allow for detection of all BMAA isomers, such as *m/z* 119 > 102, become analyte specific once a CV value is assigned. In practice a doubling in simultaneous transition monitoring saw approximately two-fold decrease in sensitivity. However, the added selectivity of the DMS reduces the burden on monitoring multiple product ion ratios for qualitative confirmation of BMAA identity. These considerations led to limiting the number of SRM transitions to two for each analyte, each with an analyte specific compensation voltage as determined in Table 2.1. Due to the possible gains in sensitivity, a method with a single transition per analyte was considered but never implemented. Instead, an approach of using the most sensitive transitions 119>102 and 119>44 for BMAA analysis rather than more selective qualifier ions 119>76 and 119>88 used elsewhere was possible because of the added selectivity of the DMS separation. By HILIC-MS, 119>102 is not optimal because of interference from BAMA, 119>44 suffers from very high baseline and poor signal-to-noise and 119>76 and 119>88 show only a third of the sensitivity. When DMS is used to eliminate interference between BMAA isomers and from ESI background, these most sensitive transitions can then be used.

One unexpected phenomenon of DMS crosstalk was observed during implementation of the HILIC-DMS-MS/MS method. This manifested itself as significant signal intensity being detected during elution of BMAA and BAMA in the transitions for whichever

analyte was second in the Analyst software's SRM table. Since these analytes were baseline resolved by DMS and the transition in which the interference was observed depended entirely on the order of the entries in the SRM table, poor DMS selectivity can be ruled out. On the other hand, crosstalk is not expected in DMS either, because the residence time of ions in the device is 20 msec and the software automatically includes a 20 msec pause between each SRM transition to compensate for this. The practical solution to this crosstalk was to insert a dummy transition between transitions for BMAA and BAMA in the SRM table with a very high CV = + 20 V. This had the effect of emptying the DMS cell of all ions before CV was switched. It is believed that this phenomenon is related to software control of the device, but a more detailed investigation is required to understand and correct it. One other possibility is that the modification described reduced the gas flow through the DMS, increasing residence time. This seems unlikely, however, as the modification was not restricting of gas flow, the gas flow-rate was metered by the instrument, and increased residence times should reduce sensitivity but an increase was observed.

The previously reported HILIC conditions [63], the two most intense product ions for each BMAA isomer (Figure 2.2) and the optimized DMS conditions (Figure 2.5-6) were combined to create a multidimensional HILIC-DMS-MS/MS method using the parameters in Table 2.1. Figure 2.3B shows the impact of the DMS separation on the HILIC-MS/MS analysis of BMAA isomers, compared to Figure 2.4A without DMS. This method showed complete selectivity between BMAA and BAMA, which are not resolved by HILIC-MS/MS alone. Since AEG and 3,4-DAB are not separated under the DMS conditions used, these species appear in each-other's DMS-SRM transitions. Of note is the approximately

70% decrease in absolute signal intensity that is observed once DMS is implemented. This can be attributed to diffusive losses in DMS and inefficient ion probing at the DMS inlet [62]. However, the elimination of ESI background by DMS, as shown in Figure 2.6, reduces the baseline and results in an increase in signal-to-noise ratio of about 4-fold compared to without DMS. Once DMS conditions are established, the per-sample run time of the HILIC-DMS-MS method is the same as it would be for HILIC-MS.

Because of the low duty cycle of the DMS, the full SRM method with continuous monitoring of all quantifier and qualifier transitions used in Figure 2.3B was not ideal for analysis of trace levels of BMAA in real samples. The duty cycle was improved by limiting the number of DMS-SRM transitions monitored at any given retention time using scheduled SRM. This method used the parameters in Table 2.1, but only monitoring each analyte at its retention time ± 45 sec.

2.3.4 Identification of BMAA Isomers in Mussel Samples

The HILIC-DMS-MS/MS method with scheduled SRM scan mode was used to analyze a variety of samples types previously reported to contain BMAA. Qualitative analysis of these samples showed the suitability of the method for selective identification of BMAA and its isomers from a variety of sample matrixes and an exceptionally low level of chemical background in all transitions monitored. In all cases the retention time of BMAA, relative to the isotope labeled standard BMAA-d_3, as well as product ion ratios between primary and secondary transitions were used as additional identification criteria. High levels of BMAA as well as 2,4-DAB and AEG were detected in the positive cycad control sample at levels in agreement with previous reports [63]. Mussel tissue reference materials and un-processed mussel samples were all found to contain BMAA, BAMA and 2,4-DAB.

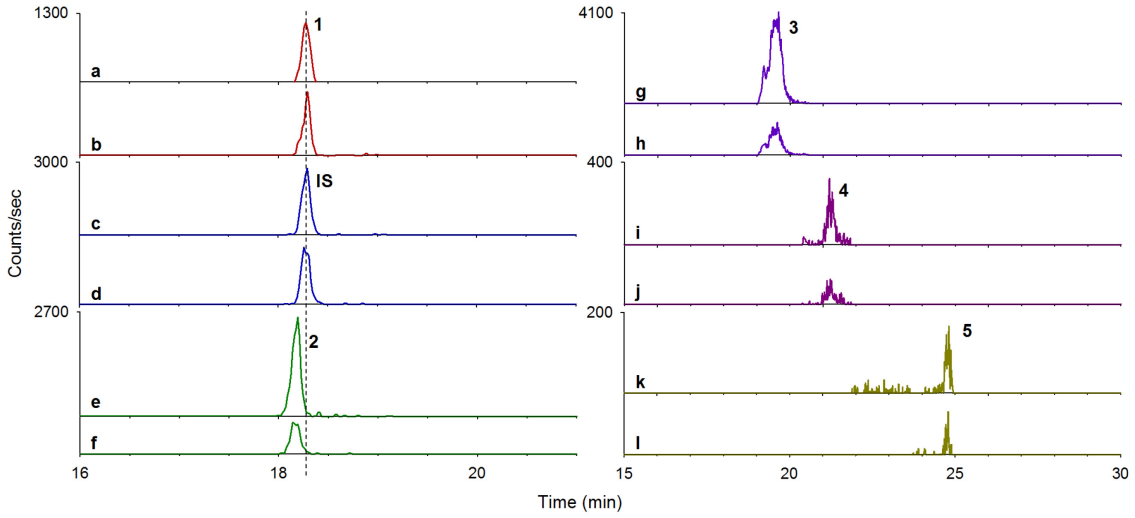

Figure 2.7: Identification of BMAA isomers in ASP-Mus mussel tissue reference material. Peak numbers correspond to analytes as in Figure 1.2 and trace labels correspond to DMS and SRM conditions in Table 2.1.

Interestingly, only 2,4-DAB was detected in the cyanobacterial reference material (RM-BGA [128]). The HILIC-DMS-MS/MS analysis of one of the mussel tissue reference materials, CRM-ASP-Mus, is shown in Figure 2.7 and revealed that BAMA was detected

at a higher intensity than BMAA and that AEG and 3,4-DAB were also tentatively detected near the LOD. The enhancement of selectivity achieved by using DMS is demonstrated by comparison of Figure 2.7 to analysis of the same sample by HILIC-MS/MS in Figure 2.8. This comparison shows the elimination of interference from BAMA and many un-identified matrix peaks as well as elimination of high baselines observed in most transitions using HILIC-MS/MS. Due to the similarity in MS/MS spectra (Figure 2.2), it would not be unreasonable to expect the possible misidentification of BAMA as BMAA without the DMS implementation, resulting in over-estimating the BMAA quantity. Matrix components can also be seen interfering with internal standard, manifesting as a peak shoulder (Figure 2.8) which are not present when DMS is utilized.

In order to investigate the DMS separation of mussel tissue matrix peaks from BMAA and its isomers further, a series of HILIC-DMS-MS/MS runs of the hydrolyzed ASP-Mus extract were carried out at a fixed CV for each run using a product ion scan of *m/*z 119. By analyzing the same sample at a range of CV values, it was possible to construct a three-dimensional plot of retention time and compensation voltage versus signal intensity, as shown in Figure 2.9. This experiment clearly demonstrates the separation of the major BMAA isomers detected in the sample (BAMA, BMAA and DAB) from the abundant isobaric interference present in the matrix. This experiment also confirmed the identity of these three analytes by matching their product ion spectra with those acquired from standards. The ability of DMS to eliminate ESI chemical background is also evident from Figure 2.9, which shows continuously eluting *m/z* 119 background species that lead to the high background observed in HILIC-MS/MS (Figure 2.3A and Figure 2.8), separated from BMAA isomers. While this experiment is not practical for routine use, it

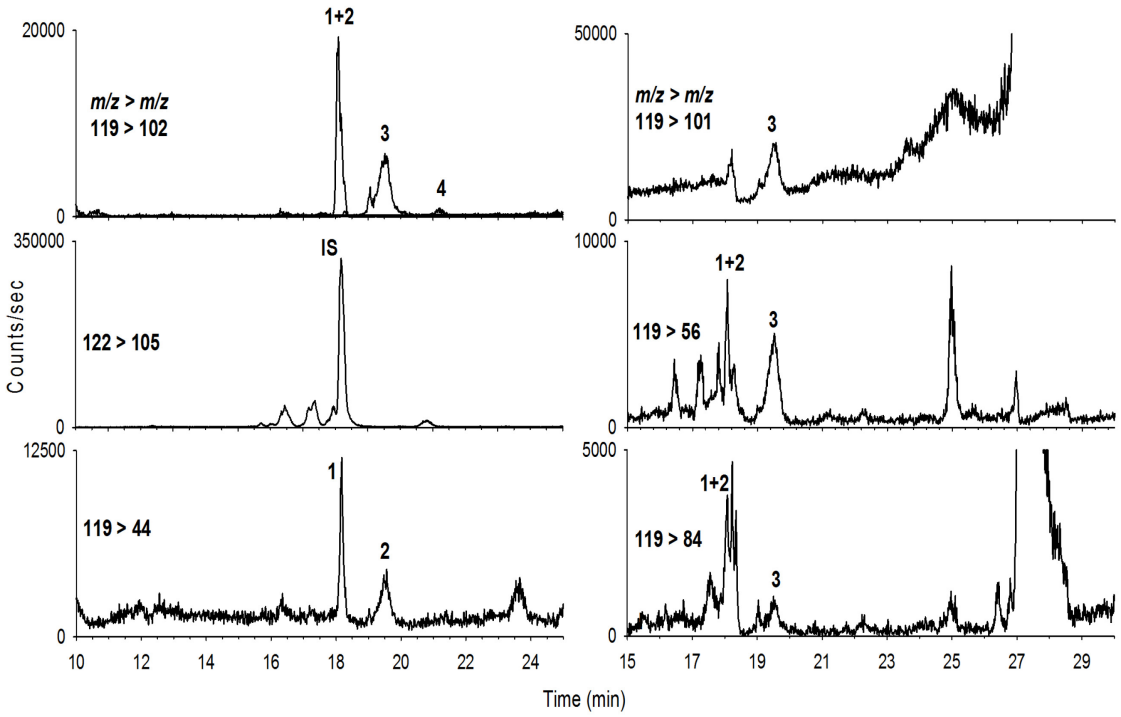

Figure 2.8: HILIC-MS/MS analysis of hydrolyzed ASP-MUS extract using selected reaction monitoring. Peak labels correspond to analytes in Figure 1.2.

is the only way to examine the DMS behavior of matrix components in a complex sample that cannot be analyzed directly by ESI-DMS-MS. It can be used to identify possible sources of interference in BMAA analysis when a new sample matrix is being considered and was an excellent way to confirm the identity of BMAA and its isomers.

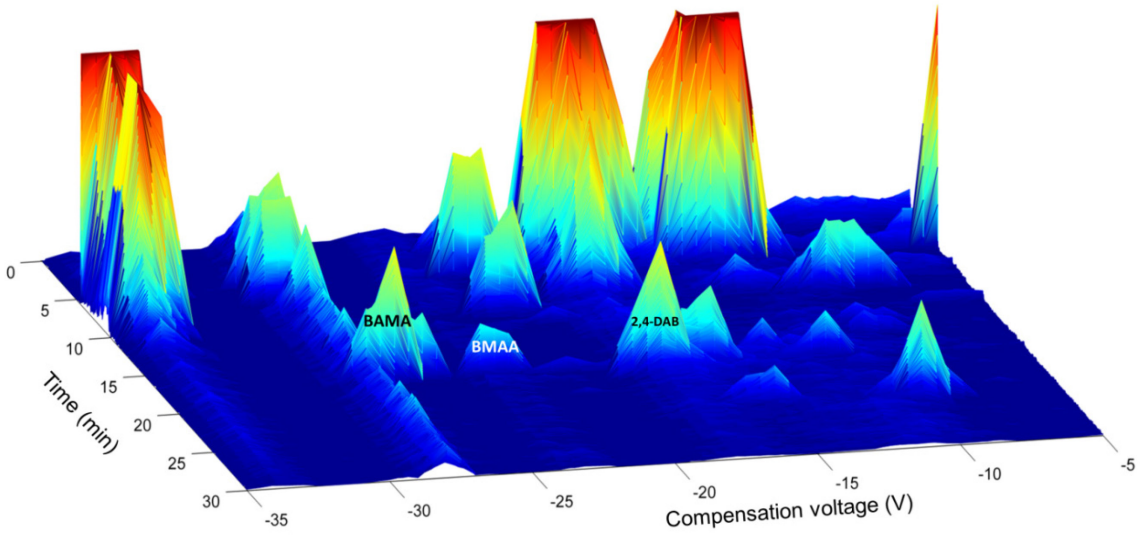

Figure 2.9: DMS separation of BMAA from isomers and matrix interference in ASP-Mus mussel tissue reference material by HILIC-DMS-MS/MS. The 3D surface plots the total ion current of a product ion scan of *m/z* 119 carried out in a series of 30 LC runs at 1 V CV intervals

2.3.5 Quantitative Analysis of BMAA with Isotope Dilution

In order to evaluate the quantitative capabilities of HILIC-DMS-MS/MS for BMAA analysis, a targeted method was developed that included only transitions for BMAA and the stable isotope labeled standard, BMAA-d_3. This method had an improved duty cycle and lower limits of detection compared to the other methods, but at the cost of not detecting other BMAA isomers. It also eliminated the potential of missing analyte signal due to shifts in retention time greater than 45 seconds.

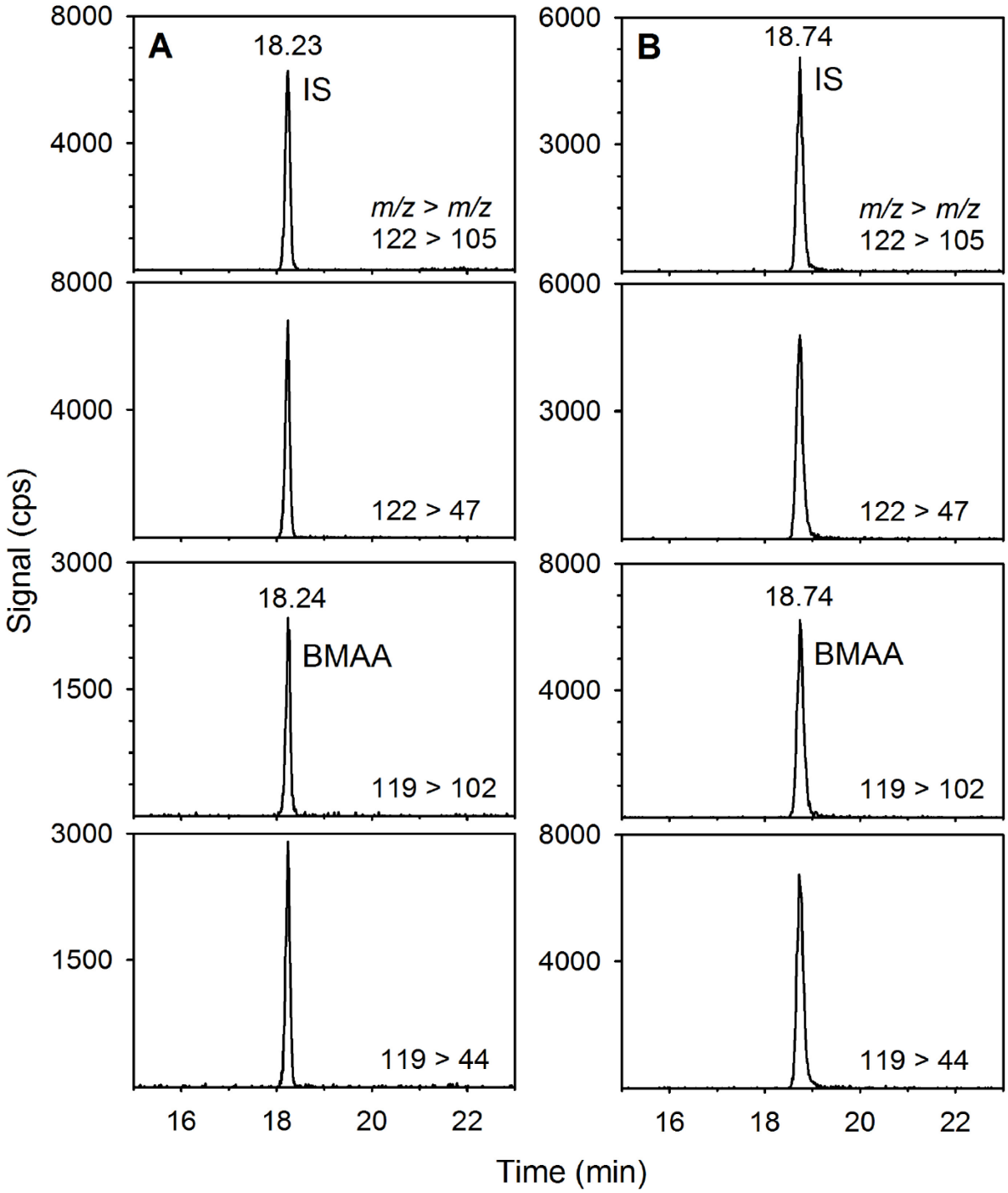

Figure 2.10: Analysis of mussel sample M1 (A) and a calibration standard (B) using the targeted HILIC-DMS-MS/MS method. Retention time shifts occurred in matrix samples compared to standards, but relative retention time between BMAA/ BMAA-d_3 were constant and used, along with product ion ratios of *m/z* 102/44 as qualitative confirmation of BMAA identity

Quantitation of BMAA in sample extracts was carried out by spiking them, along with a BMAA standard, with BMAA-d_3 after total hydrolysis to allow for double isotope dilution calibration to correct for matrix effects on ionization efficiency [132]. This is important as DMS separations only occur after ESI and are thus still susceptible to matrix suppression. Spiking was done after hydrolysis due to concerns of the internal standard exchanging protons in the acidic environment, causing an overestimation of BMAA content. An example chromatogram of this targeted HILIC-DMS-MS/MS method for analysis of mussel sample M1 by isotope dilution is shown in Figure 2.10. An isotope effect was observed in the DMS analysis of BMAA-d_3, shown in Figure 2.6C, which required slightly different CV values to be used for the analyte and the standard. This was acceptable since the primary function of isotope dilution in this workflow is to correct for matrix effects observed in ESI, which occurs prior to DMS analysis. It was also believed that any possible shifts in CV would effect BMAA and the internal standard equally, having a null effect on concentration calculations.

The standard curve of BMAA spiked with a constant level of BMAA-d_3 (Figure 2.11) showed excellent linearity ($R = 0.99991$) over 3 orders of magnitude from 0.01 to 6 μM BMAA for the ratio of BMAA/BMAA-d_3 response. An instrumental LOD of 0.4 pg on column (S/N = 3) was calculated from the chromatograms of replicate analysis of a 1 pg standard (Figure 2.11). This value was used to estimate a method LOD for BMAA in the analyzed samples of 20 ng g^{-1} dry weight, similar to those reported previously by other LC-MS/MS methods [62,64]. Since crude sample extracts were analyzed, it was necessary to use a lower injection volume (1 μL) than normal (5 μL) to minimize retention time shifts and LC peak shape degradation due to matrix effects. In the future,

sample cleanup and preconcentration will be implemented to reduce method detection limits further and reduce the effect of matrix on HILIC retention time [69].

Quantitative results of BMAA analysis of selected samples are shown in Table 2.2. As noted previously, BMAA was not detected in the cyanobacterial reference material but was present at high levels in cycad [63]. The concentrations of BMAA in mussel tissues were similar at about 1 μg g^{-1}, consistent with other recent reports [62,64,69]. Considering the controversy that has surrounded BMAA analysis [58,65] it is important to note that CRM-ASP-Mus is commercially available and could be used for comparison of BMAA detection methods in the future. The measurement of BMAA in CRM-ASP-Mus reported in Table 2.2 is preliminary and further work is required to assign a reference value to this material. Extra work is being carried out to validate one or more analytical workflows for BMAA

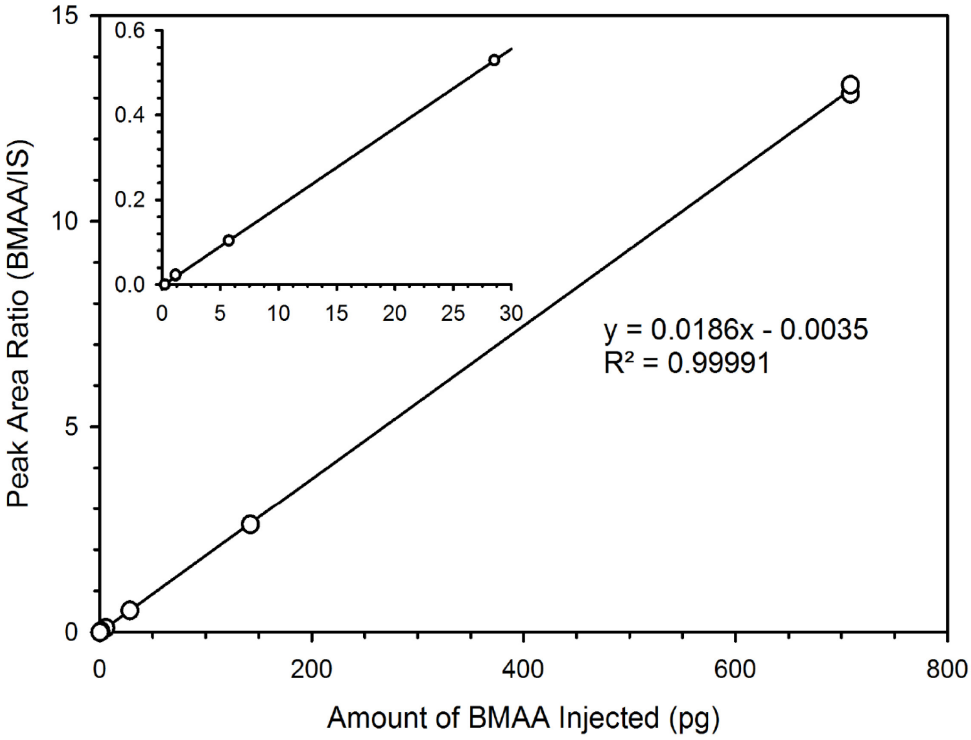

Figure 2.11: Isotope dilution calibration plot showing the ratio of BMAA/ BMAA-d_3 plotted against the amount of BMAA injected

quantitation in various matrixes and to study the chemical form of the BMAA in these samples (i.e., free or protein-bound).

Table 2.2: Quantitation of BMAA in matrix samples by HILIC-DMS-MS/MS

Sample	**Relative retention time** [a]	**Product Ion Ratio** [b]	**[BMAA] µg g^{-1} ± sd**
Cycad RM	1.0007 ± 0.0005	0.87	39 ± 1 (n=5)
RM-BGA	nd [c]	nd	nd
CRM-ASP-Mus	1.0004 ± 0.0003	0.91	1.2 ± 0.3 (n=3)
Mussels M1	1.00055 ± 0.00001	0.82	1.20 ± 0.06 (n=3)
Mussels M2	1.0007 ± 0.0009	0.88	0.95 ± 0.08 (n=3)

[a] BMAA retention time relative to BMAA-d_3 internal standard
[b] Ratio of product ion 102/44; average product ion ratio = 0.90 ± 0.04 for n = 5
[c] nd = not detected (<20 ng g^{-1})

2.4 Conclusion

Along with improving the availability of standards, exploring new analytical techniques with improved or alternative selectivity represents a promising approach to improving reliability of BMAA analysis. We have addressed both these potential improvements by considering new isomers and developing a new, highly selective, multidimensional HILIC-DMS-MS/MS method.

An investigation of the MS/MS and HILIC behavior of the new isomers demonstrated the potential for BAMA interference with BMAA. The investigation of the separation of

isomers by DMS revealed that accurate control of low % values of acetonitrile modifier in the DMS carrier gas was essential and could only be achieved by external metering. This simple modification should be equally effective in other fields where the restrictions placed on the concentration of modifier could also have limited the utility of the device.

Our optimized HILIC-DMS-MS/MS method was used to analyze a variety of matrix samples and showed detection of BMAA and BAMA in commercially available mussel tissue reference materials. The controversy still surrounding BMAA analysis and quantitation [58] and the potential public health implications of the claims being made based on BMAA detection [67,68] further underscore the need for more rigorous method validation, inter-laboratory studies and certified reference materials in this field. Work is now underway to fully validate this HILIC-DMS-MS/MS method using isotope dilution quantitation and a solid phase extraction cleanup.

2.5 Acknowledgments

The authors thank Sabrina Giddings and Krista Thomas for technical assistance and Pearse McCarron for editorial input.

CHAPTER 3: DETERMINATION OF THE NEUROTOXIN β-*N*-METHYLAMINO-L-ALANINE (BMAA) IN CYANOBACTERIA AND SEAFOOD BY CAPILLARY ELECTROPHORESIS-TANDEM MASS SPECTROMETRY[3]

3.2 Introduction

In this Chapter, capillary electrophoresis (CE) is investigated as a potential method for the determination of BMAA. As described in Chapter 1, CE has a separation mechanism complementary to the previously developed HILIC-DMS-MS/MS method. CE has a number of potential advantages for BMAA analysis, including high resolving power and the ability to distinguish isomers and chiral molecules [89]. CE has been widely used for direct analysis of small ionizable molecules such as amino acids [90]. A CE-UV method for BMAA has been reported by Baptista *et al.* [104] that demonstrated a separation of BMAA from the isomer 2,4-DAB. Unfortunately, this method suffered a poor detection limit (0.5 mg L^{-1}) due to the lack of a chromophore in BMAA, making it impractical for trace level analysis. The goals of the present study were to: (a) optimize conditions for the separation of BMAA from several isomers and co-extracted components of biological samples; (b) develop a highly selective and sensitive CE-MS/MS method for BMAA without derivatization; and (c) develop an isotope-dilution quantitation procedure with β-*N*-$^2H_3$-methylamino-L-alanine (BMAA-d_3) as internal standard.

[3] This chapter is a modified version of a manuscript that is to be submitted the journal of *Analytical and Bioanalytical Chemistry*. The authors are Elliott S. Kerrin, Robert L. White and Michael A. Quilliam. The work described is a collaboration between the National Research Council Canada, Measurement Science and Standards, Halifax, NS and Department of Chemistry, Dalhousie University, Halifax, NS.

3.3 Materials and Methods

3.3.1 Chemicals, Reagents and Samples

Acetonitrile (MeCN), methanol (MeOH), acetone, and 2-propanol (all HPLC-grade) were obtained from Caledon (Georgetown, ON, CAN). Acetic acid (AcOH) and formic acid (FA) (ACS grade, >98%) were purchased from EMD (Gibbstown, NJ, USA). Ammonium acetate, di-sodium tetraborate, sodium dihydrogen phosphate monohydrate, tri-sodium phosphate dodecahydrate were purchased from VWR International (Mississauga, ON, CAN). Ammonium hydroxide (ACS grade, 28-30% NH_3 w/v) was purchased from Fisher Scientific (Ottawa, ON, CAN). β-*N*-methylamino-L-alanine hydrochloride was obtained from Tocris Bioscience (Minneapolis, MN, USA), β-amino-*N*-methylalanine from Enamine (Kyiv, Ukraine), N-(2-aminoethyl)glycine from TCI America (Portland, OR, USA), 2,4-diaminobutyric acid dihydrochloride, hydrochloric acid and phosphoric acid (HPLC grade, 85-90%) were obtained from Sigma–Aldrich (Oakville, ON, CAN), 3,4-diaminobutyric acid dihydrochloride from FCH Group (Chernigiv, Ukraine). BMAA-d_3 was synthesized in-house as described elsewhere [62].

A mussel tissue reference material certified for the marine algal toxin domoic acid (CRM-ASP-Mus) was acquired from National Research Council Canada (Halifax, Canada). An in-house positive-control reference material made from the homogenized leaf and stem tissue of a cycad plant (Cycas debaoensis) obtained from Jurassic Plants Nursery (Halfmoon Bay, BC, CAN) and a recently developed pilot-scale cyanobacterial reference material (RM-BGA) containing other cyanotoxins [128] were also used for method testing.

3.3.2 Sample Extraction and Cleanup

Total protein hydrolysis of 50-mg freeze-dried samples was performed in 1 mL 6 M HCl in a flame-sealed glass ampoule at 110°C overnight. Samples were then dried under nitrogen at 55°C, spiked with BMAA- d_3, reconstituted in 2.5 mL 20 mM HCl, and a portion of this (25 mg tissue equivalent) was loaded onto an Oasis MCX cartridge (3 ml, 60 mg), which had been previously conditioned with 3 mL MeOH and 3 mL of 20 mM HCl. The cartridge was washed with 3 mL water and 4 mL MeOH and then BMAA was eluted in 7 mL aqueous ammonia (5% w/v). This eluent was dried under nitrogen, reconstituted with 1 mL of 2 mM HCl in water, and passed through a 0.22 μm filter (Ultrafree-MC).

3.3.3 CE-UV Method Development

All separations were performed with the Agilent G1600A capillary electrophoresis system equipped with a UV diode array detector. Fused silica capillary tubing (50 μm ID, 363 μm OD) was supplied by Molex Polymicro Technologies (USA) and cut in house to a 60 cm length with a window in the polyimide coating at 14 cm from the end. The capillary temperature was controlled by heated or cooled air. Method development was performed by injecting high concentration mixed standards (50 mbar for 5 sec) and monitoring absorbance at 192 nm. Borate (pH 9-10) and phosphate (pH 2-8) BGEs were tested for separation potential. A pH 3 phosphate BGE was optimized for concentration (from 50 to 250 mM) and for the use of organic modifiers (MeOH, MeCN, and isopropanol). System voltage (15-30 kV) and temperature (17-30°C) were also studied.

3.3.4 CE-MS Instrumentation

The CE system was coupled to a Sciex (Concord, ON, Canada) API-4000 mass spectrometer equipped with a Turbo V electrospray source. Initially, a commercial sheath-flow CE-MS adaptor kit (Sciex) was used with the sheath solvent delivered by a grounded ISCO SFC-500 microflow pump. Later, a custom interface was developed in which the CE capillary passed through a tee and was suspended in a 17 cm stainless steel tube (ID 400 µm, OD 600 µM) with a tapered tip to provided sheath flow and electrospray voltage. The exit of the CE capillary was stripped of polyimide coating, pulled to a point with heat, cut, and positioned so that it protruded from the metal tubing into the Taylor cone (Figure 3.1). This setup was suspended on an XYZ platform in place of the normal ESI source for positional control.

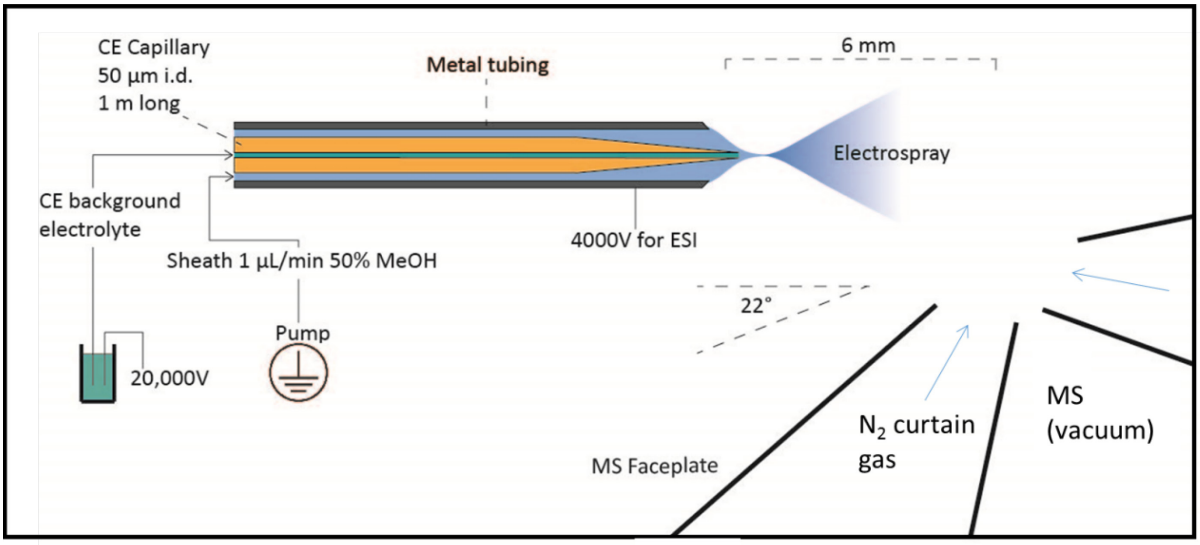

Figure 3.1: Model of Custom CE-ESI interface developed in-house.

3.3.5 CE-MS Method Development

Infusion of a low concentration mixed standard (5 μM BMAA, BAMA, AEG, 24DAB, 34DAB) in BGE at ~10 nL min-1 through the CE capillary was used to optimize MS parameters. Signal-to-noise ratio (S/N) was determined by measuring signal of infused standard solution versus blank BGE. Sheath flow (0.5 to 10 μL min^{-1}), sprayer position, spray voltage, disintegration (orifice) potential, entrance potential, exit potential, curtain and collision gas flows, desolvation gases (GS1 and GS2) were adjusted stepwise to provide maximal S/N.

Separation was optimized using the low concentration mixed standards. After a 60 sec injection at 50 mbar, BMAA and its isomers were monitored with transitions *m/z* 119→102 and 119→44, the former being used for quantitation. In addition, BMAA was selectively monitored via *m/z* 119→76 and the BMAA-d_3 was monitored via *m/z* 122→105 and 122→76, the latter being used for qualitative confirmation. A 1 M AcOH BGE (pH adjusted from 2.3 to 4.0) and a 1 M FA BGE (pH 1.9) were used for initial testing. Further optimization with FA was carried out by examining concentration from 0.5 to 5 M with 10% (v/v) MeCN to keep current below 50 μA. System voltage (15-30 kV) and capillary compartment temperature (17-30°C) were optimized for the final method. Sample stacking was optimized by examining sample loading (50 mbar for 30 – 240 sec) and sample solvent (0.2 – 20 mM HCl; 25-90% MeOH and MeCN).

3.4 Results and Discussion

3.4.1 Method Development: Analyte Selection

In addition to the commonly studied 2,4-DAB and AEG isomers, 3,4-DAB and BAMA were obtained for this study (Figure 1.2). Jiang *et al.* [61] predicted that these isomers would have the greatest potential for being present in natural samples and causing interference. Incomplete LC-MS separations of BMAA from some of these isomers have been reported in some studies, which then had to rely on the more selective but far less sensitive transitions (*m/z* 119→76 or 119→88) for selective detection [60].

3.4.2 Method Development: CE-UV

Preliminary experiments to optimize separation of BMAA and its isomers by CE were conducted using UV detection to save on mass spectrometer time. The CE-UV method proposed by Baptista *et al.* [104] was implemented as a starting point. Their proposed BGE, 20 mM sodium borate at pH 9, gave a relatively high electroosmotic flow (EOF) and it was possible to achieve resolution of BMAA and 24DAB in a fairly short analysis time, with migration times of 4.7 and 4.6 min, respectively. However, two problems were observed in our testing of this method. First, BMAA could not be resolved from AEG, although BAMA (4.9 min) was resolved. Second, it was observed that BMAA migrated close to the 4.5 min tEOF (migration time for neutral substances) under these conditions. This would make it difficult to resolve BMAA from many other compounds in a typical sample that would migrate close to tEOF.

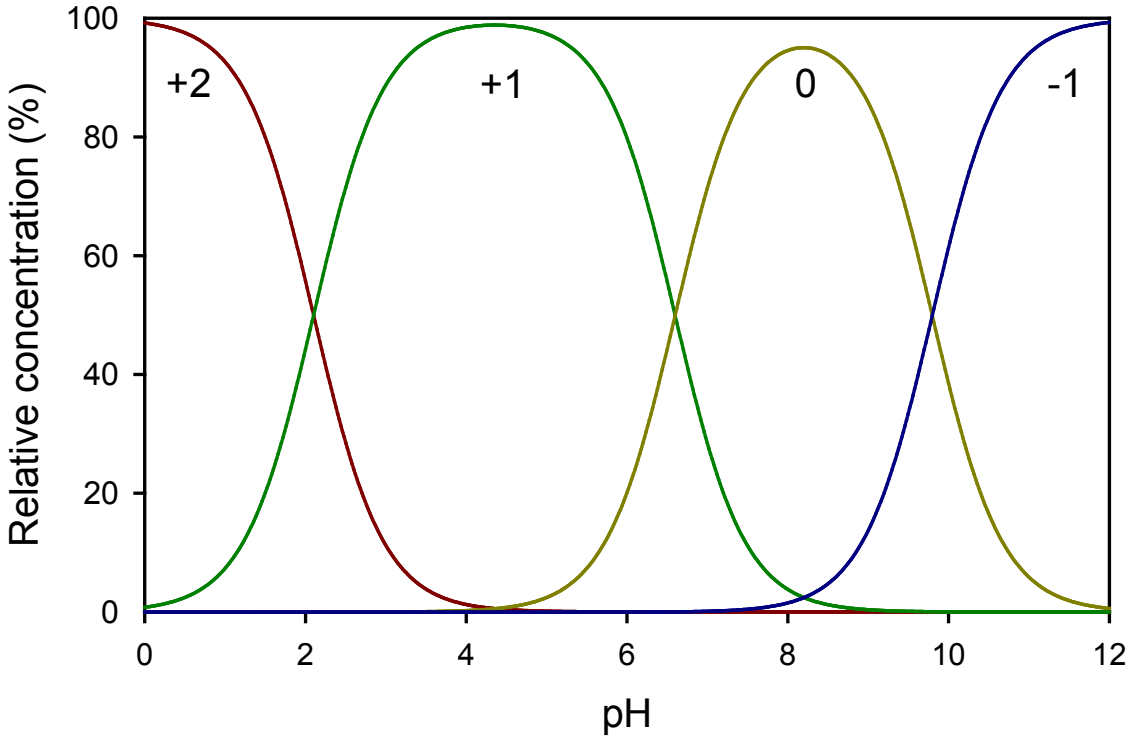

Figure 3.2: Theoretical diagram for the relative concentrations of the different charge states of BMAA as a function of solution pH.

In order to predict pH conditions under which BMAA would have greater electrophoretic mobility, the population of various charge states over a range of pHs were calculated using the published pKa values of the carboxyl (2.1), primary amine (6.6) and secondary amine (9.8) [133]. These calculations are presented in graphical form in Figure 3.2. Under Baptista's conditions of pH 9 [104], BMAA would be approximately 10% negatively charged and 90% neutral, which explains its low electrophoretic mobility. BMAA is predominantly negative in charge at a pH above 10 and positive below pH 6 (Figure 3.2). Only below pH 2 does BMAA begin to attain a predominant +2 charge state.

An attempt was made to achieve a better separation of the analytes in the negative charge state. At high pH, BMAA and the isomers migrated towards the anode against the EOF,

allowing more time for separation to occur. A high concentration (1 mM) mixed standard was analysed using 100 mM borate BGE with pH ranging from 8 to 10. At pH 10, BMAA separated further from tEOF (6.5 vs 5.0 min, respectively) but AEG still co-eluted with BMAA

Next, a series of 250 mM phosphate BGEs ranging from pH 2 to 8 were tested. As expected, separation did not occur when the analytes were in a predominantly neutral state (pH 6-8). At lower pH, the EOF was substantially reduced and only positively charged analytes migrated freely towards the cathode. The results are shown in 3.3. At pH 3.5 to 4.0, BMAA and three isomers co-eluted but good separation did occur at pH 3.0. At lower

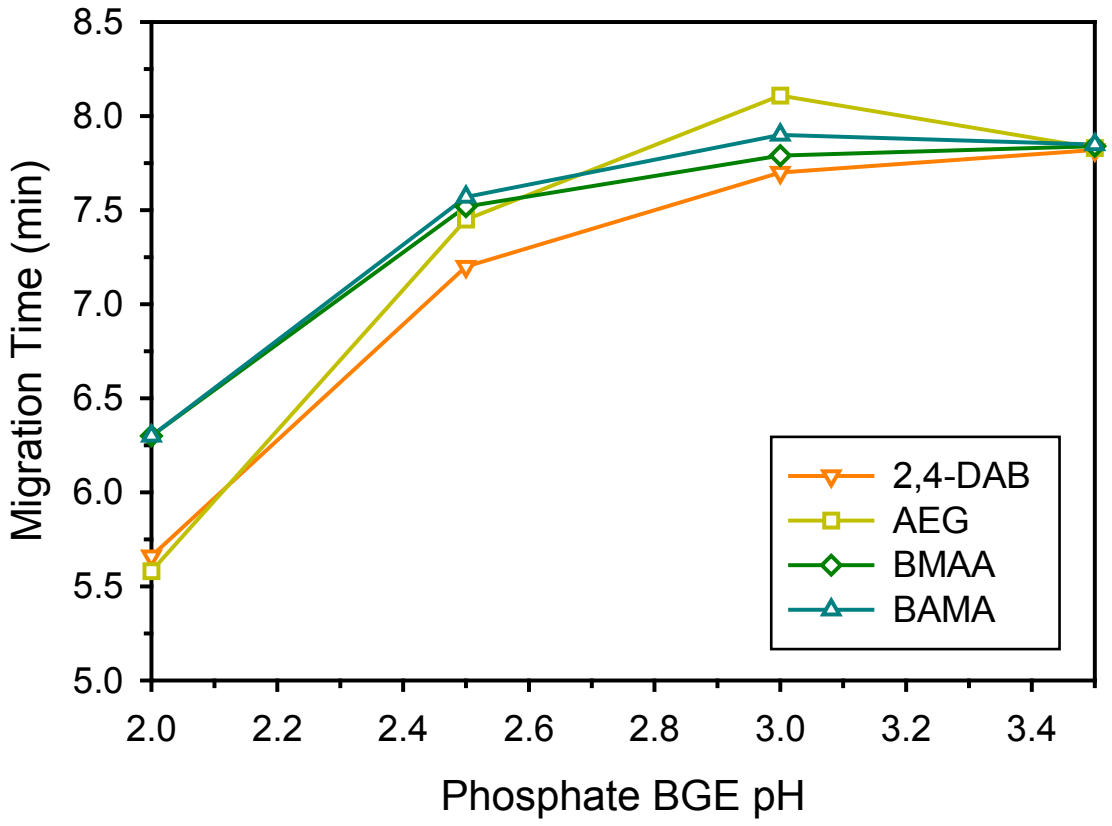

Figure 3.3: The effect of pH on migration times using 250 mM phosphate BGEs

pH values of 2.5 and 2.0, BAMA co-eluted with BMAA. At the time of this experiment, 34DAB was not available but when it was received it was found to be well resolved at most pH (see below). Additives including MeCN, MeOH, isopropanol, and cyclodextrin were explored to test effects on current and resolution but these had no positive effects on the separation. Other conditions were also optimized. Higher BGE concentrations and lower capillary temperatures increased the theoretical plates, preventing BMAA from merging with BAMA. Figure 3.4a shows a separation of mixed standards using the final conditions of phosphate buffer (250 mM, pH 3.0), 17°C capillary temperature, and 25 kV separation voltage. Relatively high sample concentrations (1 mM) were needed for CE-UV because BMAA absorbs UV radiation very weakly and only below 200 nm. The limit of detection observed for BMAA was approximately 0.25 μg mL-1, which translated to 20 mg g-1 (dry weight sample) for the extraction procedure used in this study. While UV detection was not selective or sensitive enough to be used for analysis of real samples (typically ranging from 10 ng g-1 to 100 μg g-1), it did allow for an initial exploration of separation conditions and could in the future be used for purity analysis of standards.

An extract of the mussel tissue reference material, CRM-ASP-Mus, was analyzed with the final CE-UV method to examine the separation of BMAA from co-extracted matrix compounds (Figure 3.4b). Most detected (major) sample components were observed to have migration times very different than that of BMAA and its isomers (Figure 3.4a). With a reported level of ~1.5 μg g^{-1} BMAA [62] in this CRM, however, the level of BMAA in the extract (~40 ng mL^{-1}) was far too low to be detected.

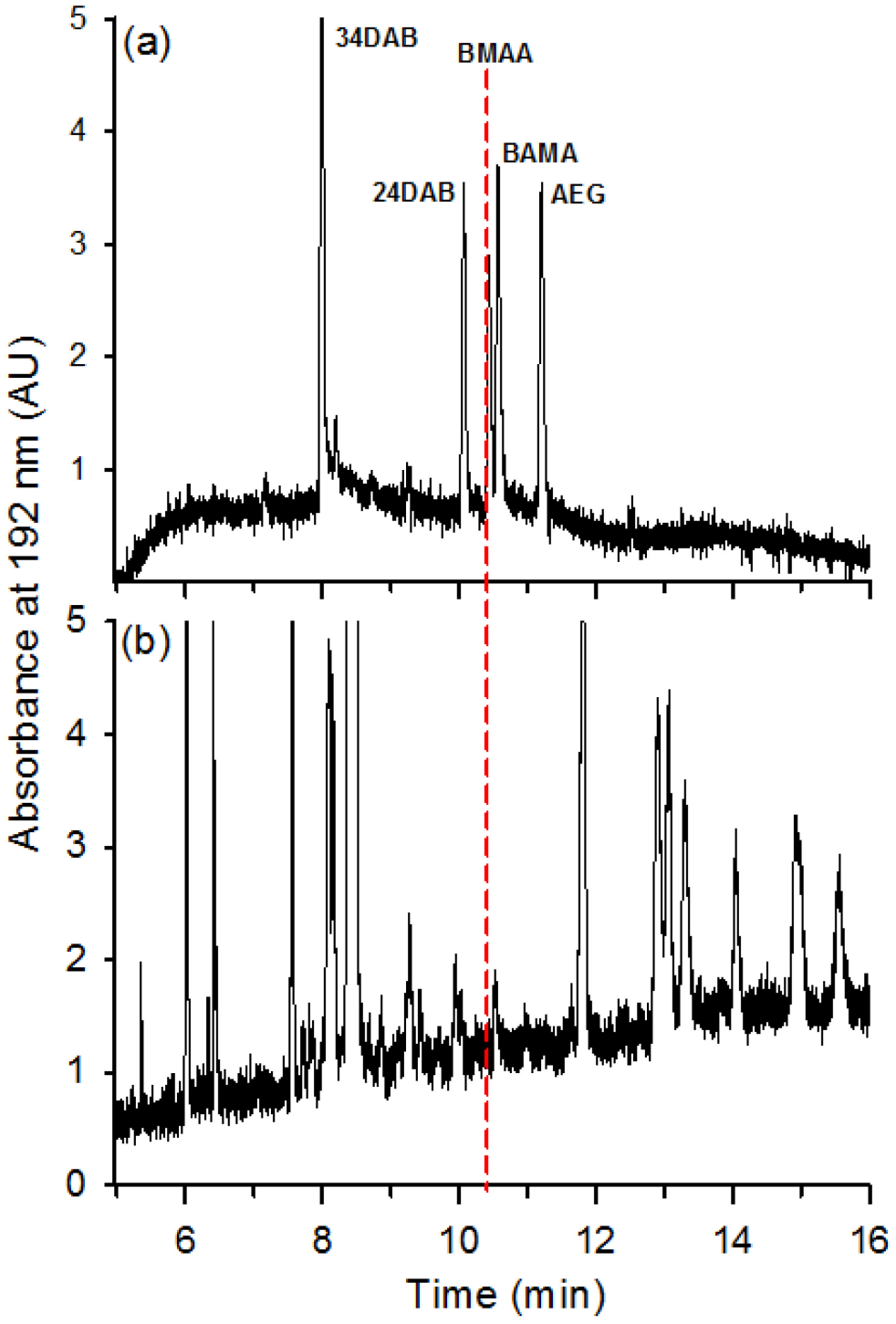

Figure 3.4: Final CE-UV method applied to: (a) a mixed standard at 1 mM each; (b) an extract of CRM-ASP-Mus. The concentration of BMAA in the CRM extract was too low to be detected.

3.4.3 Method Development: BGE for CE-MS

Interfacing CE to MS presents challenges and a number of interface designs have been reported and reviewed [105,108]. A CE system requires a completed circuit to drive the separation while the ESI source is held at high voltage (4-5 kV). A commonly used system is the coaxial sheath flow interface, which introduces an ESI compatible sheath liquid that flows around the end of the capillary and to which the ESI voltage can be applied. This setup does come with the cost of a reduction in signal-to-noise (S/N) due to sample dilution but it is easy to implement. The initial work in this project was performed with a commercially-available interface from Sciex and published by Liu *et al.* [134].

There are restrictions on BGE composition when using MS detection. In particular, a volatile electrolyte is required for optimal ESI performance. Although non-volatile BGEs have been used when EOF was suppressed, frequent system maintenance was required [120–123] and lower S/N from increased spectral background was reported [120,123,124]. These effects can be reduced by using lower concentration BGEs such as <60 mM phosphate [123]. Unfortunately, it has been found through the CE-UV experiments above that a 250 mM phosphate BGE is best for analysis of BMAA. The ionic composition of the sheath liquid is an important consideration, as besides being compatible with ESI, it must also be compatible with the BGE. The sheath acts as the CE outlet reservoir, supplying the counter-ions in order to maintain electro-neutrality in the presence of a current. If the counter ions differ from those in the BGE, a secondary separation environment is created at the cathode, which expands over the course of a run. This environment can have a different conductivity, ionic strength, molecular interactions and pH, and has been reported to cause suppressed or inverted separations [121]. In some cases, these ionic boundaries

can be minimized by using sheath counter-ions with a pKa close to that of the BGE but they were avoided here because the separation was shown with CE-UV to be very sensitive to small changes in pH.

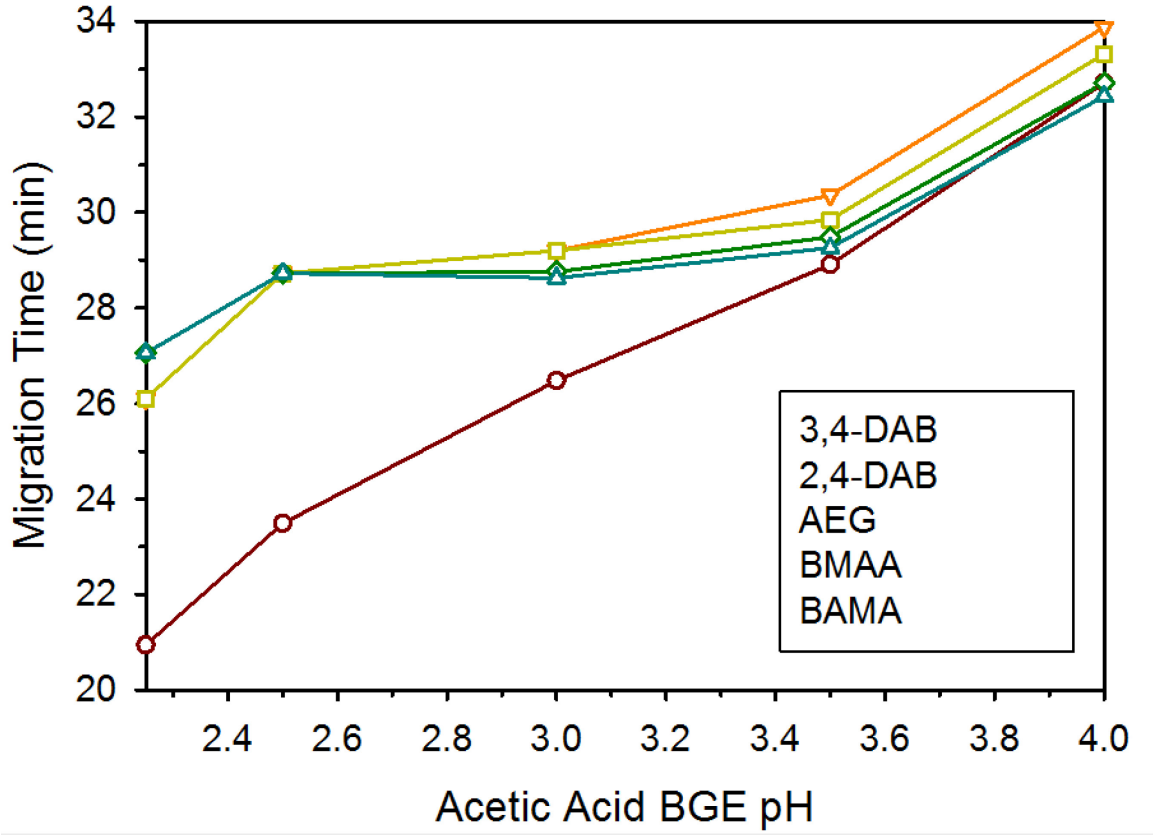

Figure 3.5: Effects of pH on migration times for an acetic acid BGE

Although the phosphate BGE developed for the CE-UV separation could not be used due to its incompatibility with ESI, comparable conditions could be produced using a BGE based on AcOH or FA, since these are fully compatible with ESI. Therefore, experiments began with a 1 M aqueous AcOH BGE (pH 3.0) and a sheath liquid of 0.1% AcOH in 50% aqueous MeOH at 10 μL min^{-1}. Connecting the CE with the MS required the use of a longer 1 m capillary and a lower separation potential of 20 kV to keep the capillary current below 50 μA to avoid damage to the MS electronics. Unfortunately this meant longer migration times of ~30 min. Initial results did show different migration times for the five isomers but the electropherograms were disappointing when compared to the CE-UV results using the pH 3.0 phosphate BGE, showing broad (0.8 min) and tailing peaks which resulted in an overall poor separation. It has been reported that phosphate BGEs often give better performance than other BGEs [120], possibly due to the formation of silanol phosphate complexes on the capillary wall, which are more easily protonated [135]. At low pH this reduces the EOF and analyte-wall adsorption that causes peak tailing. The relative migration order also differed when using the AcOH BGE compared to the phosphate BGE at the same pH. These changes could be attributed to the different electrostatic interactions of analytes with BGE ions that could affect both analyte charge and mobility.

A series of 1 M AcOH BGEs with pHs from 2.25 to 4.0 was produced through addition of HCl or NH4OH and analyte migration times were measured. A 1 M FA BGE (pH 1.9) that had been previously reported for amino acid separations [113] was also included. As shown in Figure 3.5, the same high dependency of migration time on pH was observed with the AcOH BGE as with phosphate but the migration patterns were entirely different,

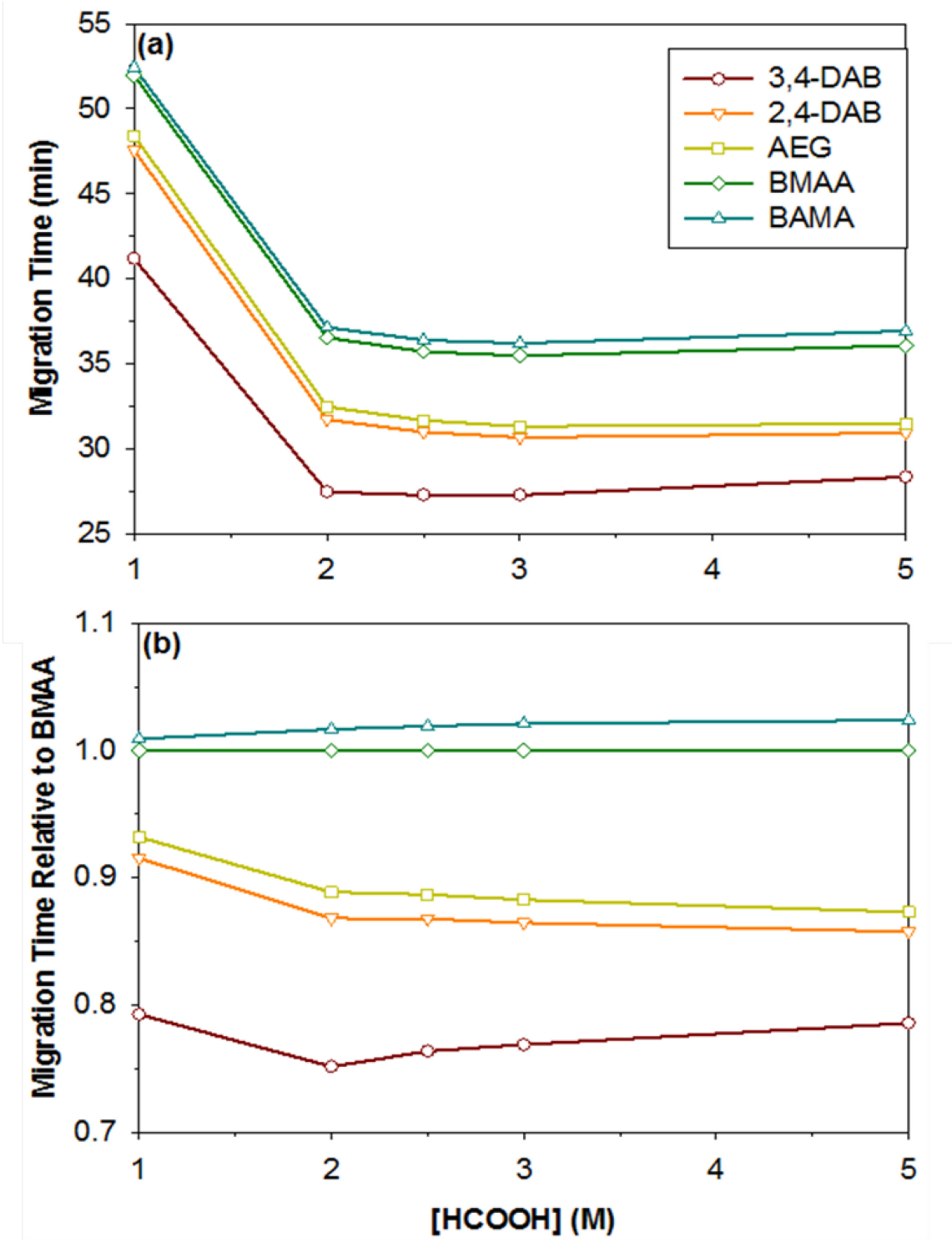

Figure 3.6: Effect of formic acid BGE concentration on migration times

highlighting the importance of the electrostatic interactions. Partial separation of all isomers was observed using an AcOH BGE at pH 3.5 and with the 1 M FA BGE at pH 1.9. The FA electropherogram was superior due to a better resolution of BMAA from the other analytes as well as a five-fold higher theoretical plate count: 21,000 for AcOH and 108,000 for FA. While the addition of MeOH and MeCN had negligible effect on separations, it was noted that 10% organic in the BGE reduced the capillary current by four-fold (48 to 12 μA). This was beneficial as the system was operating near the 50 μA system limit when using a 1 M FA BGE. Addition of 10% MeCN allowed for the exploration of BGEs containing a range of FA concentrations (0.1 to 5 M). Higher BGE concentration of 1 M FA had been reported to provide higher theoretical plate count for different amino acids [113]. There was a concern that high FA concentrations above 1 M might be detrimental to ESI but, as the EOF was negligible compared to the sheath liquid flow, there was a good chance that it would be compatible and this proved true. Theoretical plates and resolution between BMAA and BAMA (the closest analyte pair) increased with FA concentration until 1 M. Subsequent increases in FA concentration gave a slight decrease in plate count; however, the resolution between BMAA and BAMA continued to increase (Figures 3.6 and 3.7). This may be due to reductions in BGE pH, as the changes in BGE pH tend to mirror changes in resolution (Figure 3.7). A 5 M FA BGE containing 10% MeCN was chosen as the BGE, since as the gain in resolution was more than enough to offset any decreases in plate count and offered better stacking potential (see below). This is higher than any other BGE enployed in previouse studies found when reviewing literature for this study. This may be in part due to the detrimental effects that would be experienced if the capillary current was not restricted with organic modifier [135].

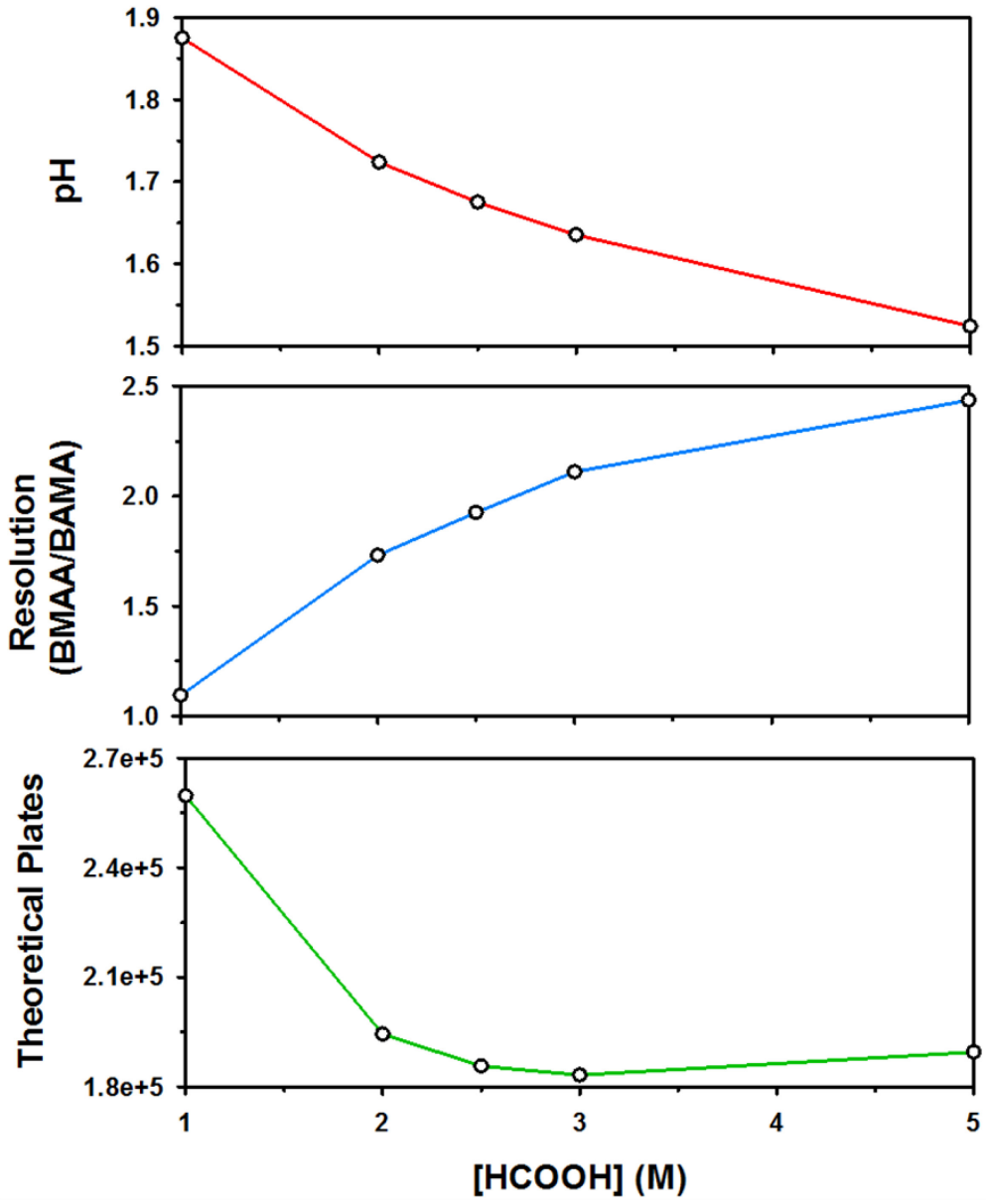

Figure 3.7: Measured pHs, theoretical plate counts and resolution of BMAA and BAMA as a function of formic acid concentration in the BGE.

3.4.4 Method Development: Improved CE-MS Interface

Initially, a commercial CE-MS adaptor [134] was used but it was determined early on that this would not be sufficient for a final method, as it proved to be unreliable and required constant supervision. Frequent partial or complete plugging of the sprayer orifice resulted in backpressure on the capillary, inconsistent increased migration times and broadening peaks, as well as poor ESI sensitivity and signal instability. Sprayer plugging was exaggerated when the ESI was turned on and off, which was required after each run to allow for capillary conditioning to avoid spraying reagents into the system. Several attempts to prevent plugging were made, including degassing and filtering all solvents, cleaning the system, and adding an in-line filter just before where the sheath entered the coaxial sprayer. Additionally, when sheath composition optimization was attempted with this setup, plugging was noticeably more problematic with a 50% MeCN composition. This suggested problems with the capillary polyamide coating dissolving in the sheath. Rather than attempting to strip the polyimide coating from the end portion of the capillary, a new approach was investigated.

A custom interface similar to that first described in 1988 by Smith *et al.* [136] was established and then adapted. In their system, a straight tube was used instead of a tapered tube that encloses the CE capillary [134], thus allowing the capillary to protrude. Such an approach resulted in a lower dead volume, as the Taylor cone formed around the CE capillary end [119]. This arrangement completely eliminated the plugging problems. Figure 3.1 shows the further modifications made in this study. Tapering the CE capillary lowered the dead volume further and allowed placement of the CE capillary exit well into the Taylor cone that emanated from the metal tube, which was also tapered. This helped to

stabilize the ESI spray and allowed a considerably lower sheath flow of 1.5 µL min^{-1} over the original 10 µL min^{-1}. An additional advantage is that a nebulizer gas was not required. While this new setup had many advantages, sprayer construction and optimization was still difficult and time consuming.

The new interface was used to examine sheath liquids composed of 25-80% MeOH, MeCN or *iso*-propanol with 0.1 % FA or ammonium formate additives. A sheath liquid composed of 50% aqueous MeOH with 0.1% FA provided the highest signal to noise for BMAA.

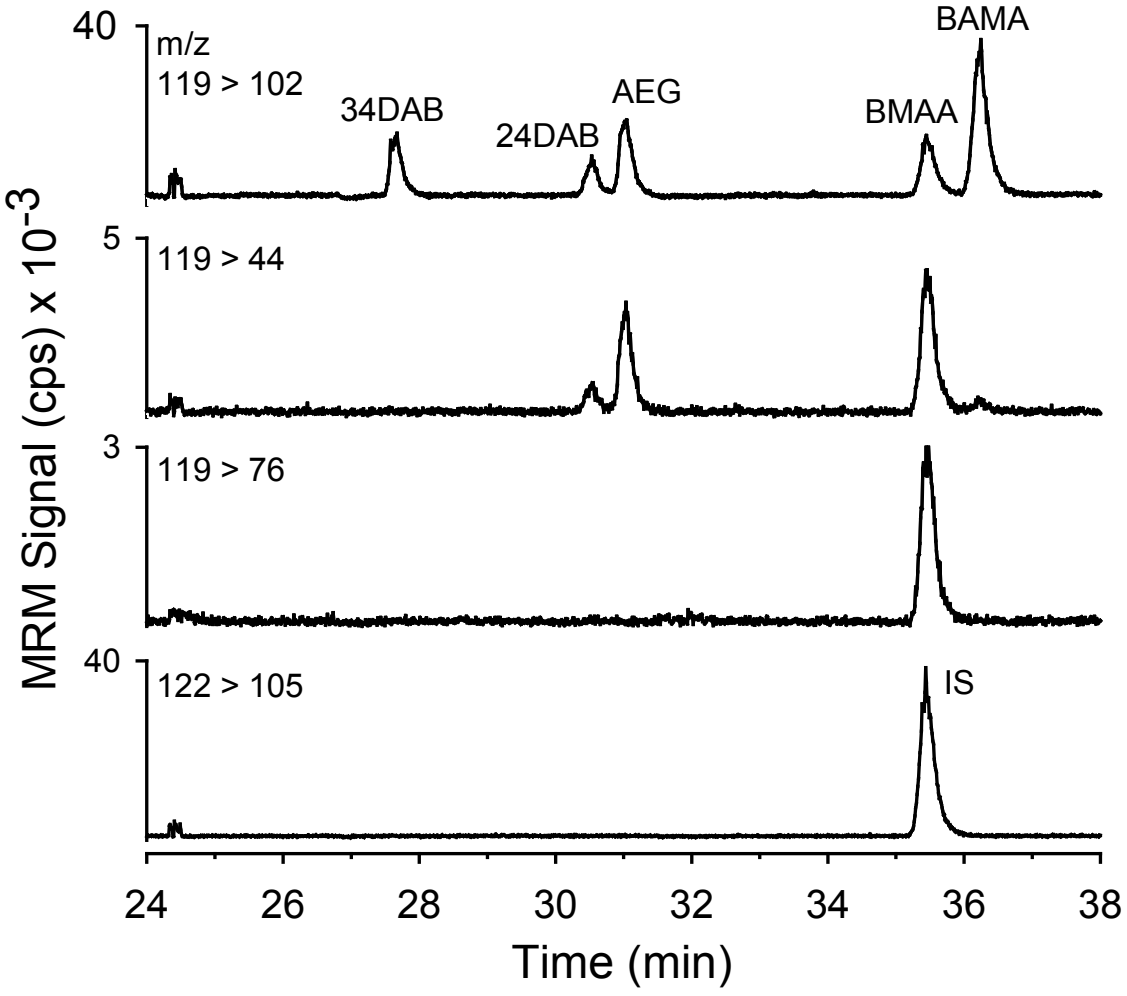

Figure 3.8: CE-MS analysis of a standard mixture using final CE-MS conditions: BGE = 5 M FA with 10% MeCN; separation voltage = 20 kV; injection: 50 mbar for 120 sec; sheath liquid: 1.5 µL/min of MeOH/H2O/FA (50:50:0.1).

3.4.5 Method Evaluation and Application to Samples

The quantitative capabilities of the CE-MS/MS method for BMAA analysis were evaluated using sensitive and selective transitions for BMAA, its four isomers and the stable isotope-labeled standard BMAA-d_3. A strong cation solid phase extraction sample cleanup procedure was used to lower conductivity in order to take advantage of field-amplified stacking [100]. The final step of the cleanup involved re-dissolution in a low conductivity solvent. MeOH was used initially as it provided the best peak shape during experimentation with standards. Unfortunately, extracts diluted in 25% or higher MeOH precipitated out of solution after injection, so a simple 2 mM aqueous HCl solvent was used instead. This still allowed for an injection of 280 seconds at 50 mbar, corresponding to an injection of ≈10% of the total capillary volume, while still maintaining good resolution between BMAA and BAMA. This stacking step actually facilitated a higher separation efficiency with theoretical plate counts up to 360,000 for samples.

Quantitation of BMAA in sample extracts was achieved by spiking with BMAA-d_3 after sample hydrolyses for isotope dilution calibration. This internal standard co-eluted exactly with BMAA, adding additional confidence when assigning peaks. An analysis of mixed standards is shown in Figure 3.8 using the final experimental conditions.

A standard curve of BMAA spiked with a constant level of BMAA-d_3 showed linearity over three orders of magnitude (R=0.9997) when plotted as BMAA/BMAA-d_3 area ratio vs. concentration, Figure 3.9. The LOD for BMAA in solution was estimated to be 0.8 µg mL^{-1} (S/N = 3 definition), which corresponded to an overall method LOD of 20 ng g^{-1} dry

weight sample. This is similar to LODs reported previously for LC-MS/MS methods [62].

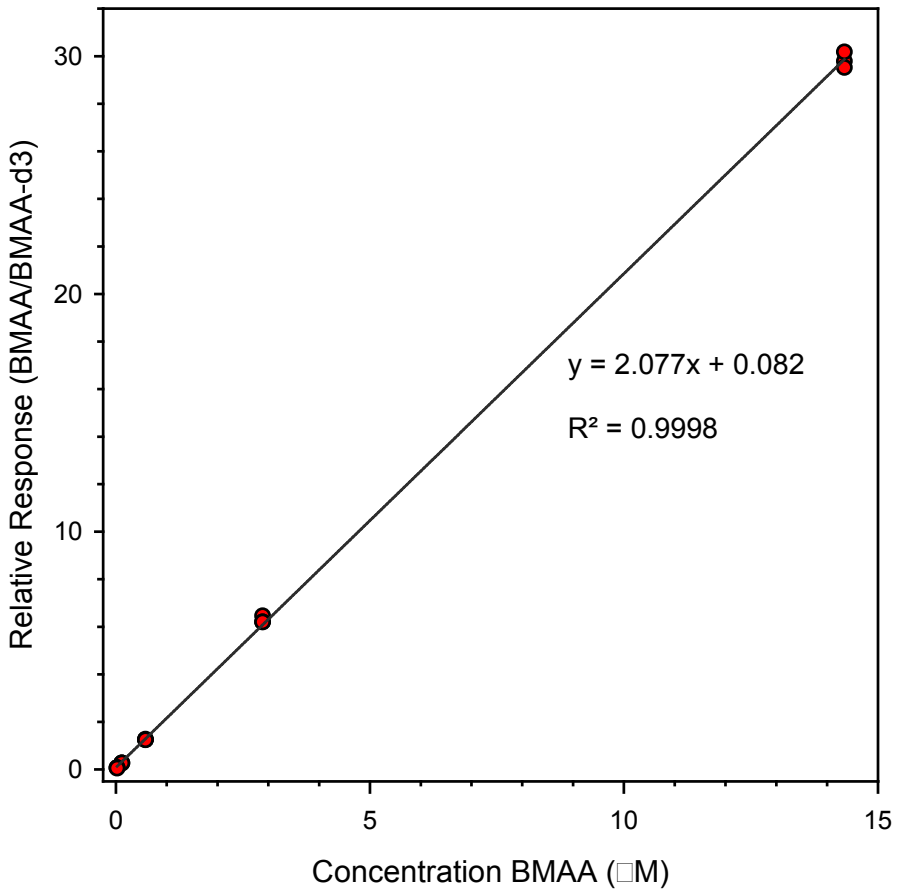

Figure 3.9: Isotope dilution calibration plot showing the ratio of BMAA/ BMAA-d_3 plotted against BMAA concentration

While this was quite satisfactory, there is still considerable potential for lowering the CE-MS LOD further as these experiments were performed on the least sensitive MS in our laboratory.

A sample chromatogram from CRM-ASP-Mus extract is shown in Figure 3.10. Full base line separation of BMAA from other peaks was achieved with no apparent interference from co-extracted matrix compounds. All of the isomers studied were confirmed to be present in this sample, as had been established previously [62]. There also appear to be

other unknown isomeric or isobaric compounds present, which reinforces the need to have the highest possible resolution and selectivity for confident determination of BMAA.

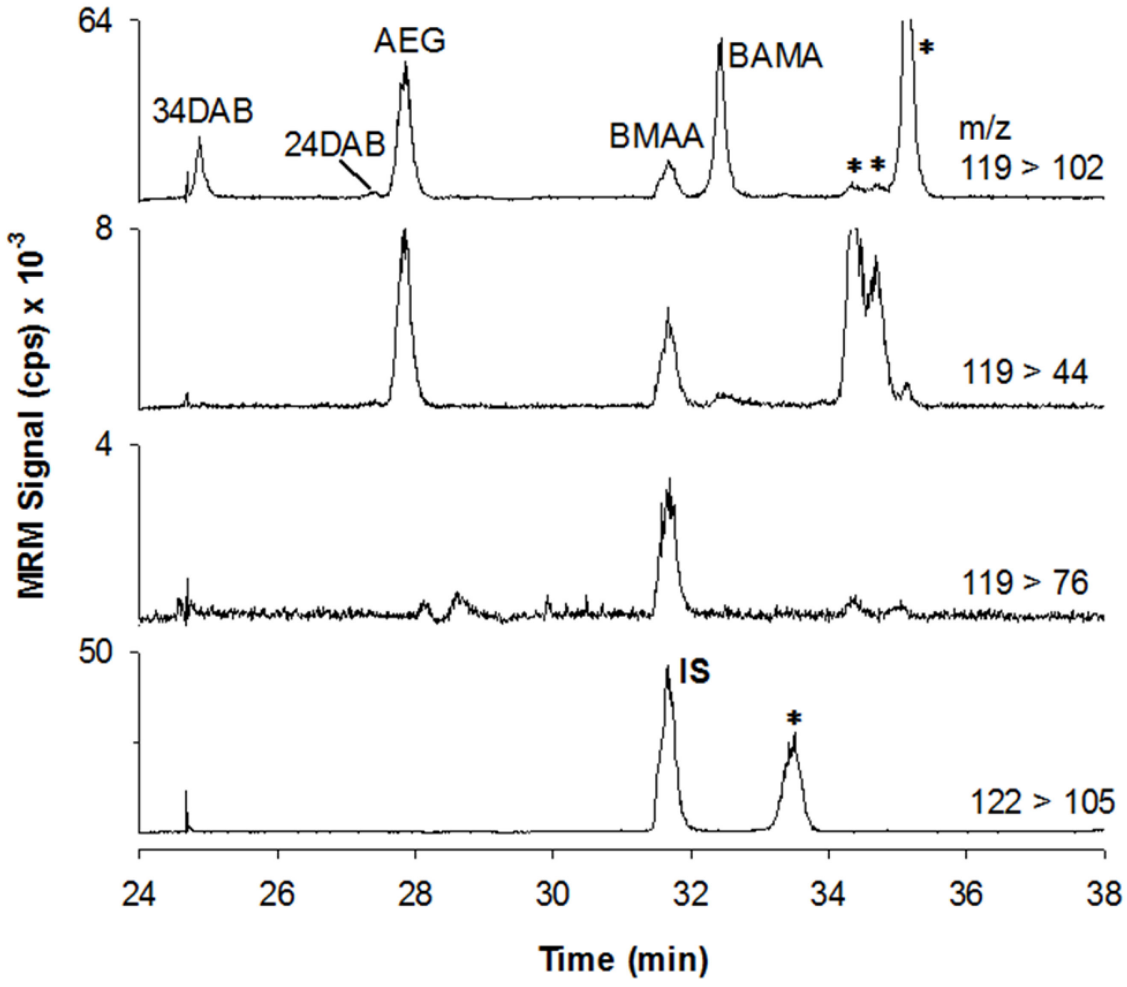

Figure 3.10: CE-MS analysis of a CRM-ASP-Mus extract using the same conditions as in Figure 3.8. The peaks marked with an asterisk are unknown sample components.

Quantitative results from BMAA analysis of selected samples are shown in Table 3.1.

Table 3.1: Quantitative results from final CE-MS method.

Sample	Relative migration time [a]	[BMAA] µg g^{-1} ± sd
CRM-ASP-Mus	1.0000	1.7 ± 0.2
Cycad	1.0000	19.6 ± 0.3
Lobster Tail	0.9994	13.8 ± 0.9
Lobster Tomalley	0.9988	3.4 ± 0.2
RM-BGA	nd [b]	nd [b]

a = BMAA migration time relative to BMAA-d_3 internal standard
b = not detected (less than 70 ng g^{-1})

As reported previously [62], BMAA was not detected in the cyanobacterial in-house reference material (RM-BGA) but was present at expected levels in cycad leaves and the CRM-ASP-Mus reference material. The result of 1.7 ± 0.2 µg g^{-1} for the latter compares fairly well with a previously reported value of 1.2 ± 0.3 µg g^{-1} as determined by HILIC-DMS-MS/MS [62], despite having different extraction and cleanup procedures. BMAA was also detected in both the tail meat and tomalley of a lobster specimen, which is consistent with recent findings [68].

3.5 Current Work

As the CE-MS/MS method was developed to be complementary to the HILIC-DMS-MS/MS method described in Chapter 2, a survey is currently underway in order to compare the effectiveness of both methods in a variety of tissue matrices. Freeze-dried samples listed in Table 3.2 were extracted as described in this Chapter and HILIC-DMS-MS/MS analysis was carried out as described in Chapter 2. CRM-FDMT was extracted in triplicate

to assess extraction variability. Three additional CRM-FDMT extracts were spiked prior to hydrolysis in order to assess the stability of the internal standard and by extension BMAA during the hydrolysis. The HILIC-DMS-MS/MS results are listed in Table 3.2. Unfortunately, there were problems with the MS system that prevented the acquisition of CE-MS/MS results in time for this thesis.

Table 3.2: Preliminary BMAA survey of aquatic matrices using HILIC-DMS-MS/MS

Sample	[BMAA] μg g^{-1}	sd*
CRM-FDMT d_3 spike after hydrolysis	4.7	0.5
CRM-FDMT d_3 spike after hydrolysis	4.5	0.3
CRM-FDMT d_3 spike after hydrolysis	4.5	0.3
CRM-FDMT d_3 spike before hydrolysis	5.0	0.5
CRM-FDMT d_3 spike before hydrolysis	5.4	0.8
CRM-FDMT d_3 spike before hydrolysis	5.3	0.4
Cycad	47	3
Lobster tail	11	1
Lobster Tomalley	3.2	0.2
Canned Lobster #1	4.6	0.3
Canned Lobster #2	1.6	0.1
Alaskan king crab	7.1	0.4
RMBGA	nd	nd
Cefas PO PST CRM1101-02939	2.2	0.1
Blowfish BI020402	nd	nd
CFIA Hot Clams	21.9	2.2
Scallop Tissue	10.8	0.9

* standard deviation from 3 replicate injections of each single sample prep

nd = not detected below LOD of 2 ng g^{-1}

A reduced LOD at 2 ng g^{-1} for the HILIC-DMS-MS/MS method was achieved through the use of the cleanup procedure, which provided a 2.5-fold pre-concentration and allowed a 5 μL injection . As expected, the HILIC-DMS-MS/MS method was able to

quantify BMAA in a variety of matrices without interference. The extraction procedure seems to have been fairly consistent, as all replicate samples are in good agreement. Some BMAA degradation appears to have occurred during sample hydrolysis but pre-spiking with an internal standard seems to have corrected for loss. Spiking prior to extraction will be incorporated into the final procedure. Samples listed are currently stored at -80 °C awaiting the CE-MS/MS repair.

3.6 Conclusion

A new analytical method with a separation selectivity that is complementary to previously reported liquid chromatography methods has been developed for the analysis of BMAA. Four isomers of BMAA were used for development and testing of the method. During optimization, each isomer demonstrated the potential for interference and all of them were in fact found to be present in various natural samples tested. Furthermore, unidentified isomeric or isobaric compounds were observed in mussel tissue matrices that have the potential to interfere with less selective methods.

Coupling CE with MS proved challenging. Initial efforts with a commercial interface produced results but suffered from plugging problems and only moderate sensitivity. The development of an in-house CE-MS interface helped to increase sensitivity and reliability.

Work is continuing on alternative extraction and cleanup methods, additional sample pre-concentration, full validation of this CE-MS method, and an extensive inter-comparison of methods for the determination of BMAA in various matrices. CE-MS will also play an important role in the current development of certified reference materials for BMAA determination at the National Research Council of Canada.

CHAPTER 4: CONCLUSIONS AND FUTURE WORK

Two novel complementary methods for the detection of underivatized BMAA were developed. The first method utilized DMS as an ion filter to create a powerful multi-dimensional HILIC-DMS-MS/MS analytical method. In order to achieve separation for BMAA from BAMA and other isomers, system modification was necessary to allow accurate control of low concentrations of acetonitrile modifier in the DMS carrier gas. This simple modification may be equally effective in other fields where the manufacturer's restrictions placed on the concentration of modifier could also have limited the utility of the device. DMS implementation was found to remove chemical noise from both ESI background and matrix compounds, allowing for a LOD of 20 ng g^{-1} dry weight, similar to chromatographic techniques that employed derivatization and sample clean-up [64]. As shown in Chapter 3, a sample cleanup led to a further decrease in the LOD to 2 ng g^{-1} by allowing for sample pre-concentration and larger injection volumes. Further improvements will be implemented by the NRC team in an upcoming project and will be included in the final validated method.

The second method employed CE as a separation technique complementary to liquid chromatography. This included the development of an in-house CE-MS interface that was more reliable than the commercial alternative. Excellent separation of BMAA from its various isomers and other sample co-extractives was achieved. The LOD for BMAA in solution was estimated to be 0.8 μg mL^{-1} (S/N = 3 definition), which corresponded to an overall method LOD of 20 ng g^{-1} dry weight sample with the cleanup method described. There remains some potential for improving the LOD through the use of a more sensitive mass spectrometer. Additionally, work is currently underway exploring alternative

extraction and cleanup methods, as well as additional sample pre-concentration. Some preliminary experiments have been conducted with a TSKgel Amide-80 stationary phase in SPE format and this showed better sample loading capabilities and ease of use than the OASIS-MCX cartridge. This procedure has the potential benefit of providing an additional dimension of selectivity similar to that of HILIC separation described in Chapter 2. If successful, these improvements will become incorporated into the final validated CE-MS method by the NRC team.

In both studies, four isomers of BMAA that had been predicted [61] to have the most potential for interference were used for development and testing, which was more than any previous study. During optimization, each isomer was shown to have the potential for interference in both analytical techniques and all of them were in fact found to be present in various natural samples tested. If not properly addressed, their presence could have led to inaccurate quantitation. As there were no previous reports of some of these isomers, it is not unreasonable to conclude that they may have been partially responsible for some of the positive findings in some studies. Furthermore, other unidentified isobaric/isomeric compounds of BMAA and the internal standard were detected in mussel and lobster matrices and these could also interfere with less selective techniques.

Both optimized methods were used to analyze a variety of matrix samples as well as commercially available reference materials. Measurements of the mussel tissue CRM-ASP-Mus were in rough agreement (1.2 ± 0.2 via HILIC-DMS-MS/MS and 1.7 ± 0.2 via CE-MS/MS) despite having different extraction and cleanup procedures. Results on cycad leaves were different (39 ± 1 via HILIC-DMS-MS/MS and 19.6 ± 0.3 via CE-MS/MS) but this was to be expected as samples were taken from different plant loci at different times.

Unfortunately at the current time these are the only samples analyzed by both methods. Work was initiated to survey a variety of tissue matrices in order to compare the effectiveness of both methods. Unfortunately, instrumentation failure coupled with time restraints limited the current results to HILIC-DMS-MS/MS only. A cross comparison of these methods should be completed before proceeding with validation.

After both methods have been fully validated, they will be used for the certification of a cyanobacterial matrix certified reference material (CRM) at the National Research Council. Such a CRM will allow others to evaluate the accuracy of their in-house methods, to establish measurement traceability, and to conduct routine QA/QC on their measurements. As BMAA was successfully detected in the previously produced CRM-ASP-Mus, assigning a certified concentration for this material may be considered. This matrix was shown to have other potentially interfering isomers/isobars present and may be a sufficiently challenging CRM for validation of analytical techniques in other laboratories.

Future work may include chemical derivatization followed by CE-UV and/or CE-MS/MS analyses. This offers the possibility of increased sensitivity and selectivity. Some preliminary experiments with different reagents such as AQC and dansyl chloride have shown promising results and will be pursued in further studies outside of this thesis. Additionally a CE-MS/MS method could be implemented to check for potentially interfering matrix components not resolved with RPLC separation.

One last possibility for future research is a search for various conjugated forms of BMAA such as peptide- or protein-bound forms as some have predicted [137], in complexes with metals [138], or in carbonate complexes [133]. There is also the possibility of metabolites such as glycosides, glucuronides, etc. being present in animal tissues. CE is selective

enough to resolve most matrix components without preventing passage to the mass spectrometer. This offers the unique possibility to search for conjugated forms of BMAA in non-hydrolysed extracts via techniques such as precursor ion and neutral loss scans.

BIBLIOGRAPHY

[1] L.P. Rowland, N.A. Shneider, Amyotrophic lateral sclerosis, New Engl. J. Med. Med. 344 (2001) 1688–1700.

[2] A.E. Renton, A. Chiò, B.J. Traynor, State of play in amyotrophic lateral sclerosis genetics., Nat. Neurosci. 17 (2014) 17–23. doi:10.1038/nn.3584.

[3] W.G. Bradley, D.C. Mash, Beyond Guam: the cyanobacteria/BMAA hypothesis of the cause of ALS and other neurodegenerative diseases, Amyotroph. Lateral Scler. 10 Suppl 2 (2009) 7–20. doi:10.3109/17482960903286009.

[4] D. Mulder, L.T. Kurland, L.L. Iriarte, Neurological Diseases on Guam, Mayo Clin. (1954) 1724–39.

[5] D. Koerner, Amyotrophic lateral sclerosis on Guam: a clinical study and review of the literature, Ann. Intern. Med. 37 (1952) 1204–1220.

[6] A. Arnold, D.C. Edgren, V.S. Palladino, Amyotrophic lateral sclerosis; fifty cases observed on Guam, J. Nerv. Ment. Dis. 117 (1953) 135–139.

[7] P.S. Spencer, P.B. Nunn, J. Hugon, a C. Ludolph, S.M. Ross, D.N. Roy, R.C. Robertson, Guam amyotrophic lateral sclerosis-parkinsonism-dementia linked to a plant excitant neurotoxin., Science. 237 (1987) 517–522. doi:10.1126/science.3603037.

[8] R.M. Garruto, R. Yanagihara, D.C. Gajdusek, Models of environmentally induced neurological disease: epidemiology and etiology of amyotrophic lateral sclerosis and parkinsonism-dementia in the Western Pacific, Environ. Geochem. Health. 12 (1990) 137–151. doi:10.1007/BF01734063.

[9] C.C. Plato, Amyotrophic Lateral Sclerosis and Parkinsonism-Dementia Complex of Guam: Changing Incidence Rates during the Past 60 Years, Am. J. Epidemiol. 157 (2003) 149–157. doi:10.1093/aje/kwf175.

[10] J. Mcconnell, Cyanobacteria, cycads, Chiroptera, and the Chamorro, Newdesk. 4 (2004) 2004.

[11] A. Hirano, L. Kurland, R. Krooth, S. Lessell, Parkinsonism-Dementia Complex, an Endemic Disease on the Island Of Guam I. Clinical Features, Brain. 84 (1961) 642–661.

[12] A. Hirano, L.T. Kurland, R.S. Krooth, S. Lessell, Parkinsonism-dementia complex, an endemic disease on the island of guam: II. Pathological Features, Brain. 84 (1961) 642–661. doi:10.1093/brain/84.4.642.

[13] U. Prasad, L.T. Kurland, Arrival of new diseases on Guam: lines of evidence suggesting the post-Spanish origins of ALS and Parkinson's dementia, J. Pac. Hist. 32 (1997) 217–228.

[14] H.R. Morris, S. Al-Sarraj, C. Schwab, K. Gwinn-Hardy, J. Perez-Tur, N.W. Wood,

J. Hardy, A.J. Lees, P.L. McGeer, S.E. Daniel, J.C. Steele, A clinical and pathological study of motor neurone disease on Guam., Brain. 124 (2001) 2215–22. http://www.ncbi.nlm.nih.gov/pubmed/11673323.

[15] K. Oyanagi, T. Makifuchi, T. Ohtoh, K.C.T. Van Der Schaaf, D.C. Gajdusek, T.N. Chase, Amyotrophic lateral sclerosis of Guam : the nature of the neuropathological findings, Acta Neuropathol. (1994) 405–412.

[16] P.S. Spencer, Guam ALS / Parkinsonism-Dementia : A Long-Latency Neurotoxic Disorder Caused by " Slow Toxin (s)" in Food ?, Can. J. Neurol. Sci. 14 (1987) 347–357.

[17] F. Gros-Louis, C. Gaspar, G.A. Rouleau, Genetics of familial and sporadic amyotrophic lateral sclerosis, Biochim. Biophys. Acta. 1762 (2006) 956–72. doi:10.1016/j.bbadis.2006.01.004.

[18] M.W. Duncan, J.C. Steele, I.J. Kopin, S.P. Markey, 2-Amino-3-(methylamino)propanoic acid (BMAA) in cycad flour: An unlikely cause of amyotrophic lateral sclerosis and parkinsonism-dementia of Guam, Neurology. 40 (1990) 767–772.

[19] S. Yoshida, Y. Uebayashi, T. Kihira, J. Kohmoto, I. Wakayama, S. Taguchi, Y. Yase, Epidemiology of motor neuron disease in the Kii Peninsula of Japan, 1989-1993: Active or disappearing focus?, J. Neurol. Sci. 155 (1998) 146–155. doi:10.1016/S0022-510X(97)00300-6.

[20] D.C. Gajdusek, A.M. Salazar, Amyotrophic lateral sclerosis and parkinsonian syndromes in high incidence among the Auyu and Jakai people of West New Guinea, Neurology. 32 (1982) 107–126.

[21] P.G. Ince, G. Codd, Return of the cycad hypothesis - does the amyotrophic lateral sclerosis/parkinsonism dementia complex (ALS/PDC) of Guam have new implications for global health?, Neuropathol. Appl. Neurobiol. 31 (2005) 345–53. doi:10.1111/j.1365-2990.2005.00686.x.

[22] J.C. Steele, P.L. McGeer, The ALS/PDC syndrome of Guam and the cycad hypothesis, Neurology. 70 (2008) 1984–1990. doi:10.1212/01.wnl.0000312571.81091.26.

[23] R.M. Garruto, D.C. Gajdusek, K. Chen, Amyotrophic lateral sclerosis and parkinsonism-dementia among Filipino migrants to Guam, Ann Neurol. 10 (1981) 341–350.

[24] J. Torres, L.L. Iriarte, L.T. Kurland, Amyotrophic Lateral Sclerosis Among Guamanians in California, Calif. Med. 86 (1957) 385–388.

[25] R.M. Garruto, D.C. Gajdusek, K. Chen, Amyotrophc Lateral Sclerosis among Chamorro Migrants from Guam, Ann. Neurol. 8 (1980) 612–619.

[26] J.A. Brody, A.H. Edgar, M.M. Gillespie, Amyotrophic Lateral Sclerosis No Increase Among US Construction Workers in Guam, JAMA. 240 (1978) 551–552.

[27] P.A. Cox, O.W. Sacks, Cycad neurotoxins, consumption of flying foxes, and ALS-PDC disease in Guam, Neurology. 58 (n.d.) 956–959. http://cat.inist.fr/?aModele=afficheN&cpsidt=13576002 (accessed February 22, 2016).

[28] D.E. Kohne, C.J. Gibbs, L. White, S.M. Tracy, W. Meinke, R.A. Smith, Virus detection by nucleic acid hybridization: Examination of normal and ALS tissues for the presence of poliovirus, J. Gen. Virol. 56 (1981) 223–233.

[29] D.C. Mash, Cyanobacterial toxins in neurodegeneration, Am. Acad. Neurol. 14 (2008) 138–149.

[30] Y. Yase, S. Yoshida, T. Kihira, I. Wakayama, J. Komoto, Kii ALS dementia, Neuropathology. 21 (2001) 105–109. doi:10.1046/j.1440-1789.2001.00303.x.

[31] K. Kikugawa, R. Nakano, T. Inuzuka, Y. Kokubo, Y. Narita, S. Kuzuhara, S. Yoshida, S. Tsuji, A missense mutation in the SOD1 gene in patients with amyotrophic lateral sclerosis from the Kii Peninsula and its vicinity, Japan, Neurogenetics. 1 (1997) 113–115.

[32] S. Lattante, A. Conte, M. Zollino, M. Luigetti, A. Del Grande, G. Marangi, A. Romano, A. Marcaccio, E. Meleo, G. Bisogni, P.M. Rossini, M. Sabatelli, Contribution of major amyotrophic lateral sclerosis genes to the etiology of sporadic disease, Neurology. 79 (2012) 66–72. doi:10.1212/WNL.0b013e31825dceca.

[33] C.J. Gibbs, D.C. Gajdusek, Amyotrophic lateral sclerosis, Parkinson's disease, and the amyotrophic lateral sclerosis-Parkinsonism-dementia complex on Guam: a review and summary of attempts to demonstrate infection as the aetiology, J. Clin. Pathol. Suppl. (R. Coll. Pathol). 25 (1972) 132–40. doi:10.1136/jcp.s3-6.1.132.

[34] J.A. Brody, A. Hirano, R.M. Scott, Recent neuropathologic observations in amyotrophic lateral sclerosis and parkinsonism-dementia of Guam, Neurology. 21 (1971) 528–536.

[35] E.J. Kasarskis, L. Tandon, M. a Lovell, W.D. Ehmann, Aluminum, calcium, and iron in the spinal cord of patients with sporadic amyotrophic lateral sclerosis using laser microprobe mass spectroscopy: a preliminary study., J. Neurol. Sci. 130 (1995) 203–8. http://www.ncbi.nlm.nih.gov/pubmed/8586987.

[36] B. Mjoberg, E. Hellquist, H. Mallmin, U. Lindh, Aluminum, Alzheimer's disease and bone fragility, Acta. Orthop. Scand. 68 (1997) 511–514. doi:10.3109/17453679708999016.

[37] F.O. Johnson, W.D. Atchison, The role of environmental mercury, lead and pesticide exposure in development of amyotrophic lateral sclerosis, Neurotoxicology. 30 (2009) 761–765. doi:10.1016/j.neuro.2009.07.010.

[38] H. Nagata, S. Miyata, S. Nakamura, M. Kameyama, Y. Katsui, Heavy metal concentrations in blood cells in patients with amyotrophic lateral sclerosis, J. Neurol. Sci. 67 (1985) 173–8. http://www.ncbi.nlm.nih.gov/pubmed/3981218.

[39] F. Yoshimasu, M. Yasui, Y. Yase, Y. Uebayashi, S. Tanaka, S. Iwata, S. Sazuhisa, C. Gajdusek, C.J. Gibbs, K.-M. Chen, Studies on Amyotrophic Lateral Sclerosis by Neutron Activation Analysis-2. Comparative Study of Analytical Results on Guam, Folia Psychiatr. Neurol. 34 (1980).

[40] F. Yoshimasu, M. Yasui, Y. Yase, Y. Uebayashi, S. Tanaka, S. Iwata, S. Sazuhisa, C. Gajdusek, C.J. Gibbs, K.-M. Chen, Studies on Amyotrophic Lateral Sclerosis by Neutron Activation Analysis-3. Systematic Analysis of Metals on Guamanian ALS and PD Cases, Folia Psychiatr. Neurol. 36 (1982).

[41] M.G. Whiting, Toxicity of cycads, Econ. Bot. 17 (1963) 270–302. doi:10.1007/BF02860136.

[42] A. Vega, E. Bell, α-amino-β-methylaminopropionic acid, a new amino acid from seeds of Cycas czrcznal, Phytochemistry. 6 (1967) 759–762.

[43] P.A. Cox, S. Banack, S. Murch, O. Sacks, Commentary on: return of the cycad hypothesis ? does the amyotrophic lateral sclerosis/Parkinsonism dementia complex (ALS/PDC) of Guam have new implications for global health?, Neuropathol. Appl. Neurobiol. 32 (2006) 679–682. doi:10.1111/j.1365-2990.2006.00796.x.

[44] V.T. Karamyan, R.C. Speth, Animal models of BMAA neurotoxicity : A critical review, 82 (2008) 233–246. doi:10.1016/j.lfs.2007.11.020.

[45] M.A. Al-Sammak, D.G. Rogers, K.D. Hoagland, Acute β-N-methylamino-L-alanine toxicity in a mouse model, J. Toxicol. 2015 (2015) 1–9. doi:10.1155/2015/739746.

[46] M. Lee, P.L. McGeer, Weak BMAA toxicity compares with that of the dietary supplement beta-alanine, Neurobiol. Aging. 33 (2012) 1440–1447. doi:10.1016/j.neurobiolaging.2010.11.024.

[47] V. le Verche, B. Ikiz, A. Jacquier, S. Przedborski, D.B. Re, Glutamate pathway implication in amyotrophic lateral sclerosis: What is the signal in the noise?, J. Receptor. Ligand Channel Res. 4 (2011) 1–22. doi:10.2147/JRLCR.S6504.

[48] X. Liu, T. Rush, J. Zapata, D. Lobner, β-N-methylamino-L-alanine induces oxidative stress and glutamate release through action on system Xc(-), Exp. Neurol. 217 (2009) 429–33. doi:10.1016/j.expneurol.2009.04.002.

[49] S. Lopicic, M. Stanojevic, P. Dhruba, D. Pavlovic, M. Prostran, V. Nedeljkov, Excitatory amino acid β-N-methylamino-L-alanine is a putative environmental neurotoxin, J. Serbian Chem. Soc. 76 (2011) 479–490. doi:10.2298/JSC100629047L.

[50] S.A. Banack, H.E. Johnson, R. Cheng, P.A. Cox, F.O. Paper, Production of the neurotoxin BMAA by a marine cyanobacterium, Mar. Drugs. 5 (2007) 180–196. doi:10.3390/md504180.

[51] E.D. Brenner, D.W. Stevenson, R.W. McCombie, M.S. Katari, S. Rudd, K.F.X. Mayer, P.M. Palenchar, S.J. Runko, R.W. Twigg, G. Dai, R. Martienssen, P.N.

Benfey, G.M. Coruzzi, Expressed sequence tag analysis in Cycas, the most primitive living seed plant, Genome Biol. 4 (2003) R78. doi:10.1186/gb-2003-4-12-r78.

[52] T.E. Marler, L.R. Snyder, C.A. Shaw, Toxicon Cycas micronesica (Cycadales) plants devoid of endophytic cyanobacteria increase in β-methylamino-alanine, Toxicon. 56 (2010) 563–568. doi:10.1016/j.toxicon.2010.05.015.

[53] S.A. Banack, P.A. Cox, Biomagnification of cycad neurotoxins in flying foxes: implications for ALS-PDC in Guam, Neurology. 61 (2003) 387–389. doi:10.1212/01.WNL.0000078320.18564.9F.

[54] P.A. Cox, S.A. Banack, S.J. Murch, Biomagnification of cyanobacterial neurotoxins and neurodegenerative disease among the Chamorro people of Guam., Proc. Natl. Acad. Sci. U. S. A. 100 (2003) 13380–3. doi:10.1073/pnas.2235808100.

[55] S.J. Murch, P.A. Cox, S.A. Banack, A mechanism for slow release of biomagnified cyanobacterial neurotoxins and neurodegenerative disease in Guam, Proc. Natl. Acad. Sci. U. S. A. 101 (2004) 12228–12231. doi:10.1073/pnas.0404926101.

[56] P.A. Cox, S.A. Banack, S.J. Murch, U. Rasmussen, G. Tien, R.R. Bidigare, J.S. Metcalf, L.F. Morrison, G.A. Codd, B. Bergman, Diverse taxa of cyanobacteria produce β-methylamino-alanine, a neurotoxic amino acid, Proc. Natl. Acad. Sci. U. S. A. 102 (2005) 5074–5078. doi:10.1073/pnas.0501526102.

[57] J. Rosén, K.-E. Hellenäs, Determination of the neurotoxin BMAA (β-N-methylamino-L-alanine) in cycad seed and cyanobacteria by LC-MS/MS (liquid chromatography tandem mass spectrometry), Analyst. 133 (2008) 1785–1789. doi:10.1039/b809231a.

[58] E.J. Faassen, Presence of the neurotoxin BMAA in aquatic ecosystems: what do we really know?, Toxins (Basel). 6 (2014) 1109–38. doi:10.3390/toxins6031109.

[59] J. Rosen, E. Westerberg, S. Schmiedt, K.E. Hellenas, BMAA detected as neither free nor protein bound amino acid in blue mussels, Toxicon. 109 (2016) 45–50. doi:10.1016/j.toxicon.2015.11.008.

[60] D. Réveillon, V. Séchet, P. Hess, Z. Amzil, Systematic detection of BMAA (β-N-methylamino-l-alanine) and DAB (2,4-diaminobutyric acid) in mollusks collected in shellfish production areas along the French coasts, Toxicon. 110 (2016) 35–46. doi:10.1016/j.toxicon.2015.11.011.

[61] L. Jiang, B. Aigret, W.M. De Borggraeve, Z. Spacil, L.L. Ilag, Selective LC-MS/MS method for the identification of BMAA from its isomers in biological samples, Anal. Bioanal. Chem. 403 (2012) 1719–30. doi:10.1007/s00216-012-5966-y.

[62] D.G. Beach, E.S. Kerrin, M.A. Quilliam, Selective quantitation of the neurotoxin BMAA by use of hydrophilic-interaction liquid chromatography–differential

mobility spectrometry–tandem mass spectrometry (HILIC–DMS–MS/MS), Anal. Bioanal. Chem. 407 (2015) 8397–8409. doi:10.1007/s00216-015-9012-8.

[63] P. McCarron, A.C. Logan, S.D. Giddings, M. Quilliam, Analysis of β-N-methylamino-L-alanine (BMAA) in spirulina-containing supplements by liquid chromatography-tandem mass spectrometry, Aquat. Biosyst. 10 (2014) 5. doi:10.1186/2046-9063-10-5.

[64] M. Lampinen Salomonsson, A. Hansson, U. Bondesson, Development and in-house validation of a method for quantification of BMAA in mussels using dansyl chloride derivatization and ultra performance liquid chromatography tandem mass spectrometry, Anal. Methods. 5 (2013) 4865. doi:10.1039/c3ay40657a.

[65] E.J. Faassen, F. Gillissen, M. Lürling, A comparative study on three analytical methods for the determination of the neurotoxin BMAA in cyanobacteria, PLoS One. 7 (2012) e36667. doi:10.1371/journal.pone.0036667.

[66] T. Krüger, B. Mönch, S. Oppenhäuser, B. Luckas, LC-MS/MS determination of the isomeric neurotoxins BMAA (beta-N-methylamino-L-alanine) and DAB (2,4-diaminobutyric acid) in cyanobacteria and seeds of Cycas revoluta and Lathyrus latifolius, Toxicon. 55 (2010) 547–57. doi:10.1016/j.toxicon.2009.10.009.

[67] S.A. Banack, T. Caller, P. Henegan, J. Haney, A. Murby, J.S. Metcalf, J. Powell, P. Alan, E. Stommel, Detection of cyanotoxins, β-N-methylamino-L-alanine and microcystins, from a lake surrounded by cases of amyotrophic lateral sclerosis, Toxins (Basel). 7 (2015) 322–336. doi:10.3390/toxins7020322.

[68] S.A. Banack, J.S. Metcalf, W.G. Bradley, P.A. Cox, Detection of cyanobacterial neurotoxin β-N-methylamino-l-alanine within shellfish in the diet of an ALS patient in Florida, Toxicon. 90 (2014) 167–173. doi:10.1016/j.toxicon.2014.07.018.

[69] D. Réveillon, E. Abadie, V. Séchet, L. Brient, V. Savar, M. Bardouil, P. Hess, Z. Amzil, Beta-N-methylamino-L-alanine: LC-MS/MS optimization, screening of cyanobacterial strains and occurrence in shellfish from Thau, a French Mediterranean Lagoon, Mar. Drugs. 12 (2014) 5441–5467. doi:10.3390/md12115441.

[70] S. Banack, J.S. Metcalf, Z. Spáčil, T.G. Downing, S. Downing, A. Long, P.B. Nunn, P. Cox, Distinguishing the cyanobacterial neurotoxin β-N-methylamino-L-alanine (BMAA) from other diamino acids, Toxicon. 57 (2011) 730–8. doi:10.1016/j.toxicon.2011.02.005.

[71] I.A. Buryakov, E. V. Krylov, & Nazarov, E. G., U.K. Rasulev, A new method of separation of multi-atomic ions by mobility at atmospheric pressure using a high-frequency amplitude-asymmetric strong electric field, Int. J. Mass Spectrom. Ion Process. 128 (1993) 143–148.

[72] A.A. Shvartsburg, Differential ion mobility spectrometry: nonlinear ion transport and fundamentals of FAIMS, CRC Press, 2008.

[73] A.A. Shvartsburg, F. Li, K. Tang, R.D. Smith, High-resolution FAIMS Using New Planar Geometry Analyzers, Anal. Chem. 78 (2006) 3706–3714. doi:10.1021/ac052020v.

[74] J.T. Kapron, M. Jemal, G. Duncan, B. Kolakowski, R. Purves, Removal of metabolite interference during liquid chromatography/tandem mass spectrometry using high-field asymmetric waveform ion mobility spectrometry, Rapid Commun. Mass Spectrom. 19 (2005) 1979–1983. doi:10.1002/rcm.2016.

[75] T. Klassen, S. Szwandt, J.T. Kapron, A. Roemer, Validated quantitation method for a peptide in rat serum using liquid chromatography/high-field asymmetric waveform ion mobility spectrometry, Rapid Commun. Mass Spectrom. 23 (2009) 2301–2306. doi:10.1002/rcm.

[76] S. Prasad, M.W. Belford, J.J. Dunyach, R.W. Purves, On an aerodynamic mechanism to enhance ion transmission and sensitivity of faims for nano-electrospray ionization-mass spectrometry, J. Am. Soc. Mass Spectrom. 25 (2014) 2143–2153. doi:10.1007/s13361-014-0995-8.

[77] P.R.S. Baker, A.M. Armando, J.L. Campbell, O. Quehenberger, E. Dennis, Three-dimensional enhanced lipidomics analysis combining UPLC, differential ion mobility spectrometry, and mass spectrometric separation strategies, J. Lipid Res. 55 (2014) 2432–42. doi:10.1194/jlr.D051581.

[78] H. Gao, S. Deng, R.S. Obach, Unbiased scanning method and data banking approach using ultra-high performance liquid chromatography coupled with high-resolution mass spectrometry for quantitative comparison of metabolite exposure in plasma across species analyzed at different dates, Anal. Chem. 87 (2015) 11771–11776. doi:10.1021/acs.analchem.5b03469.

[79] B.B. Schneider, T.R. Covey, S.L. Coy, E. V. Krylov, E.G. Nazarov, Planar differential mobility spectrometer as a pre-filter for atmospheric pressure ionization mass spectrometry, Int. J. Mass Spectrom. 298 (2010) 45–54. doi:10.1016/j.ijms.2010.01.006.

[80] R.W. Purves, A.R. Ozog, S.J. Ambrose, S. Prasad, M. Belford, J.J. Dunyach, Using gas modifiers to significantly improve sensitivity and selectivity in a cylindrical FAIMS device, J. Am. Soc. Mass Spectrom. 25 (2014) 1274–1284. doi:10.1007/s13361-014-0878-z.

[81] J.L. Campbell, M. Zhu, W.S. Hopkins, Ion-molecule clustering in differential mobility spectrometry: Lessons learned from tetraalkylammonium cations and their isomers, J. Am. Soc. Mass Spectrom. 25 (2014) 1583–91. doi:10.1007/s13361-014-0939-3.

[82] B.B. Schneider, T.R. Covey, S.L. Coy, E. V. Krylov, E.G. Nazarov, Chemical effects in the separation process of a differential mobility/Mass spectrometer system, Anal. Chem. 82 (2010) 1867–1880. doi:10.1021/ac902571u.

[83] R. Guevremont, R. Purves, D. Barnett, FAIMS apparatus and method using carrier gas of mixed composition, 6,774,360, 2004.

[84] P. Camilleri, ed., Capillary Electrophoresis: Theory and Practice, Second Edition, CRC Press, 1997.

[85] S. Hjertén, Free zone electrophoresis, Chromatogr. Rev. 9 (1967) 122–219.

[86] R. Virtanen, Zone electrophoresis in a narrow-bore tube employing potentiometric detection-theoretical and experimental study, Acta Polytech. Scand. Technol. Ser. 123 (1974) 1–67.

[87] J.A. Olivares, N.T. Nguyen, C.R. Yonker, R.D. Smith, On-line mass spectrometric detection for capillary zone electrophoresis, Anal. Chem. 59 (1987) 1230–1232. doi:0003-2700/67/0359-1230$01.50.

[88] P. Hommerson, A. Khan, G.J. de Jong, G.W. Somsen, Ionization techniques in capillary electrophoresis-mass spectrometry: principles, design, and application, Indian J. Exp. Biol. 47 (2009) 987–992. doi:10.1002/mas.

[89] G.N. Okafo, P. Camilleri, Direct chiral resolution of amino acid derivatives by capillary electrophoresis, J. Microcolumn Sep. 5 (1993) 149–153. doi:10.1002/mcs.1220050210.

[90] J.-S. Jeong, S.-K. Kim, S.-R. Park, Capillary electrophoresis mass spectrometry with sheathless electrospray ionization for high sensitivity analysis of underivatized amino acids, Electrophoresis. 33 (2012) 2112–21. doi:10.1002/elps.201200005.

[91] P. James, ed., Proteome Research: Mass Spectrometry, Springer Science & Business Media, 2000.

[92] L. Sun, G. Zhu, X. Yan, M.M. Champion, N.J. Dovichi, Capillary zone electrophoresis for analysis of complex proteomes using an electrokinetically pumped sheath flow nanospray interface, Proteomics. 14 (2014) 622–628. doi:10.1002/pmic.201300295.

[93] M. Gong, K.R. Wehmeyer, A.M. Stalcup, P.A. Limbach, W.R. Heineman, Study of injection bias in a simple hydrodynamic injection in microchip CE, Electrophoresis. 28 (2007) 1564–1571. doi:10.1002/elps.200600616.

[94] S. Orlandini, R. Gotti, S. Furlanetto, Multivariate optimization of capillary electrophoresis methods: A critical review, J. Pharm. Biomed. Anal. 87 (2014) 290–307. doi:10.1016/j.jpba.2013.04.014.

[95] S. Furlanetto, S. Orlandini, I. Giannini, G. Beretta, S. Pinzauti, Pitfalls and success of experimental design in the development of a mixed MEKC method for the analysis of budesonide and its impurities, Electrophoresis. 30 (2009) 633–643. doi:10.1002/elps.200800626.

[96] P. Schmitt-Kopplin, N. Hertkorn, A. Garrison, D. Freitag, A. Kettrup, Influence of borate buffers on the electrophoretic behavior of humic substances in capillary zone electrophoresis, Anal. Chem. 70 (1998) 3798–3808. doi:10.1016/j.carres.2009.03.019.

[97] Z.K. Shihabi, Stacking in capillary zone electrophoresis, J. Chromatogr. A. 902 (2000) 107–117. doi:10.1016/s0021-9673(00)00743-3.

[98] M. Zdena, P. Gebauer, P. Bocek, Contemporary sample stacking in analytical electrophoresis, Electrophoresis. 32 (2011) 116–126. doi:10.1002/elps.201400313.

[99] J.P. Quirino, S. Terabe, Sample stacking of cationic and anionic analytes in capillary electrophoresis, J. Chromatogr. A. 902 (2000) 119–35. doi:10.1016/S0021-9673(00)00812-8.

[100] D.S. Lian, S.J. Zhao, J. Li, B.L. Li, Progress in stacking techniques based on field amplification of capillary electrophoresis, Anal. Bioanal. Chem. 406 (2014) 6129–6150. doi:10.1007/s00216-014-8062-7.

[101] A.A. Kazarian, E.F. Hilder, M.C. Breadmore, Online sample pre-concentration via dynamic pH junction in capillary and microchip electrophoresis, J. Sep. Sci. 34 (2011) 2800–2821. doi:10.1002/jssc.201100414.

[102] E. Baidoo, P. Benke, C. Neususs, M. Pelzing, Capillary electrophoresis-Fourier transform ion cyclotron resonance mass spectrometry for the identification of cationic metabolites via a pH-mediated stacking-transient isotachophoretic method, Anal. Chem. 80 (2008) 3112–3122. http://pubs.acs.org/doi/abs/10.1021/ac800007q\npapers3://publication/uuid/7F9015C6-BFE1-4153-BC2B-5C3CC779E71C.

[103] J.P. Quirino, S. Terabe, Approaching a million. Fold sensitivity increase in capillary electrophoresis with direct ultraviolet detection: Cation-selective exhaustive injection and sweeping, Anal. Chem. 72 (2000) 1023–1030. doi:10.1021/ac990344b.

[104] M.S. Baptista, R.C.C. Cianca, V.R. Lopes, C.M.R. Almeida, V.M. Vasconcelos, Determination of the non protein amino acid β-N-methylamino-l-alanine in estuarine cyanobacteria by capillary electrophoresis, Toxicon. 58 (2011) 410–4. doi:10.1016/j.toxicon.2011.08.007.

[105] G. Bonvin, J. Schappler, S. Rudaz, Capillary electrophoresis-electrospray ionization-mass spectrometry interfaces: Fundamental concepts and technical developments, J. Chromatogr. A. 1267 (2012) 17–31. doi:10.1016/j.chroma.2012.07.019.

[106] C.W. Klampfl, Recent advances in the application of capillary electrophoresis with mass spectrometric detection, Electrophoresis. 27 (2006) 3–34. doi:10.1002/elps.200500523.

[107] P. Schmitt-Kopplin, M. Frommberger, Capillary electrophoresis-mass spectrometry: 15 years of developments and applications, Electrophoresis. 24 (2003) 3837–3867. doi:10.1002/elps.200305659.

[108] P. Pantůčková, P. Gebauer, P. Boček, L. Křivánková, Recent advances in CE-MS: Synergy of wet chemistry and instrumentation innovations, Electrophoresis. 32 (2011) 43–51. doi:10.1002/elps.201000382.

[109] R. Ramautar, A.A.M. Heemskerk, P.J. Hensbergen, A.M. Deelder, J.M. Busnel, O.A. Mayboroda, CE-MS for proteomics: Advances in interface development and application, J. Proteomics. 75 (2012) 3814–3828. doi:10.1016/j.jprot.2012.04.050.

[110] V. Sanz-Nebot, E. Balaguer, F. Benavente, J. Barbosa, Comparison of sheathless and sheath-flow electrospray interfaces for the capillary electrophoresis-electrospray ionization-mass spectrometry analysis of peptides, Electrophoresis. 26 (2005) 1457–1465. doi:10.1002/elps.200410087.

[111] S. Akamatsu, T. Mitsuhashi, Development of a simple analytical method using capillary electrophoresis-tandem mass spectrometry for product identification and simultaneous determination of free amino acids in dietary supplements containing royal jelly, J. Food Compos. Anal. 30 (2013) 47–51. doi:10.1016/j.jfca.2013.01.006.

[112] K.T. Rodrigues, D. Mekahli, M.F.M. Tavares, A. van Schepdael, Development and validation of a CE-MS method for the targeted assessment of amino acids in urine, Electrophoresis. 37 (2016) 1039–1047. doi:10.1002/elps.201500534.

[113] T. Soga, D.N. Heiger, Amino acid analysis by capillary electrophoresis electrospray ionization mass spectrometry, Anal. Chem. 72 (2000) 1236–1241. doi:10.1021/ac990976y.

[114] N. Shama, S.W. Bai, B.C. Chung, B.H. Jung, Quantitative analysis of 17 amino acids in the connective tissue of patients with pelvic organ prolapse using capillary electrophoresis-tandem mass spectrometry, J. Chromatogr. B Anal. Technol. Biomed. Life Sci. 865 (2008) 18–24. doi:10.1016/j.jchromb.2008.01.027.

[115] P. Kusy, K. Klepárník, Z. Aturki, S. Fanali, F. Foret, Optimization of a pressurized liquid junction nanoelectrospray interface between CE and MS for reliable proteomic analysis, Electrophoresis. 28 (2007) 1964–1969. doi:10.1002/elps.200600640.

[116] M. Hashimoto, Y. Ishihama, M. Tomita, T. Soga, Microelectrospray interface with coaxial sheath flow for high-resolution capillary electrophoresis/mass spectrometry separation, Rapid Commun. Mass Spectrom. 21 (2007) 3479–3584. doi:10.1002/rcm.

[117] Y.R. Chen, M.C. Tseng, G.R. Her, Design and performance of a low-flow capillary electrophoresis-electrospray-mass spectrometry interface using an emitter with dual beveled edge, Electrophoresis. 26 (2005) 1376–1382. doi:10.1002/elps.200410159.

[118] X. Zhong, E.J. Maxwell, D.D.Y. Chen, Mass transport in a micro flow-through vial of a junction-at-the-tip capillary electrophoresis-mass spectrometry interface, Anal. Chem. 83 (2011) 4916–4923. doi:10.1021/ac200636y.

[119] L. Sun, G. Zhu, Z. Zhang, S. Mou, N.J. Dovichi, Third-Generation Electrokinetically Pumped Sheath-Flow Nanospray Interface with Improved Stability and Sensitivity for Automated Capillary Zone Electrophoresis–Mass Spectrometry Analysis of Complex Proteome Digests, J. Proteome Res. (2015)

2312–2321. doi:10.1021/acs.jproteome.5b00100.

[120] S.L. Nilsson, C. Andersson, P.J.R. Sjöberg, D. Bylund, P. Petersson, M. Jörntén-Karlsson, K.E. Markides, Phosphate buffers in capillary electrophoresis/mass spectrometry using atmospheric pressure photoionization and electrospray ionization, Rapid Commun. Mass Spectrom. 17 (2003) 2267–2272. doi:10.1002/rcm.1182.

[121] F. Foret, T.J. Thompson, P. Vouros, B.L. Karger, P. Gebauer, P. Boček, Liquid sheath effects on the separation of proteins in capillary electrophoresis/electrospray mass spectrometry, Anal. Chem. 66 (1994) 4450–4458. doi:10.1021/ac00096a010.

[122] R.L. Sheppard, X. Tong, J. Cai, J.D. Henion, Chiral separation and detection of terbutaline and ephedrine by capillary electrophoresis coupled with ion spray mass spectrometry, Anal. Chem. 67 (1995) 2054–2058.

[123] H. Stutz, G. Bordin, A.R. Rodriguez, Capillary zone electrophoresis of metal-binding proteins in formic acid with UV- and mass spectrometric detection using cationic transient capillary isotachophoresis for preconcentration., Electrophoresis. 25 (2004) 1071–1089. doi:10.1002/elps.200305806.

[124] G.A. Ross, Capillary Electrophoresis– Mass Spectrometry: Practical Implementation and Applications, LC•GC Eur. (2001) 2–6.

[125] A.A. Shvartsburg, R.D. Smith, A. Wilks, A. Koehl, D. Ruiz-Alonso, B. Boyle, Ultrafast differential ion mobility spectrometry at extreme electric fields in multichannel microchips, Anal. Chem. 81 (2009) 6489–6495. doi:10.1021/ac900892u.

[126] B.B. Schneider, E.G. Nazarov, F. Londry, P. Vouros, T.R. Covey, Differential mobility spectrometry/mass spectrometry history, theory, design optimization, simulations, and applications, Mass Spectrom. Rev. (2015). doi:10.1002/mas.21453.

[127] I.W. Burton, M.A. Quilliam, J.A. Walter, Quantitative H NMR with external standards: Use in preparation of calibration solutions for algal toxins and other natural products, Anal. Chem. 77 (2005) 3123–3131. doi:10.1021/ac048385h.

[128] C. Hollingdale, K. Thomas, N. Lewis, K. Bekri, P. McCarron, M.A. Quilliam, Feasibility study on production of a matrix reference material for cyanobacterial toxins, Anal. Bioanal. Chem. (2015) 5353–5363. doi:10.1007/s00216-015-8695-1.

[129] N. Pang, C. Yan, Study of field mobilities dependence and direct separation of acidic phytohormones by differential mobility spectrometry-mass spectrometry, Int. J. Mass Spectrom. 362 (2014) 48–55. doi:10.1016/j.ijms.2013.12.025.

[130] D.G. Beach, J.E. Melanson, R.W. Purves, Analysis of paralytic shellfish toxins using high-field asymmetric waveform ion mobility spectrometry with liquid chromatography-mass spectrometry, Anal. Bioanal. Chem. 407 (2015) 2473–2484. doi:10.1007/s00216-015-8488-6.

[131] B. Kolakowski, M. McCooeye, Z. Mester, Compensation voltage shifting in high-field asymmetric waveform ion mobility spectrometry-mass spectrometry, Rapid Commun. Mass Spectrom. 20 (2006) 3319–3329. doi:10.1002/rcm.

[132] E. Pagliano, Z. Mester, J. Meija, Reduction of measurement uncertainty by experimental design in high-order (double, triple, and quadruple) isotope dilution mass spectrometry: application to GC-MS measurement of bromide, Anal. Bioanal. Chem. (2013) 1–9. doi:10.1007/s00216-013-6724-5.

[133] P.B. Nunn, P. O'Brien, The interaction of β-N-methylamino-L-alanine with bicarbonate: an 1H-NMR study, FEBS Lett. 251 (1989) 31–35. doi:10.1016/0014-5793(89)81423-1.

[134] C.C. Liu, J.F. Alary, P. Vollmerhaus, M. Kadkhodayan, Design, optimisation, and evaluation of a sheath flow interface for automated capillary electrophoresis-electrospray-mass spectrometry, Electrophoresis. 26 (2005) 1366–1375. doi:10.1002/elps.200410133.

[135] R.M. Mccormick, Capillary zone electrophoretic separation of peptides and proteins using low ph buffers in modified silica capillaries, Anal. Chem. 60 (1988) 2322–2328. doi:10.1021/ac00172a003.

[136] R.D. Smith, C.J. Barinaga, H.R. Udseth, Improved electrospray ionization interface for capillary zone-mass spectrometry, Anal. Chem. 60 (1988) 1948–1952. doi:10.1021/ac00169a022.

[137] E.A. Bell, The discovery of BMAA, and examples of biomagnification and protein incorporation involving other non-protein amino acids, Amyotroph. Lateral Scler. 10 Suppl 2 (2009) 21–25. doi:10.3109/17482960903268700.

[138] W.B. Glover, C.M. Liberto, W.S. McNeil, S.A. Banack, P.R. Shipley, S.J. Murch, Reactivity of β-methylamino-L-alanine in complex sample matrixes complicating detection and quantification by mass spectrometry, Anal. Chem. 84 (2012) 7946–7953. doi:10.1021/ac301691r.